Study on Residual Stress and Mechanical Behavior of intermetallic Compound Layer in Diffusion Bonding of Mg/Al Alloy

Yunlong Ding

CONTENTS

Chapter 1 Introduction

1.1 Background and development on bonding technology of magnesium alloy and aluminum alloy

In recent years, with the rapid development of the transportation, aerospace and, national defense and military industry, and the economic development demand for energy, the expectation of lightweight structure of transportation machinery such as automobile and aviation is getting higher and higher. As the lightest metal [1], magnesium alloys have received more and more attentions because of the low density, high specific strength, excellent castability, outstanding vibration or shock energy absorption function. As the use of magnesium alloys, the weight of components can be reduced [2]. But it's formability in cold working is poor, tearing and cracking always occur. What's more, magnesium alloy can be corroded easily. However, aluminum alloys have attractive mechanical and metallurgical properties, good moldability and excellent corrosion resistance [3,4,5,6]. It is well known that aluminum alloys are also widely used in aerospace, automotive, machinery, electrical and chemical industry [7,8,9]. If aluminum alloy can be bonded with magnesium alloy and form a kind of composite material, not only would the flexibility and availability be improved substantially, but also the weight and cost would be reduced obviously. Therefore, the combination of superior functions of magnesium alloy and aluminum alloy becomes one direction of the research on lightweight of vehicle structure.

In the field of studying the joint of magnesium alloys and aluminium alloys, which belongs to dissimilar-metal joints. There are many welding processes have been applied. Such as electron beam welding, resistance welding, explosive welding, friction stir welding, laser welding and vacuum diffusion bonding [10]. Dissimilar-metal joints are used widely in various industrial applications due to both technical and economic reasons. The adoption of dissimilar-metal combinations provides possibilities for the flexible design of the product by using each material

efficiently, benefiting from the specific properties of each material in a functional way. Welding is one of the most widely used methods for welding process of metals. Therefore, despite there are many difficulties, efforts have also been made to apply these methods to join dissimilar metals. These difficulties include issues related to metallurgical incompatibility, the formation of brittle phases, the separation of high and low melting phases due to chemical mismatch, and large residual stresses that may be caused by physical mismatch [11].

Fusion welding technology includes many welding techniques, such as commonly used conventional metal shielded arc, tungsten gas protection arc, gas metal arc and submerged arc welding. They also include processes characterized by high energy density, such as plasma arc, electron beam and laser beam welding. In addition to fusion welding, several other types of joining techniques can be used and are often associated with the difficulty of producing dissimilar metal joints. These methods include pressure welding, friction welding, resistance welding and diffusion welding, as well as brazing and welding, bonding and mechanical joining. Most of these techniques can eliminate the problem of fusion because base metals remain solid during the bonding process. Therefore, they are better than fusion in this regard. However, the conditions of usage may make a particular process unsuitable, and welding and bonding can not be candidates for high temperature applications, whereas mechanical connections are not acceptable for leak proof connections. In addition, the required joint geometry may make friction welding difficult to be applied. Diffusion welding often provides superior technical advantages for bonding small, dissimilar metal parts, but this process is quite time-consuming.

The electron beam welding

Relying on high energy density, electron beam welding (EBW) still has a great industrial interest [12]. This trend may be due to the rapid growth of EBW equipment and the economic benefits of using the process in mass volume production. More importantly, EBW can meet the high quality requirements of products [13,14]. The basic EBW equipment is composed of a welding chamber, an electron beam gun,

power supply system, vacuum pump system and control system.

The simplified diagram of the EBW process is shown in Fig.1.1.
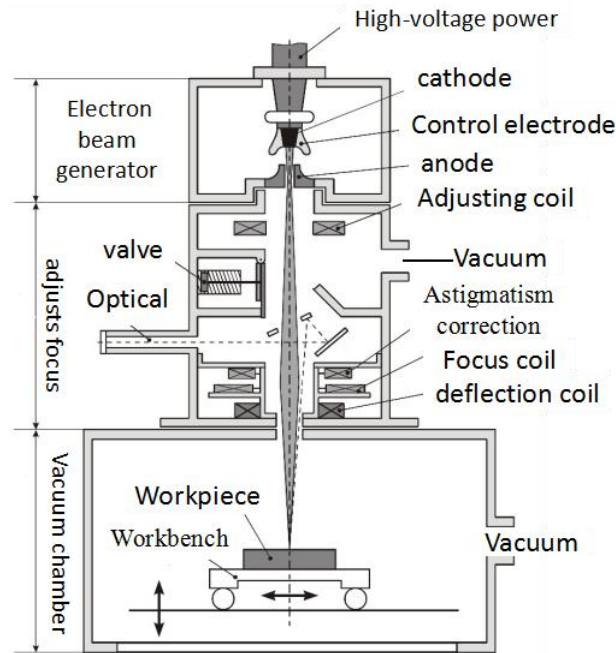
Fig.1.1 Simplified diagram of the EBW process

As an industrial welding process, EBW is mainly used in the nuclear industry, aircraft and aerospace industries. Due to the high quality and reliability requirements of welding area, EBW has also been successfully used in a variety of applications, such as the workshop of medium thickness welding and the parts requiring for high precision welding. Recently, the welding of heavy engineering parts has been realized due to high power level. In all of these cases, EBW of dissimilar metals was frequently used for investigations due to the advancement in equipment, and the ability to carry out sundry welding projects. The operation of an EBW is based on the principle of using kinetic energy of electrons as the heating source to melt the metals to be welded. These electrons are generated by heating the negatively charged filament to the temperature range of its thermionic emission, and the electron is emitted at that temperature range. The electron is accelerated by the electric field between the negatively charged bias electrode, which is slightly below the cathode, and the anode, then through the hole in the anode and form a beam. The electron

beam can be focused under the condition of vacuum and strikes the metal surface to be welded. About 95% of the electron kinetic energy is converted to heat. Typical voltage and current are respectively 30-175kV and 50-1000mA. The minimum weld width is about 0.8mm, and the obtained power density is as high as 1010 wm^{-2} [15]. One of EBW's main features is the ability to use the "keyhole" mechanism for deep penetration welding. Therefore,The EB weldments can achieve a high depth-to-width ratio. This characteristic not only can realize single-pass welding of thick plates, but also can perform the welding of relatively thin plates with a high travel speed. The advantages of EBW are shown as follows [16]:

1. The total amount of needed heat is low, so the thermal influence area is not easy to grow once more, and the workpieces are less deformed.

2. The high depth-width ratio can be obtained when welding task is carried out with small hole welding.

3. Single-beam electron beam welding can be used for welding up to 4 inches of material.

4. High purity welding environment (vacuum) can reduce the pollution of oxygen and nitrogen to metals.

5. A high vacuum or medium vacuum welding method can be used to weld closed containers that require internal vacuum maintenance.

6. The electron beam can use magnetic deflection to produce various shapes or use magnetic oscillations to improve welding quality or increase penetration.

7. Focusing the electron beam has a considerable depth of field, can be applied to a range of distances ranging from welding.

8. A fully welded, single-pass weld with approximately parallel sides and approximately symmetrical shrinkage can be obtained.

9. Dissimilar metals and materials with high thermal conductivity, can be welded. such as magnesium alloy and aluminium alloy, copper.

The EBW technique also has it's limitations which are shown as follows:

1. The connector must be precisely positioned under the electron beam.

2. I-bezel butt joint is required.

3. The workpieces usually must be clamped tightly.

4. Rapid cooling will cause cracks in the heat affected area, make the material brittle and leave pores in the weld.

5. The cost of quipment is expensive.

6. For vacuum and medium vacuum welding, the vacuum chamber should be large enough to accommodate the entire assembly. The time required to   evacuate the vacuum chamber will affect the cost of the product.

7. Because the electron beam can be deflected by the magnetic field, so the device used for fixation on the electron beam path should be non-magnetic material or the correctly demagnetized metal material.

8. All EBWs must have radiological protection to ensure that no one is exposed to x-rays produced by electron beam welding.

9. For non-vacuum EBW, the advisable ventilation is required to ensure that ozone and   other harmful gases produced during the EBW welding process are discharged.

Laser welding process

Laser welding process is a kind of welding technology with high power density [17,18]. Laser welding process offers great potential for the design of new products. Compared with other welding processes, less heat is added to the workpieces, which results in a smaller heat affected zone and lower panel deformation. In addition, it is advanced for it's high productivity, high weld quality, low distortion, manufacturing flexibility, and facility for automation [19,20,21]. Therefore, it has become an important industrial process because of its advantages as a welding process over the other widely used joining techniques.

Laser welding has the characteristics of parallel fusion zone, narrow weld width and high penetrability. These advantages come from its high power density, which makes laser welding one of the keyhole welding processes [22]. The simplified diagram is shown in Fig.1.2.
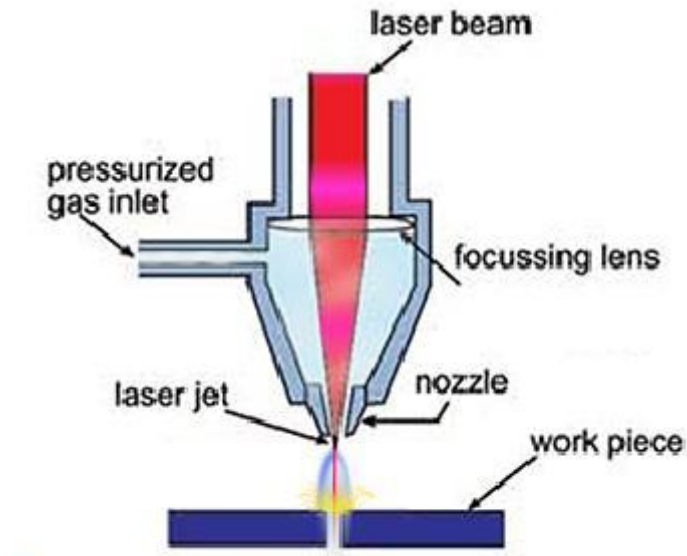
Fig.1.2 Simplified diagram of the LW process

The laser welding input parameters determine the shape of the laser welding bead 'keyhole' [23], because of the combination of these parameters control the heat input. In order to obtain good welding quality, the combination of output power, welding speed, focus position, shielding gas and position accuracy should be selected correctly [24]. The Response Surface Method is widely used to predict the geometry and mechanical properties of weld bead in many welding processes [25-29]. In the process of laser welding, the temperature dependence of the phase change of material properties, laser absorption and plasma reflection are very complex phenomena occurring in a very short time. The traditional experiment and error approaches based on welding experiment have encountered many difficulties in optimizing laser welding. In order to extend the industrial application of laser welding and make the process more reliable, numerical simulation of welding process has been used as the basis for optimizing welding parameters, which can control the welding process properly [30].

Explosive welding

Explosive welding and vacuum diffusion welding processes can stop the metals from being welded, because the substrate metal remains solid state during the bonding

process. Explosive welding is a special type of welding method, which is based on the high energy produced by the explosion [31,32], and it is well known for its capability, which can directly join a large variety of both similar and dissimilar combinations of metals that can not be completed by any other techniques [33-36]. Furthermore, Due to its ability to distribute high energy density through explosion, this process can join with high surface area [37–40]. Explosive welding is a solid-state welding process that can control explosive detonations to force two or more metals together at high pressure and high velocity oblique impact. The explosive charge when detonated accelerates the plates to a speed at which a metallic bond can be formed between the metal components during the collision. The metal plates collide with each other at high speed by using explosives. In the high-speed oblique collision of the metal plate, if the impact angle β and the impact velocity Vp are in the required range for bonding, a high-speed jet stream can be formed between the metal plates [41,42]. The simplified diagram of the explosive welding process is shown in Fig.1.3 (a) and (b).
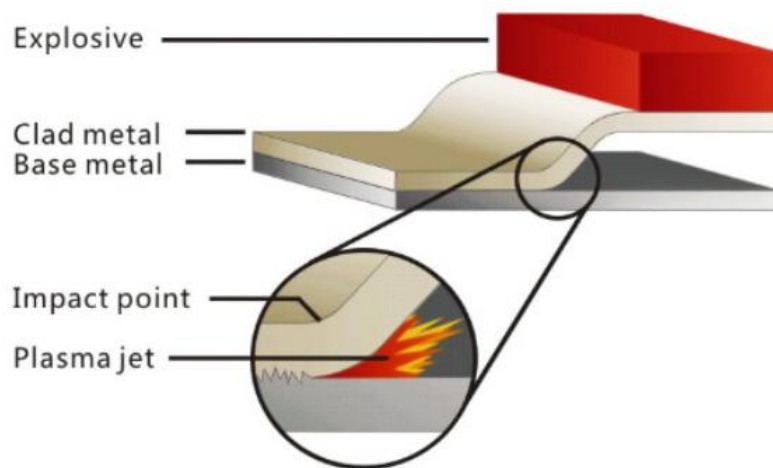
Fig.1.3 (a) Simplified diagram of the explosive welding process
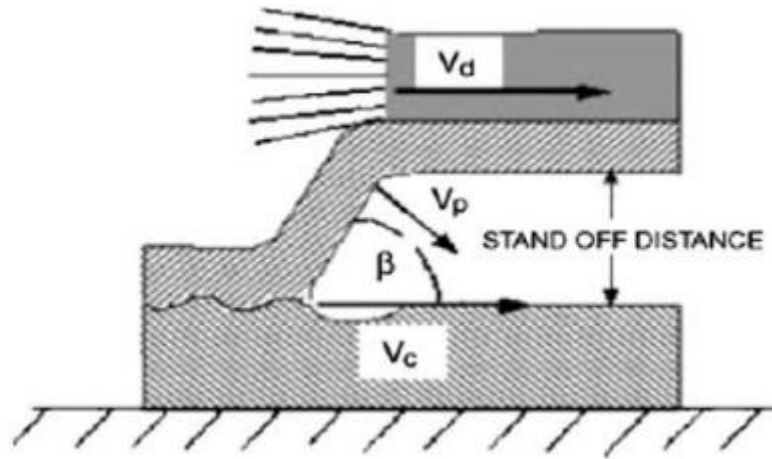
Fig.1.3 (b) Simplified diagram of the explosive welding process

The oxide film is harmful to the establishment of metallurgical welding. The oxide film is blown off the interface by jet. Then the metal plate is sprayed with a spray to remove any surface film. At the point of collision, the original clean surface is gathered together under very high pressure. The pressure must be high enough and for a sufficient length of time to achieve inter-atomic bonding. The velocity Vc of the collision point can be used for controlling the bonding time. The high pressure also results in considerable local plastic deformation of the metal in the bonding area [43,44]. This kind of welding is metallurgy in nature, and usually is stronger than the weaker material.

The quality of welding area depends greatly on the careful control of process parameters. The parameters include material surface preparation, plate separation or departure distance, explosive load or explosive ratio, detonation energy and detonation velocity V_d. The selection of parameters is based on the mechanical characteristics, density and shear wave velocity of each part [45]. Considerable progress has been made to determine the optimum operational parameters for producing acceptable bonds. In this paper, the welding window of various parameters such as collision velocity - collision angle or flying plate velocity - collision angle are proposed [46–49]. It is the most important factor to choose the explosive that can produce the required detonation velocity for obtaining consistent well welds. Related

8

research has reported that the collision velocity Vc and the plate velocity Vp should be smaller than the sound velocity in any part to be welded [50,51]. The velocity of sound in engineering materials is typically 4.5–6 km/s, while the detonation velocity in common explosive (plastic explosive) is typically 6–7 km/s. The high speed explosives are not available for explosive welding [52,53]. In this reason, a mixture of ammonium nitrate and fuel oil and an inert substance such as sand or perlite is always used with the condition of detonation velocity typically between 2 and 3 km/s. The required explosive must also provide uniform detonation so that a collision velocity that will be uniform from the start to end of the weld can be obtained. The type and amount of explosions in unit area are selected to achieve the necessary detonation energy and detonation velocity. The wave interface is the characteristic of explosive welding. Wave formation in explosive welding can be regarded as a special case of normal phenomena of inter facial wave formation in a certain flow environment. The formation of waveform appears to be the result of velocity distribution variety and periodic disturbance of material. The cladding of plate and concentric cylinder constitutes the main commercial application of explosive welding. The advantages of the explosive package include: The joining of dissimilar metals; The bonding of thin sheet with thick plate; Weld the metals that are after heat treatment and cold worked together without changing their mechanical properties; the absence of heat affected zone in the clad plates and the simplicity and speed of operation for achieving welding with cost reduction and strength or corrosion properties [54].

Diffusion bonding

Diffusion welding is an advanced solid-state welding process that is based on solid state diffusion [55,56], wherein the atoms of two solid metal surfaces are dispersed over time. This is usually completed at elevated temperatures that are about 50-70% of the materials' absolute melting temperatures [57]. The heating and cooling rates of diffusion bonding are slow, so the atom can fully diffuse in the welding course. During the diffusion process, coalescence of contacting surface is produced with minimum macroscopic deformation by diffusion controlled processes which are

induced by applying heat and pressure for a finite interval [58]. So with the usage of diffusion bonding technology these defects produced during fusion welding could be avoided, and improve the structure stability and mechanical properties [59]. At present, diffusion bonding technology has been applied in the welding of dissimilar materials. Such as Ti/Al, Fe3Al/18-8 steel and Al/18-8 steel [60-62]. And it is most commonly used to weld "sandwiches" of alternating layers of thin metal foil, and metal wires or filaments [63]. Currently, the diffusion bonding method is widely used in the joining of high-strength and refractory metals within the aerospace and nuclear industries.

The advantages and applicability of the diffusion bonding process are as follows: diffusion bonding does not involve fluid fusion, and usually does not contain filler metals. The total weight does not increase, and the bonding layer tends to show the strength and heat resistance of the base metal at the same time. The material will not bear or bear small plastic deformation. The introduced residual stresses were very few and there was no contamination from the welding process. It can be performed theoretically on an arbitrary connection surface without increasing processing time; In fact, the surface is often limited by the required pressure and physical constraints. It can be carried out with similar and dissimilar metals, active and refractory metals, or pieces of different thicknesses.

Because of its relatively high cost, diffusion bonding is most often used for workpieces that are difficult or impossible to weld in other ways. Examples include welding materials, which are usually impossible to fuse with liquid. Such as zirconium and beryllium; Extremely high melting materials such as tungsten; The alternating layers of different metals must be maintained at high temperatures; And very thin honeycomb foil structure [64-67].

The advantages:

1. The welding layer has the same physical and mechanical properties as the basic material.

2. The diffusion welding process can produce high quality joints, in which there is

no discontinuity and porosity. In other words, the welded workpiece can be processed and heat treated.

3. Diffusion welding can build high-precision parts with complex shapes. Moreover, diffusion is flexible.

4. Diffusion bonding can be widely used and can be used to join similar or dissimilar materials and can be used for the processing of composite materials.

5. This process is not very difficult to approach, and the cost of implementing diffusion bonding is not very high.

6. The plastic deformation of materials welded by diffusion bonding method can be reduced .

Applicability:

Diffusion bonding is mainly used to create complex forms for electronics, aerospace and nuclear industries. Compared with other connection technology (such as explosion welding), need quite a long time because of the connection, so the quantity of components is small, and are mostly automatic manufactured. However, due to different requirements, some of the time interval could be accomplished in few minutes. In an attempt to reduce fastener count, labor costs, and quantities of parts, diffusion bonding, in conjunction with super-plastic forming, is also used when creating complex forms of metal sheets. Multiple sheets are stacked atop one another and bonded in specific sections. The stack is then piled into a mold and gas pressure makes the sheets to fill the mold. This is often accomplished with the usage of titanium or aluminum alloys for parts needed in the aerospace industry. Typical materials that are welded include titanium, beryllium, and zirconium. In many military aircraft, diffusion bonding will help save expensive strategic materials and reduce manufacturing costs. For some aircraft, the quantities of diffusion bonding components have exceeded 100, these includes fuselages, outboard and inboard actuator fittings, landing gear trunnions, and nacelle frames.

1.2 Purpose of this research

As it is reported, compared with other welding process diffusion bonding technology

has so many advantages. However, although diffusion bonding process was applied, the intermetallic compounds of Mg and Al, such as Al_3Mg_2 and $Al_{12}Mg_{17}$ will form in the diffusion layer. Due to brittleness of intermetallic compound, the mechanical behaviors of composite materials are not as well as expected, so that maybe the applications of Mg/Al composite materials will be limited. Therefore, it's significant to investigate the microstructure and evaluate the mechanical properties of bonded material, in addition, take measures to refine the microstructure and improve the mechanical behavior. So evaluation of the residual stress and mechanical properties in the bonding layer were carried out in this study. In order to refine the microstructure of diffusion zone, and reveal the effect of microscopic structure on the mechanical behavior. Hot rolling technology was applied to roll the plate before diffusion bonding. What's more, annealing process was also applied after diffusion bonding.

References

[1] Zhao L.M., Zhang Z.D., Effect of Zn alloy interlayer on interface microstructures and strength of diffusion-bonded Mg-Al joints [J]. Scripta Materialia. 58 (2008) pp.283-286.

[2] L. Commin a, M. Dumont, J.-E. Masse, L. Barrallier, Friction stir welding of AZ31 magnesium alloy rolled sheets: Influence of processing parameters[J]. Acta Materialia. 57 (2009) pp.326–334.

[3] SHE Qing-yuan, YAN Hong-ge, CHEN Ji-hua, SU Bin, YU Zhao-hui, CHEN Chao, XIA Wei-jun, Microstructure characteristics and liquation behavior of fiber laser welded joints of Mg−5Zn−1Mn−0.6Sn alloy sheets [J]. Transactins of Nonferrous Metals Society of China. 57 (2017) pp.812−819.

[4] Liu L. M., Liu F., Effect of Ce on microstructures and properties of Mg/Al butt joint welded by gas tungsten arc with Zn–30Al–xCe filler metal [J]. Science and Technology of Welding and Joining. 18 (2013) pp.414-420.

[5] Liu Liming, Liu Fei, Zhu Meili, Study on Mg/Al weld seam based on Zn-Mg-Al ternary alloy [J]. Materials. 7 (2014) pp.1173-1187.

[6] Yan Y.B., Zhang Z.W., Shen W., Wang J.H., Zhang L.K., Chin B.A., Microstructures and properties of magnesium AZ31B-aluminum 7075 explosively welded composite plate [J]. Materials Science and engineering A. 527 (2010) pp.2241-2245.

[7] Li Xianrong, Liang Wei, Zhao Xingguo, Zhang Yan, Fu Xiaopeng, Liu Fencheng, Bonding of Mg and Al with Mg-Al eutectic alloy and its application in aluminum coating on magnesium [J]. Journal of Alloys and Compounds. 471 (2009) pp.408-411.

[8] Liu Fei, Ren Daxin, Liu Liming, Effect of Al foils interlayer on microstructures and mechanical properties of Mg-Al butt joints welded by gas tungsten arc welding filling with Zn filler metal [J]. Materials and Design. 46 (2013) pp.419-425.

[9] Zhu Bo, Liang Wei, Li Xianrong, Interfacial microstructures, bongding strength

and fracture of magnesium-aluminum laminated composite plates fabricated by direct hot pressing[J]. Materials Science and Engineering A. 528 (2011) pp.6584-6588.

[10] Li Ma, Dingyong He, Xiaoyan Li and Jianmin Jiang, Microstructures and mechanical properties of magnesium alloy AZ31B brazed Joint using a Zn-Mg-Al filler metal[J]. J. Mater. Sci. Technol. 26 (2010) pp.743-746.

[11] Z. Sun R. Karppi b, The application of electron beam welding for the joining of dissimilar metals: an overview. Journal of Materials Processing Technology. 59 (1996) pp.257 -267.

[12] Qi Yunlian , Deng Ju, Hong Quan, Zeng Liying, Electron beam welding, laser beam welding and gas tungsten arc welding of titanium sheet. Materials Science and Engineering. A280 (2000) pp.177–181.

[13] Kutsuna, M., Yan, Q.U, Study on porosity formation in laser welds of aluminum alloys (Report 2)—mechanism of porosity formation by hydrogen magnesium. J. Light Met. Weld. Constr. 36 (11) (1998) pp.1–17.

[14] Ion, J.C, Laser beam welding of wrought aluminum alloys. Sci. Technol. Weld. Joining. 5 (5) (2000) pp.265–276.

[15] Crafer, R. C, Improved welding performance from a 2 kW axial flow CO2 laser welding machine. Advances in welding processes. Fourth international conference. Cambridge, England: The Welding Institute. (1978) p.267.

[16] Electron beam welding.http://www.maihanji.com/baike/showbk _2201.Html.

[17] K.Y.Benyounis, A.G.OlabiM, S.J.Hashmi, Effect of laser welding parameters on the heat input and weld-bead profile. Journal of Materials Processing Technology. 164–165 (2005) pp.978-985.

[18] C. Dharmendra, K.P. Rao, J. Wilden, S. Reich, Study on laser welding–brazing of zinc coated steel to aluminum alloy with a zinc based filler. Materials Science and Engineering A. 528 (2011) pp.1497–1503.

[19] X. Cao, W. Wallace, J.-P. Immarigeon, and C. Poon, Research and progress in laser welding of wrought aluminum alloys. II. Metallurgical Microstructures, Defects, and Mechanical Properties. Materials and Manufacturing Processes. 18/1

(2003) pp.23–49.

[20] Kutsuna, M., Yan, Q.U, Study on porosity formation in laser welds of aluminum alloys (Report 2)—mechanism of porosity formation by hydrogen magnesium. J. Light Met. Weld. Constr. 36 (11) (1998) pp.1–17.

[21] Ion, J.C. Laser beam welding of wrought aluminum alloys. Sci. Technol. Weld. Joining. 5 (5) (2000) pp.265–276.

[22] W. M. Steen, Laser Material processing, Springer, London. (1991).

[23] C. Dawes, Laser welding. Abington Publishing, New York. NY (1992).

[24] Q. Huang, J. Hagstroem, H. Skoog and G. Kullberg, Effect of laser parameter variation on sheet metal welding. Inter. J. for the Joining of Materials. 3/3 (1991) pp.79-88.

[25] D. Kim et al, Modelling and optimisation of a GMA welding process by genetic algorithm and response surface methodology, INT. Journal of PROD. RES. 40/7 (2002) pp.1699-1711.

[26] V. Gunaraj and N. Murugan, Application of response surface methodology for predicting weld bead quality in SAW of pipes, Journal of Mater. Processing Technology. 88 (1999) pp.266-275.

[27] K.Y. Benyounis, A. H. Bettamer, A.G. Olabi and M.S.J. Hashmi, Predicting the impact strength of spiral-welded pipe joints in SAW of low carbon steel. Proceedings of IMC21, Limerick Ireland. Sep. (2004).

[28] V. Gunaraj and N. Murugan, Prediction of Heat- Affected Zone Characteristics in SAW of Structural Steel Pipes. Welding Journal, American Welding Society. Jan. (2002) pp.94-98.

[29] T.T. Allen, R.W. Richardson, D.P. Tagliable and G.P. Maul, Statistical process Design for Robotic GMA Welding of Sheet Metal. Welding Journal, American Welding Society. May (2002) pp.69-77.

[30] S.A. Tsirkas, P.Papanikos, Th. Kermanidis, Numerical simulation of the laser welding process in butt-joint specimens. Journal of Materials Processing Technnology. 134 (2003) pp.59-69.

[31] Mustafa Acarer, Behcet Gulenc, Fehim Findik, Investigation of explosive

welding parameters and their effects on microhardness and shear strength. Materials and Design. 24 (2003) pp.659–664.

[32] Ahmet Durgutlu, Behcet Gulenc, Fehim Findik, Examination of copper/stainless steel joints formed by explosive welding. Materials and Design. 26 (2005) pp.497–507.

[33] Fehim Findik, Recent developments in explosive welding, Review. Materials and Design. 32 (2011) pp.1081–1093.

[34] A.G. Mamalis, A. Szalay, N.M. Vaxevanidis, D.I. Pantelis, Macroscopic and microscopik phenomena of nickel/titanium "Shapememory" bimetalic strips fabricated by explosive cladding and rolling, Mater. Sci. Eng. A. 188 (1994) pp.267–275.

[35] A. Abe, Numerical study of the mechanism of wavy interface generation in explosive welding, JSME Int. J. 40 (3) (1997) pp.395–401.

[36] V. Balasubramanian, M. Rathinasabapathi, K. Raghukandan, Modelling of process parameters in explosive cladding of mildsteel and aluminium, J. Mater. Process. Technol. 63 (1997) pp.83–88.

[37] A.G. Mamalis, A. Szalay, N.M. Vaxevanidis, D.I. Pantelis, Macroscopic and microscopik phenomena of nickel/titanium "Shapememory" bimetalic strips fabricated by explosive cladding and rolling, Mater. Sci. Eng. A. 188 (1994) pp.267–275.

[38] A. Abe, Numerical study of the mechanism of wavy interface generation in explosive welding, JSME Int. J. 40(3) (1997) pp.395–401.

[39] V. Balasubramanian, M. Rathinasabapathi, K. Raghukandan, Modelling of process parameters in explosive cladding of mildsteel and aluminium, J. Mater. Process. Technol. 63 (1997) pp.83–88.

[40] Nizamettin Kahraman, Behcet Gulenc, Microstructural and mechanical 7properties of Cu–Ti plates bonded through explosive welding process. Journal of Materials Processing Technology. 169 (2005) pp.67–71.

[41] Blazynsky TZ, Explosive forming welding and compaction. Applied Science Publishers LTD. (1983).

[42] Rughue N, Characterization of explosive weld interface. In: Proc intern sympres stud mat sci eng, Chennai, India. December (2004).

[43] Akbari Mousavi SAA, Al-Hassani STS, Numerical and experimental studies of mechanism of wavy interface formations in explosive/impact welding. J Mech Phys Sol. 12 (2005) pp.251–279.

[44] Akbari Mousavi SAA, Al-Hassani STS, Burley SJ, Simulation of explosive welding using the Williamsburg equation of state to model low detonation velocity explosives. Int J Imp Eng. 31 (2005) pp.719–734.

[45] Crossland B, Williams JD, Explosive welding. Met Rev. 15 (1970) pp.79–100.

[46] Loyer A, Talerman M, Hay DR, Explosive welding: the weldability window for dissimilar metals and alloys. In: Third int symp use exp ene manuf metallic mat new prop. (1976) p.43.

[47] Wittman RH, Use of explosive energy in manufacturing metallic materials of new properties. In: Second int symp, Marianski, Lazne, Czechoslovakia. (1973).

[48] SW, Wittman RH, Computer selection of the optimum explosive loading and welding geometry. In: Proc fifth int conf high ener rate fab. 4(2) (1975) pp.1–16.

[49] AA, Simonov VA, Zakcharenko ID, Investigations on explosive welding parameters for arbitrary combinations of metals and alloys. In: Proc sixth int conf high ener rate fab. 4(1) (1975) p.1024.

[50] Bahrani AS, Crossland B, Explosive welding and cladding: an introductory survey and preliminary results. Proc Inst Mech Eng. 79 (1964) p.264.

[51] Birkhoff G, MacDougall DP, Pugh EM, Taylor G, Explosive with lined cavities. J Appl Phys. 19 (1948) pp.563–582.

[52] Abrahamson GR, Permanent periodic surface deformations due to a traveling jet. J Appl Mech. 83 (1961) pp.519–528.

[53] Wylie HK, Williams PEG, Crossland B, Further experimental investigation of explosive welding parameters. In: Proc second int conf cen high ener fab. 1(3) (1971) pp.1–43.

[54] Hammerschmidt M, Kreye H, Microstructure and bonding mechanism in explosive welding. Met Char Exp Weld Zone. 37/7 (1984) pp.12–21.

[55] O. Torun, A. Karabulut, B. Baksan, I. Celikyurek, Diffusion bonding of AZ31 using a silver interlayer. Materials and Design. 29 (2008) pp.2043–2046.

[56] Ren Jiangwei, Li Yajiang, Feng Tao, Microstructure characteristics in the interface zone of Ti/Al diffusion bonding. Materials Letters. 56 (2002) pp.647–652.

[57] C.S. Lee, H. Li, R.S. Chandel, Vacuum-free diffusion bonding of aluminium metal matrix composite. Journal of Materials Processing Technology. 89-90 (1999) pp.326-330.

[58] W.A. Owczarski, D.F. Paulonis, Application of diffusion welding in the USA. Welding Journal. 60 (2) (1981) pp.22– 33.

[59] Liu Penga, Li Yajianga, Geng Haoranb, Wang Juan, Investigation of interfacial structure of Mg/Al vacuum diffusion-bonded joint. Vacuum. 80 (2006) pp.395–399.

[60] Ren JW, Li YJ, Feng T, Microstructure characteristics in the interface zone of Ti/Al diffusion bonding. Mater Lett. 56 (5) (2002) pp.647–652.

[61] Li YJ, Wang J, Mater Sci Technol. 12 (1) (2004) pp.45–48.

[62] Liu P, Li YJ, Wang J, Guo JS, Vcuum brazing technology and microstructure near the interface of Al/18-8 stainless steel. Mater Res Bull. 38 (9–10) (2003) pp.1493–1499.

[63] VanDyke Kevin, Streeter Gigi, Dreher Jon, Leyrer Larry, Diffusion bonding. (2012). retrieved 2016-02-17

[64] Schrader George F, Elshennway Ahmad K, Manufacturing Processes and Materials (4th illustrated ed.). ISBN 0872635171. pp.319–320.

[65] Chawla Krishan K, Composite Materials: Science and Engineering. Materials research and engineering (2nd illustrated ed.). ISBN 0387984097. p.174.

[66] Jacobson David M, Giles Humpston, Principles of Brazing. 1st ed. Ohio: ASM International. USA. (2005) pp.11–14.

[67] Zhao L.M., Zhang Z.D., Effect of Zn alloy interlayer on interface microstructures and strength of diffusion-bonded Mg-Al joints [J]. Scripta Materialia. 58 (2008) pp.283-286.

Chapter 2 Effect of annealing temperature on microstructure and mechanical properties of the combined Mg/Al alloy

2.1 Introduction

Heat treatment is a group of industrial and metalworking processes used to alter the physical, and sometimes chemical, properties of a material. The most common application is metallurgical. Heat treatment is a a comprehensive process, in which metal or alloy in solid state is heated to a certain temperature in a certain medium, and maintained at this temperature for a certain period of time, then cool down at a certain rate.

Heat treatment generally does not change the shape and the overall chemical composition of the workpiece, But make the component obtain special mechanical behaviors or improve the usage performance of the workpiece by changing the internal microstructure, or change the chemical composition of the surface.

The characteristic of heat treatment is to improve the inherent quality of the workpiece, however, the transform of the inherent quality is generally not visible to the naked eye. Generally speaking, heat treatment process is made up by three procedures, which are heating, holding and cooling. Sometimes it only contains heating and cooling processes. These processes are interconnected and can't be interrupted. Throughout the production process of metals or alloys, the appropriate heat treatment could be applied to improve the performance of metal materials.

The cast metal components usually need low temperature annealing to eliminate internal stress, or complete annealing, or normalizing, Sometimes the components also need the treatment of tempering after quenching (aging). Heat treatment of ingots, during pressure process or finished products, and heat treatment is one of the major processes in the manufacture of semi-finished products and machine parts in the metallurgical enterprises and machinery factory. Heat treatment, as an intermediate process, can improve some machinability (such as forgeability, machinability, etc.) of

a workpiece; if it's used as a final operation, it can make the metals and alloys meet the required mechanical, physical, and chemical properties, in addition, it can ensure the products meet the specified quality requirements.

In the aspect of affecting the depth and diversity of structural changes of metals, heat treatment is more effective than machining and other treatments. Heat treatment can also be combined with chemical treatment, deformation processing and magnetic field effect, to improve the performance of metal materials further more.

In order to make the metal components obtain the required mechanical properties, physical properties and chemical properties. In addition to the rational choice of materials and a variety of forming processes, the heat treatment process is often essential. For example, steel is the most widely used material in the machinery industry. Its complex microstructure can be controlled by heat treatment to obtain the required mechanical properties and physicochemical properties.

In addition, aluminum, copper, magnesium, titanium and its alloys can also be treated to change their mechanical, physical and chemical properties, in order to obtain different usability. Such as aluminum generally need to be strengthened to improve the strength, in order to achieve the required mechanical properties. Conventional heat treatment process of magnesium alloy is divided into two categories, which are annealing and solution aging treatment.

2.1.1 Heat treatment methods of magnesium alloys

Annealing can significantly reduce the hardness of magnesium alloy products, and at the same time, increase their plasticity, which is beneficial for some subsequent processing. Depending on the application requirements and the properties of the alloy, for the deformed magnesium alloy, high temperature full annealing (o) and low temperature stress relief annealing (T_2) can be applied.

The purpose of annealing:

1. Reduce the hardness, and make it easy to cut the workpieces.

2. Improve the microstructure and mechanical properties.

3. To improve the microstructure for the preparation of quenching.

4. Eliminate internal stress.

Fully annealing can eliminate the work-hardening effect of magnesium alloy during plastic deformation, further more, restore and enhance its plasticity and make it easy for the subsequent deformation processing. During fully annealing, recrystallization and grain growth will occur, so the temperature can not be too high, and the annealing time can neither be too long. If the magnesium alloy contains rare earth elements, its recrystallization temperature will increase. The microstructures of AM60, AZ61, AZ60, AZ31 magnesium alloy treated by hot rolling or hot extrusion annealing can be improved. Stress relief annealing can reduce or eliminate the residual stress generated in the deformed magnesium alloy products during hot and cold processing, forming, correcting and welding. And the residual stress in castings or ingots can also be eliminated [1].

1. Solution treatment

For obtaining aging enhancement, the premise is a supersaturated solid solution. First heating to the appropriate temperature, which belongs to the single phase solid solution phase zone, and holding for appropriate time so that the alloy elements in the original microstructure dissolved in the matrix metal completely to form a supersaturated solid solution. The process above is called solution heat treatment.

According to the Hmue - Rothery rule, If the difference between the radius of the atoms of solvent and solute exceeds 14%～15%, the solid solubility of this solvent in this kind of solute will not be very great. The radius of Mg atom is 3.2nm. So the solid solubility of the elements, such as Li, Al, Ti, Cr, Zn, Ge, Yt, Zr, Nb, Mo, Pd, Ti, Pb, Bi will be obviously. In addition, if the negative charge of a given element has a great difference with that of Mg, for example, when the difference of Gordy's negative charge is more than 0.4, it is impossible to have a significant solid solubility. That is because Mg and the element tend to form stable compounds rather than solid solutions.

2. Artificial aging

Precipitation hardening is an important mechanism of magnesium alloy

21

reinforcement(especially room temperature strength), in alloys, when the solid solubility of the alloy elements decreases as the temperature decreases, then aging enhancement may be produced. The alloy with this feature is solutionized at high temperature to obtain an unstable supersaturated solid solution, then carry out aging treatment at a lower temperature to produce a dispersion precipitation phase. The sliding dislocation interacts with the precipitation phase to make the yield strength increase and the magnesium alloy is strengthened:

$$T_{yield} = (2aGb)/L + T_a \qquad\qquad (2\text{-}1)$$

Where T_{yield} is the yield strength of the precipitated alloy; T_a is the yield strength of the precipitated matrix ; (2aGb/L) is the stress required to bend the dislocations between precipitates.

Due to the high diffusion activation energy, the vast majority of magnesium alloys are not sensitive to the natural aging, after quenching process, the quenched state can be maintained at room temperature for a long time. A part of the magnesium alloy, after forming by casting or processing, are without solid solution treatment, but directly treated by artificial aging. This process is very simple, the stress of the workpiece can be eliminated, and its tensile strength can also be increased slightly. For the Mg-Zn series alloys, when the thermal deformation processes are completed, they are often directly treated by the artificial aging process to obtain the aging enhancement effect, then the products at T5 state can be obtained.

3. Solution treatment plus artificial aging

Artificial aging after solution quenching (T6) can improve the yield strength of magnesium alloy, but will reduce the partial plasticity, this process is mainly used for Mg-Al-Zn and Mg-RE-Zr alloy. In order to give full play to the aging strengthening effect, the high zinc content alloy, such as Mg-Zn-Zr alloy can also be treated with T6 processing [2,3]. During the T6 treatment, the supersaturated solid solutions obtained by the solution treatment will decompose and precipitate the second phase during artificial aging. The precipitation process and the characteristics of the precipitation phase are impacted by the alloying system, the aging temperature and the added

elements. The situation is very complicated. In addition, for the different series of magnesium alloy, the heat treatment process is different; for the different types of workpieces, heat treatment process is not the same.

For the extrusion components of magnesium alloy, after demoulding process, forced air cooling or water cooling is used for quenching, aiming at obtaining fine and uniform microstructure. However, in the quenching process, the directly contacting between the cooling water and hot mold is forbidden, otherwise it will lead to mold cracking.

The main states of extruded magnesium alloys are T5, T6 and F. T5 is the state that the artificial aging is applied after quenching process on-line; T6 is the state of solution treatment and artificial aging; F is the original processing state that is the squeezing state. Solution treatment can increase the strength, make the toughness maximize , and improve the shock resistance. The process, combining the solution treatment and the artificial aging, can achieve the maximum hardness and strength, but toughness will decrease a little. Magnesium alloys will contain residual stresses after hot working, forming, straightening and welding. Therefore, stress relief annealing should be performed.

2.1.2 Heat treatment methods of aluminium alloys

1. Annealing

The product is heated to a certain temperature and holding for a certain time, then cooling at a certain cooling rate to room temperature.

(1) The uniform annealing of the ingot: holding for a long-term at high temperature and then cooling at a certain speed (high, medium, low and slow) to make the chemical composition, the microstructure and properties of the ingot uniform, so that the plasticity of materials can improved by about 20%, the extrusion force can be reduced approximately by 20%. The extrusion speed can be increased approximately by 15%, at the same time, the quality of the material surface treatment is improved.

(2) Intermediate annealing, also known as partial annealing, or the annealing between

processes, is a kind of heat treatment method, which is under a lower temperature and hold for a short time aiming at improving the plasticity of the material and eliminating the processing stress in the material, what's more, benefiting the continuous process or obtain some properties,

(3) Fully annealing, also known as finished product annealing, is to hold for a certain time at a high temperature, in order to obtain soften microstructure under fully recrystallized state, the microstructure possesses the best plasticity and lower strength.

2. Solution quenching

The heat-treatable aluminum alloy material is heated to a higher temperature and hold for a certain period of time to make the second phase or other soluble components in the material fully dissolve into the aluminum matrix to form a supersaturated solid solution. Then the supersaturated solid solution is cooled to room temperature by fast cooling method, it's an unstable state, because of the state of high energy, the solute atoms will precipitate at any time. But the plasticity is very well so that it can be cold processed or used for straightening process.

(1) Online quenching

For some alloys, whose quenching sensitivity are not high, can be taken for the solid solution process with the high temperature during squeezing, and then air-cooled (T5) or water-cooled (T6) for quenching to obtain a certain microstructure and performance.

(2) Offline quenching

For some quenching sensitive alloy materials, they must be reheated to a higher temperature in a special heat treatment furnace and hold for a certain period of time, then transferred into the water or oil in 15 seconds for quenching to obtain a certain microstructure and performance. According to the difference of equipment, offline quenching can be divided into these categories, such as: salt bath quenching, air quenching, vertical quenching, horizontal quenching.

3. Aging: for the materials, which have been solution quenched, if located in room temperature or higher temperature environment for a period of time, the unstable supersaturated solid solution will decompose, and the second phase particles will

precipitate from the supersaturated solid solution (or precipitate), then distribute around the α (AL) aluminum grains, and result in strengthening effect, this effect is called precipitation (precipitation) strengthen.

(1) Natural aging: Some alloys (such as 2024, etc.) can produce precipitation strengthening effect at room temperature, which is called natural aging effect.

(2) Artificial aging: Some alloys (such as 7075, etc.) can not produce precipitation strengthen at room temperature obviously, but it is obvious at higher temperatures, which is known as artificial aging.

Artificial aging can be divided into under-aging and over-aging.

① Under- aging: In order to obtain a certain performance, control the lower aging temperature and hold for a shorter aging time.

② Over-aging: In order to obtain some special properties and better comprehensive performance, the aging process is carried out at a higher temperature or a longer holding time.

③ Multi-stage aging: In order to obtain some special properties and good comprehensive performance, the aging process is divided into several stages.

Such as two stages aging and three stages aging.

4. Regression treatment: In order to improve the plasticity, easy to cold forming or correct the geometric tolerance. For the products, which have been treated for quenching aging, when they are at high temperature and heated for a short time, they can reinstate to the state just after quenching. This phenomenon is called regression.

2.2 Diffusion equation

For the diffusion bonding process of magnesium alloy sheet and aluminium alloy sheet, the diffusion of element Mg and element Al between magnesium alloy sheet and aluminium alloy sheet have to be taken account. Diffusion phenomenon can be analyzed by **Fick's law**, which is shown in equation (2-2):

$$\frac{\partial C}{\partial t} = D \frac{\partial^2 C}{\partial x^2} \tag{2-2}$$

Where C is the concentration of element, and D is the Diffusion coefficient of

element,which represents the diffusion property of element [4]. In addition, generally speaking, the diffusion coefficient D is a function of element concentration， and the function is expressed as equation (2-3):

$$D = K_0 \exp(K_1 C) \tag{2-3}$$

Where K_0， K_1 are coefficient. Generally，if the variety of microstructure is ignored, The diffusion equation for element concentration C is displayed as equation (2-4):

$$\dot{C} = div(DgradC) \tag{2-4}$$

The boundary condition used for diffusion analysis is displayed as equation (2-5):

$$-D_c gradC \bullet \mathbf{n} = \beta_c (C - C_w) \tag{2-5}$$

Where β_c is the diffusion coefficient of surrounding gas etc, and C_w is the concentration of the surrounding element.

2.2.1 Diffusion analysis by finite element method

The diffusion equation is represented by equation (2-3) and (2-4). For diffusion analysis in coupled analyzes, as a boundary condition, the boundary penetration of elements on the surface of the continuum may be taken into consideration. The extent of element penetration at such boundaries is given in the form of the boundary penetration rate of the element defined as below.

$$q = D_s (C_e - C_s) \tag{2-6}$$

Where q is the amount of element entering from the interface, D_s is the boundary penetration rate of element, C_e is element concentration in external environment, and C_s is the element concentration on the surface of the object.

For the formulation of the diffusion analysis by the finite element method, the region V is first divided into a finite number of elements [5]. The element concentration C at any time t within each element is assumed as the product of the shape function $[N]$ and the element concentration Ce of the node, which is shown in below.

26

$$C = [N]\{C\}^e \qquad (2\text{-}7)$$

By using the principle of the weighted residual method, the residual errors of the element concentration approximated by the above equation and the true solution become zero in average for the concentration distribution of the chemical components in the region, so the element concentration at the node can be obtained by the following integral equation. That is to say, the weight function and the residual error are orthogonalized by the following equation.

$$\int_V W_i \left\{ \dot{C} - div(DgradC) \right\} dV + \int_{s_h} W_i \left\{ gradC \bullet \mathbf{n} + \beta_c (C)(C - C_w) \right\} ds = 0 \qquad (2\text{-}8)$$

Where the Galerkin method is applied to the above equation, That is to say, a shape function N_i is used as the weight function W_i. If the element concentration at the node is expressed as $C_j (j = 1 \cdots n)$, then the equation as follows can be obtained.

$$\sum_{j=1}^{N} \left\{ \left(\int_V D(C) gradN_i \bullet gradN_j dV + \int_{s_h} N_i \beta_c (C) N_j dV \right) C_j + \int_V N_i N_j dV \, \dot{C}_i \right\}$$
$$- \int_{s_h} N_i \beta_C (C) C_w ds = 0 \qquad (2\text{-}9)$$

When this formula is rewritten in matrix form, it becomes a simplified form as follows:

$$[H_c]\{C\} + [P_c]\{\dot{C}\} + \{Q_c\} = \{0\} \qquad (2\text{-}10)$$

Where the matrix and vector are represented as follows:

$$[H_c] = \sum [H_c]^e, \ [P_c] = \sum [P_c]^e, \ \{Q_c\} = \sum \{Q_c\}^e \qquad (2\text{-}11)$$

As the above, the diffusion equation for the entire region was obtained. The diffusion coefficient D included in this equation is dependent on the element concentration. Therefore, the matrix $[H_c]$, $[P_c]$, and $\{Q_c\}$ become the functions of element concentration.

Therefore, using the difference approximation method, equation (2-10) can be applied as follows. At first, Assuming that the change of element concentration C from time $t - \Delta t$ to t matches the primary function relationship, the following equation is

obtained.

$$\left\{\dot{C}\right\}_t = \frac{\left\{C\right\}_t - \left\{C\right\}_{t-\Delta t}}{\Delta t} \tag{2-12}$$

So the equation (2-12) can be represented as follows:

$$\left([H_c] + \frac{[P_c]}{\Delta t}\right)\{C\}_t = \frac{[P_c]}{\Delta t}\{C\}_{t-\Delta t} - \{Q_c\} \tag{2-13}$$

Where $\{C\}$ represents the vector of element concentration at time t. If the matrix $[H_c]$, $[P_c]$, and $\{Q_c\}$ approximately do not change from time $t - \Delta t$ to t, the results at time $t - \Delta t$ are $[H_c]_{t-\Delta t}$, $[P_c]_{t-\Delta t}$, and $\{Q_c\}_{t-\Delta t}$. So the equation (2-13) can be rewritten as follows:

$$\left([H_c]_{t-\Delta t} + \frac{[P_c]_{t-\Delta t}}{\Delta t}\right)\{C\}_t = \frac{[P_c]_{t-\Delta t}}{\Delta t}\{C\}_{t-\Delta t} - \{Q_c\}_{t-\Delta t} \tag{2-14}$$

Therefore, if $\{C\}$, $[H_c]$, $[P_c]$, and $\{Q_c\}$ at the previous time step are already known, it is possible to obtain $\{C\}$ at the subsequent stage from the above equation.

2.3 Calculation method of Mg/Al volume ratio in the intermetallic compounds

Definition：there are a substance which is constituted by element Mg and Al. The volume is V_0, and the unit is liter (L).

Atomic weight, volume, weight, mass, and relative atomic mass are represented by C, V, G, m and A_r. Avogadro's constant, atomic number, amount of substance and molar concentration are represented by NA, M, n and C_B. When 1 is attached to each symbol, it indicates each unit of Mg, in the conditon of attaching 2, it indicates each unit of Al. For example, the atomic weight of Al is C_1, the atomic weight of Al is C_2.

The atomic number ratio of Mg and Al is expressed by the following equation.

$$\frac{M_1}{M_2} = \frac{C_1 \cdot Ar_2}{C_2 \cdot Ar_1} \tag{2-15}$$

The molar concentration of Mg is written as the following equation.

$$C_{B1} = \frac{M_1}{V_0 \cdot N_A} \qquad (2\text{-}16)$$

The unit is mol/L.

The amount of substance of Mg can be represented as equation (2-17)

$$n_1 = \frac{G_1}{Ar_1 \cdot g} \qquad (2\text{-}17)$$

Where g is the gravitational acceleration. Because volume is the of amount of substance n and molar concentration C_B, so the volume of Mg can be expressed as equation (2-18).

$$V_1 = \frac{n_1}{C_{B1}} \qquad (2\text{-}18)$$

When take the equation (2-16) and (2-17) into equation (2-18), then the volume of Mg can be represented as the following equation.

$$V_1 = \frac{G_1 \cdot V_0 \cdot N_A}{C_1 \cdot g} \qquad (2\text{-}19)$$

Similarly, the volume of Al can be expressed as the equation (2-20).

$$V_2 = \frac{G_2 \cdot V_0 \cdot N_A}{C_2 \cdot g} \qquad (2\text{-}20)$$

Therefore, the volume ratio of Mg and Al in this substance is represented as equation (2-21).

$$\frac{V_1}{V_2} = \frac{G_1 \cdot C_2}{G_2 \cdot C_1} \qquad (2\text{-}21)$$

According to the quantitative analysis results of EDS, since the values of atomic weight C and weight G are known, so the ratio of the volume can be obtained.

2.4 Experiment on diffusion bonding of Mg/Al alloy

At first, the cast AZ31 magnesium alloy was cut together with 6061 aluminum alloy

sheets according to the size 50mm*12mm*2mm. Then the oxide layers on the surface of substrate were polished by using abrasive papers #400, and the ground samples were wiped with acetone before joining. After that, the materials were put into the furnace, then closed the door of the furnace.

The next work is to turn on the switch of the pump for vacuum. When the degree of vacuum reached -0.1MPa, turned off the switch, and at the same time, open the embolus of the argon gas cylinder and the intake valve to insert argon gas into the furnace until the barometer pointer turned back to 0. Then opened the exhaust valve.

The most important step is the set of temperatures and time for the diffusion joining process. According to the phase diagram (shown in Fig.2.1), the joining temperature was set at 440℃, and heating time is 10 minutes, holding time is 1 hour. After the temperature setting, turned on the power, the controller started to work, temperature increased gradually. After cooling down to room temperature in the furnace, specimens were successfully joined.
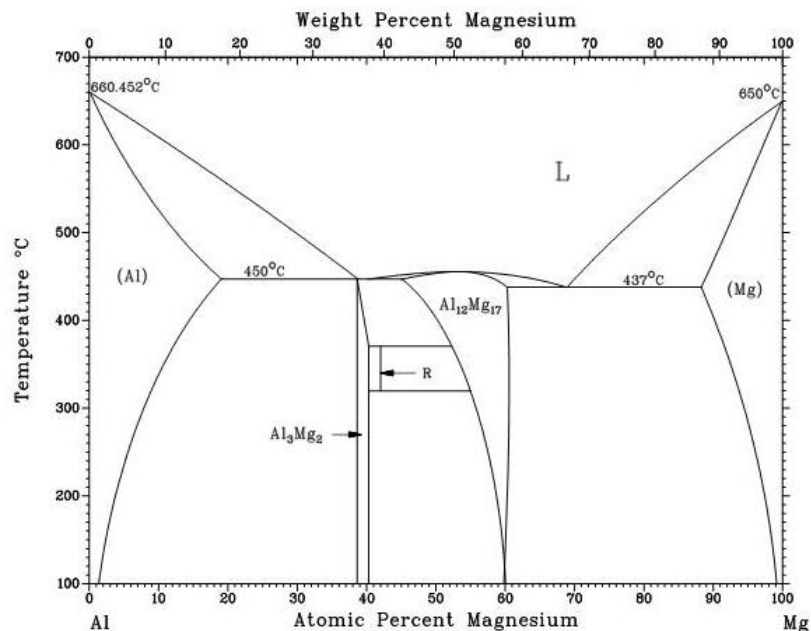
Fig.2.1 Phase diagram of magnesium alloy

2.5 Annealing process on diffusion bonded Mg/Al alloy

After the diffusion bonding experiment, in order to refine the microstructures and

improve the mechanical properties of bonding layers, the samples were used for the annealing treatment experiments. At first, turn on the switch of the pump for vacuum. When the degree of vacuum reached -0.1MPa, turned off the switch of pump, and at the same time, open the embolus of argon gas cylinder and intake valve to insert argon gas into the furnace until the barometer pointer turned back to 0. Then opened the exhaust valve.

The second step is to set the annealing temperatures and time for annealing treatment process. According to the phase diagram (shown in Fig.2.1), According to the Mg-Al phase graph and annealing experience. The heat treatment temperatures were set as 200℃, 225℃, 250℃, 275℃ and 300℃, and the holding time was 60min, heating rate is 42℃/min, holding time is 1 hour. After the temperature setting, turned on the power, then the controller started to work, and temperature increased gradually. After cooling down to room temperature in the furnace, the annealing were completed.

2.6 Evaluation on microstructure of the diffusion layers

For the purpose of studying the effect of annealing temperatures on the microstructures and properties of interfaces, a series of specimens that were treated at different conditions were cut crossing diffusion zone. Then inlaid the component containing diffusion layers into resin for making the specimens to investigate the microstructures. The sections were ground by the grinder with abrasive papers (GRIT 240, 600, 800, 1200). And polished with polishing compound until the microstructure of diffusion zone can be observed clearly. The microstructures and element distribution of the joints were studied respectively by SEM and EPMA. At last, the crystal index was investigated and identified with the usage of X-ray diffraction (XRD).

2.6.1 Investigation on microstructure with the applicaton of SEM

Temperature is the most important condition for heat treatment process, therefore, the microstructures of the bonding interfaces treated at different temperature were

observed. Firstly, the ground specimen inlaided in resin was set on the holder and put into the equipment for microstructure investigation. Secondly, waiting for a moment until the vacuum is ready. Then turn on the high voltage and increase the voltage from 1kv to 15 kv gradually. The third is to adjust the position of sample until it come into the visual area of the screen. The last step is to select the area which will be observed, and adjust the magnification, then scan the surface of sample and save the results. The specimens treated at different conditions were all observed.

The microstructures of joints annealed at 200℃, 225℃, 250℃, 275℃ and 300℃ are shown in Fig.2.2 (b), (c), (d), (e) and (f) respectively, While (a) shows the microstructures of joints without annealing treatment. It can be thought that the diffusion layers with heat treatment can be seen clearly including layer A, layer B, layer C shown in Fig.2.2 (a), (b), (c), (d), (e) and (f). What's more, it can be known that the width of diffusion layers increases with the increasing annealing temperatures. That is because diffusion rate turns faster with the increasing temperatures.

| (a) Without annealing | (b) 200℃ |

32

| (c) 225℃ | (d) 250℃ |
| (e) 275℃ | (f) 300℃ |
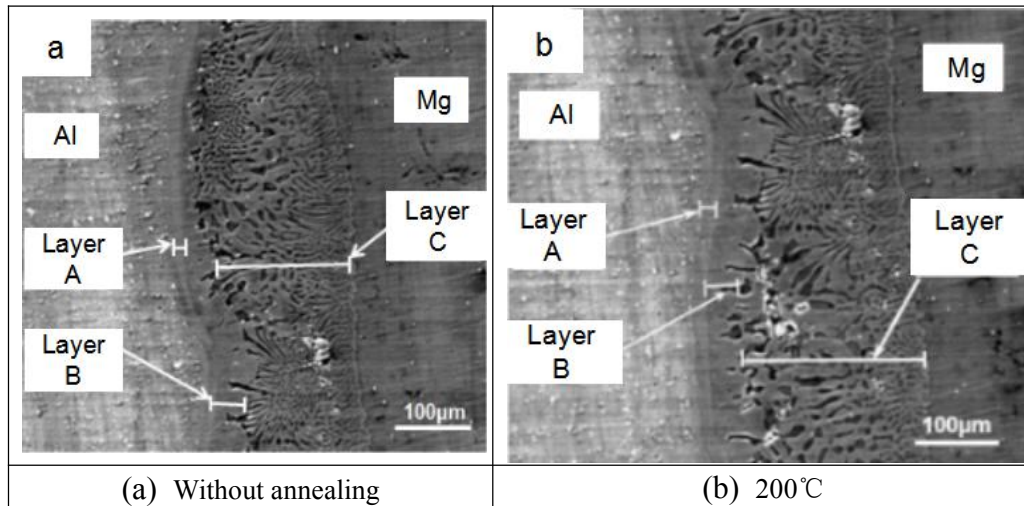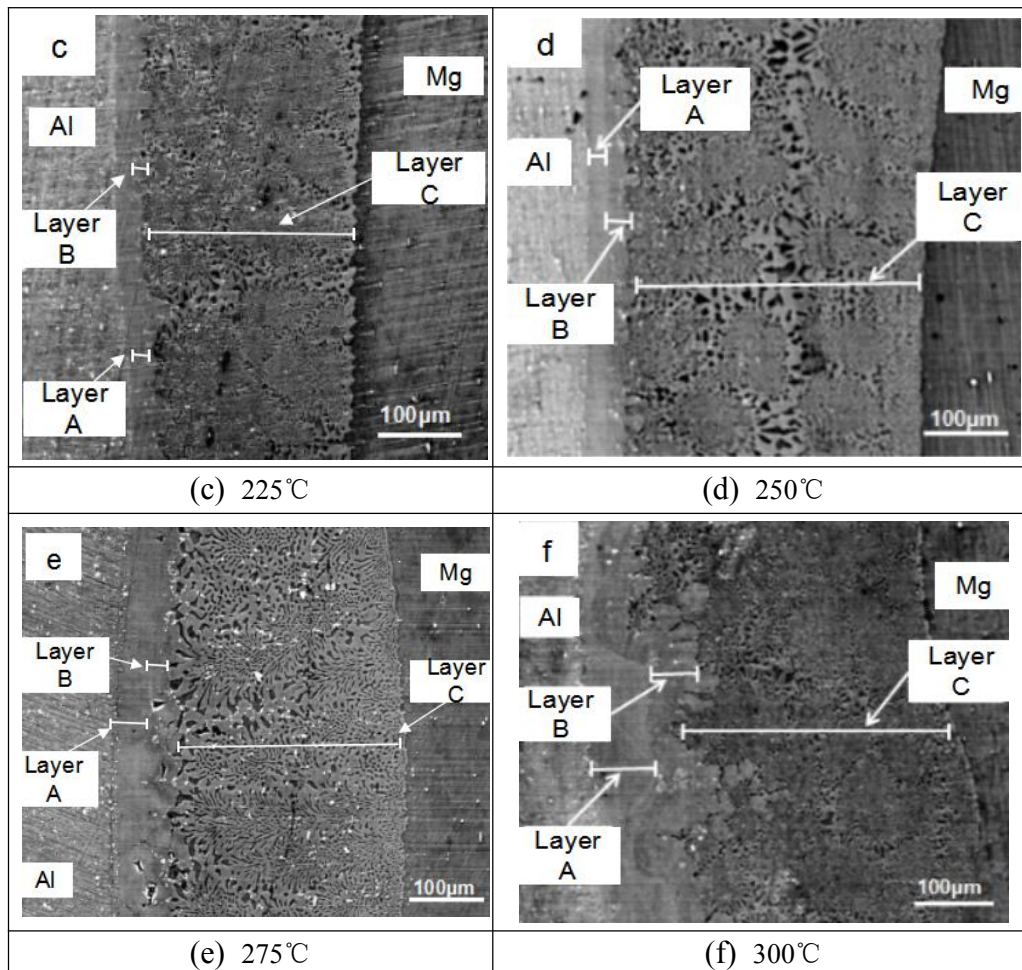
Fig.2.2 The microstructure of the diffusion zone

2.6.2 Analysis of element distribution based on EPMA

The element analysis was carried out with the application of EPMA. Cooling water and protection gas need to be applied before the equipment was started. At first, the specimens were stuck with conductive tape respectively, and put into the different position of the holder. Secondly, the holder was put into the device called EPMA, then wait for about 30 minutes until the vacuum state is ready. The third step is to open the electronic optical system, add the high voltage and adjust the magnitude of the current to 10^{-9}, then select the position of sample, and adjust the focus, contrast and brightness until the clear optical image and SEM image can be observed. The next step is to set the scanning range as 400μm*400μm. Based on confirming the electronic optical conditions, the scan was started. When the scan on one sample was over, save the results of element analysis, then change the observing place for the

analysis of another specimen. At last, the specimens without annealing, annealed at 200℃, 225℃, 250℃, 275℃ and 300℃ were all analyzed.

After the data processing, the results of element analysis are shown in the Figs from Fig.2.3 to Fig.2.8. According to the results, it can be thought that the diffusion layers can be seen clearly. The different colors stand for the quantities of elements that were detected. The quantities increase with the change of colors from black to white. For example, as it is shown on the left side of Fig.2.6. it's the analysis result of Mg element.

The pink zone is the side of magnesium alloy, the black zone is Al alloy. The blue and green zone is the diffusion layer near Al side, the area between pink zone and green zone is the diffusion layer near Mg side. The quantify of magnesium element decrease along the direction from Mg alloy to Al alloy, while the quantify of Al element changes contrary with Mg element in the same direction.
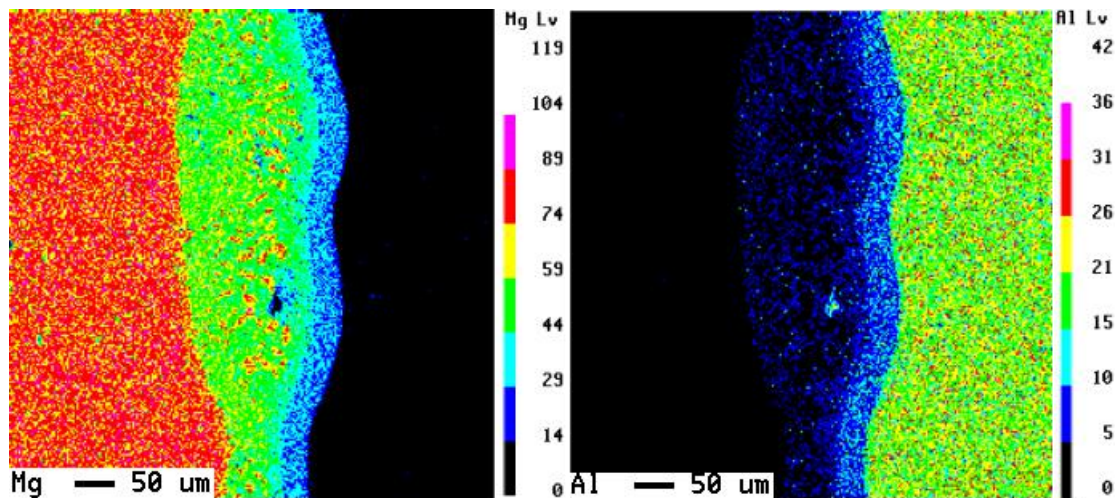
Fig.2.3 The distribution of element under the condition of annealing absence
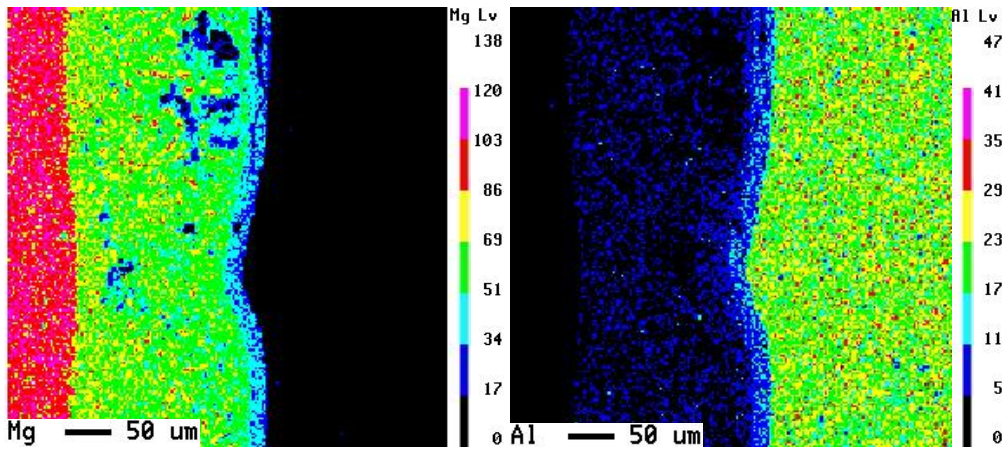
Fig.2.4 The result of surface scan for element analysis (annealing at 200℃)
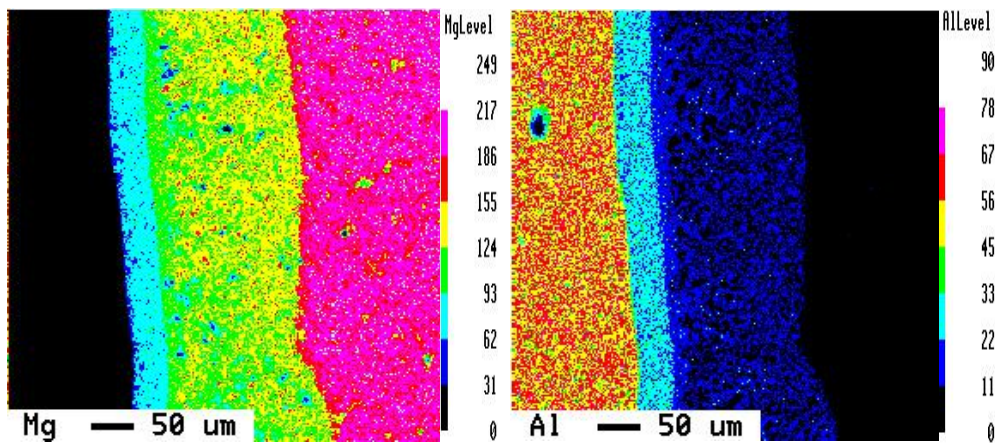
Fig.2.5 The investigation on element distribution after annealing at 225℃
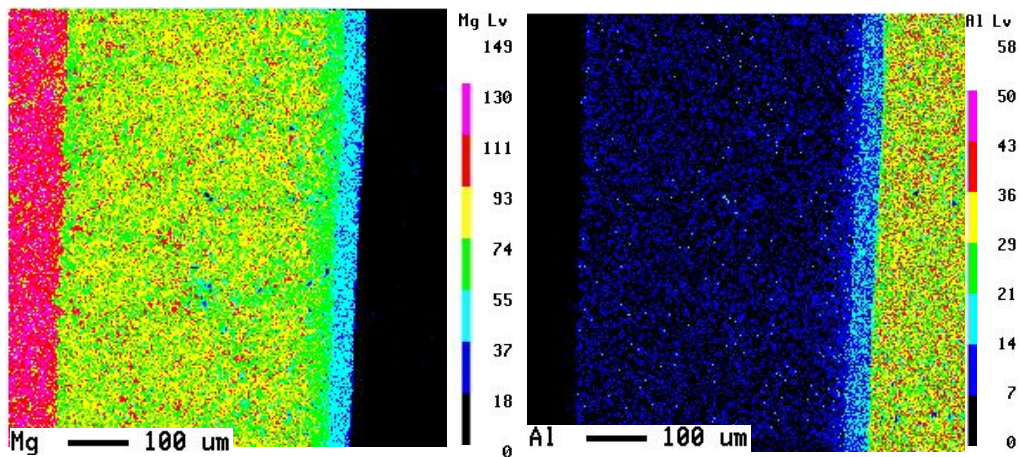
Fig.2.6 The analysis on element distribution in diffusion zone (annealing at 250℃)
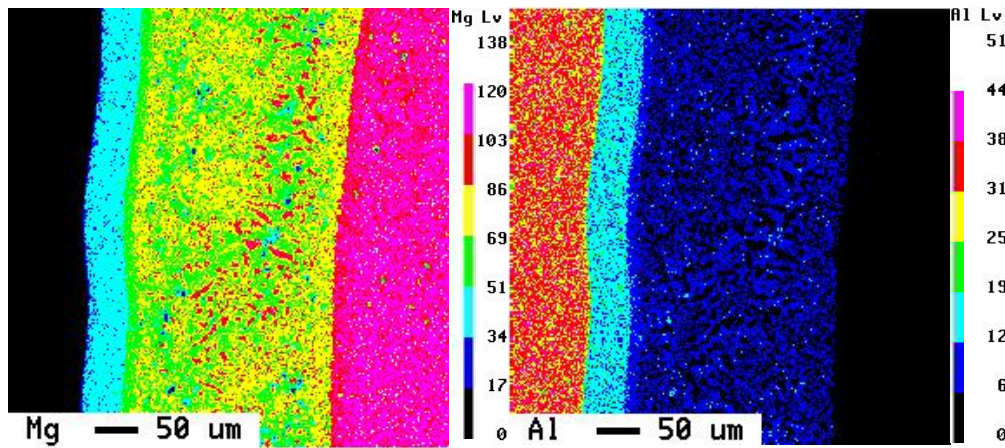
Fig.2.7 The element distribution in diffusion layers of specimen annealed at 275℃
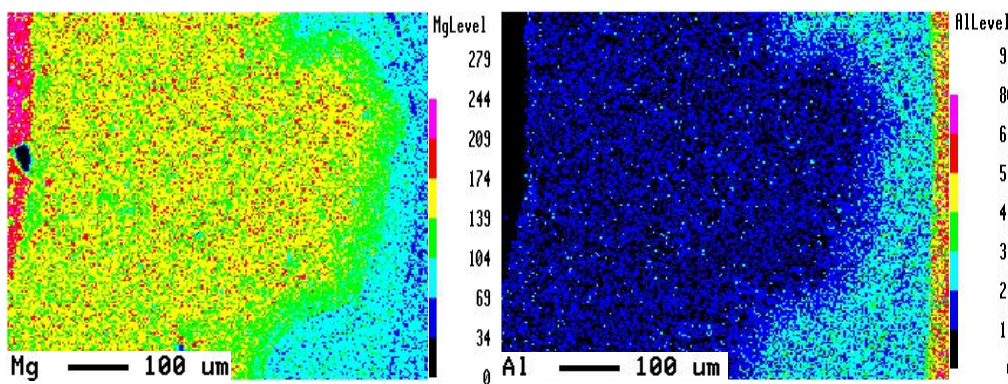
Fig.2.8 The result of surface scan on element detection (annealing at 300℃)

The results of line scanning is shown in Fig.2.9. It can be seen that the diffusion layers widen with the increase of heat treatment temperature. The contents of magnesium element and aluminum element vary with the range of temperatures. when without annealing, The width of diffusion layer is approximately 0.15mm. The width of diffusion layer of the specimen with heat treatment at 200℃ is about 0.18mm. In the case of annealing at 225℃, the width of diffusion zone is 0.29mm. In the condition of 275℃, the width of diffusion layer is about 0.44mm. However, when treated at 300℃, The thickness of diffusion layer is about 0.46mm. The result after treated at 250℃ is shown in Fig.2.9 (d). The width of diffusion layer is approximately 0.42mm. The reason for the variation of diffusion layers' width is the diversity of annealing temperature. Diffusion rates of elements increase with the increasing temperatures, therefore, diffusion layers are the widest when annealed at 300℃.

36
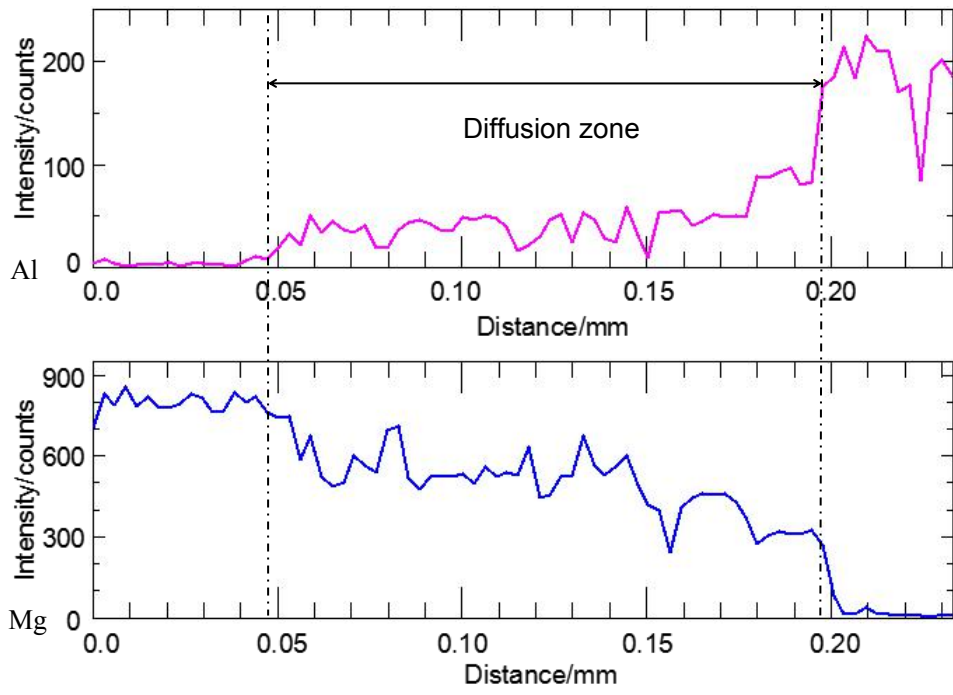
(a)
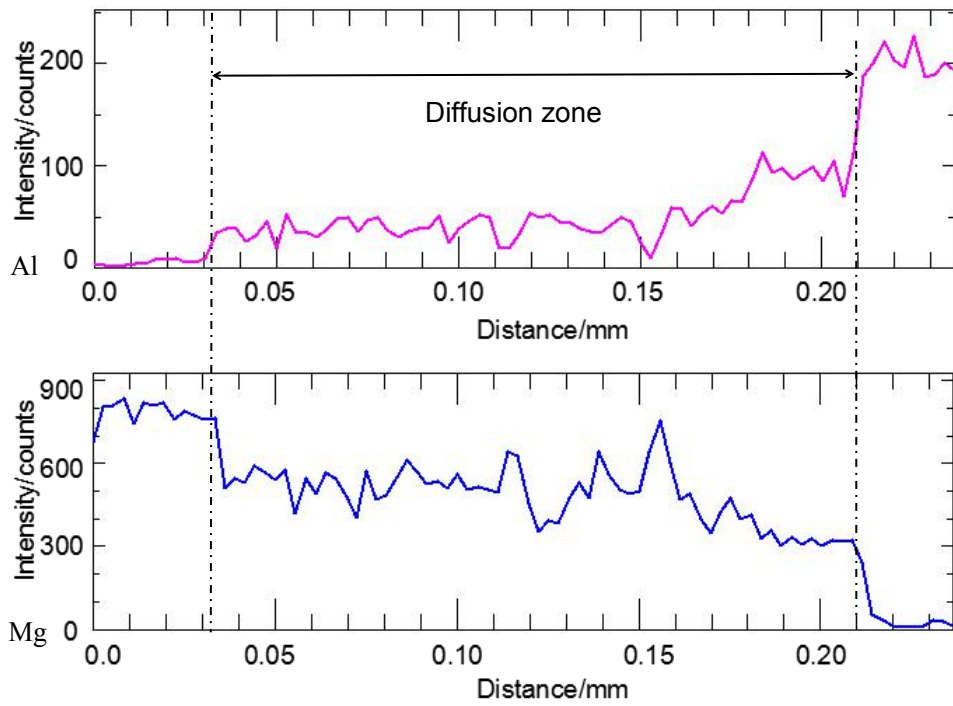
(b)
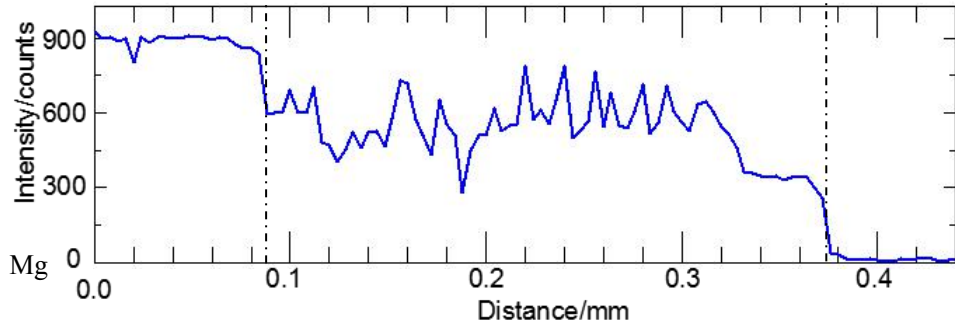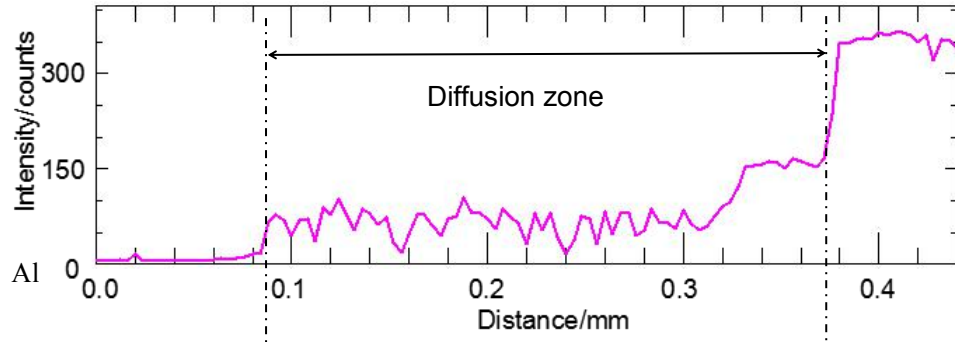
(c)
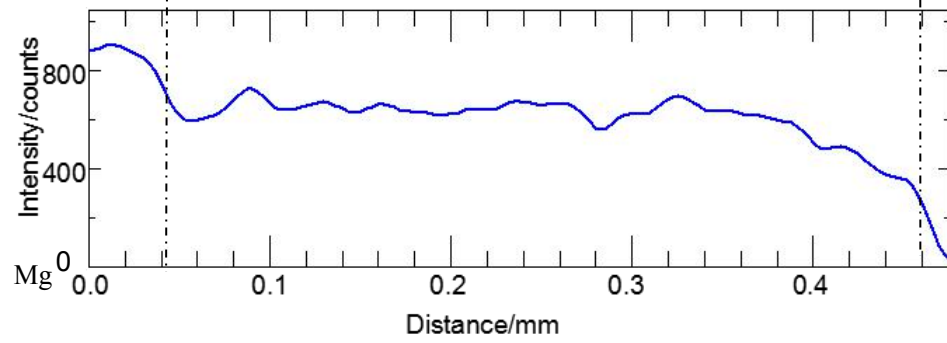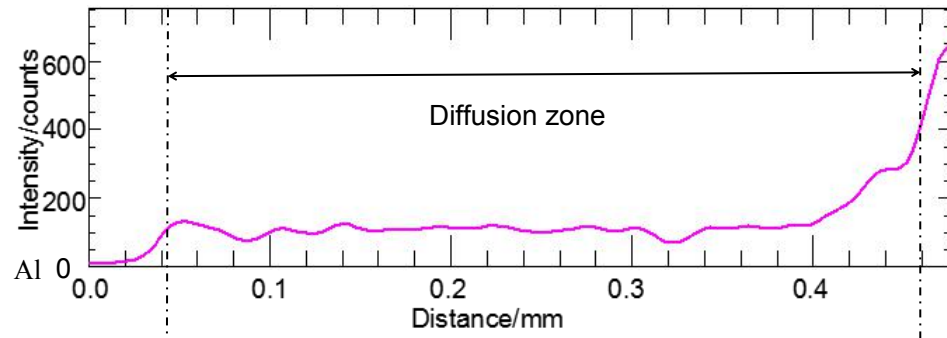
(d)
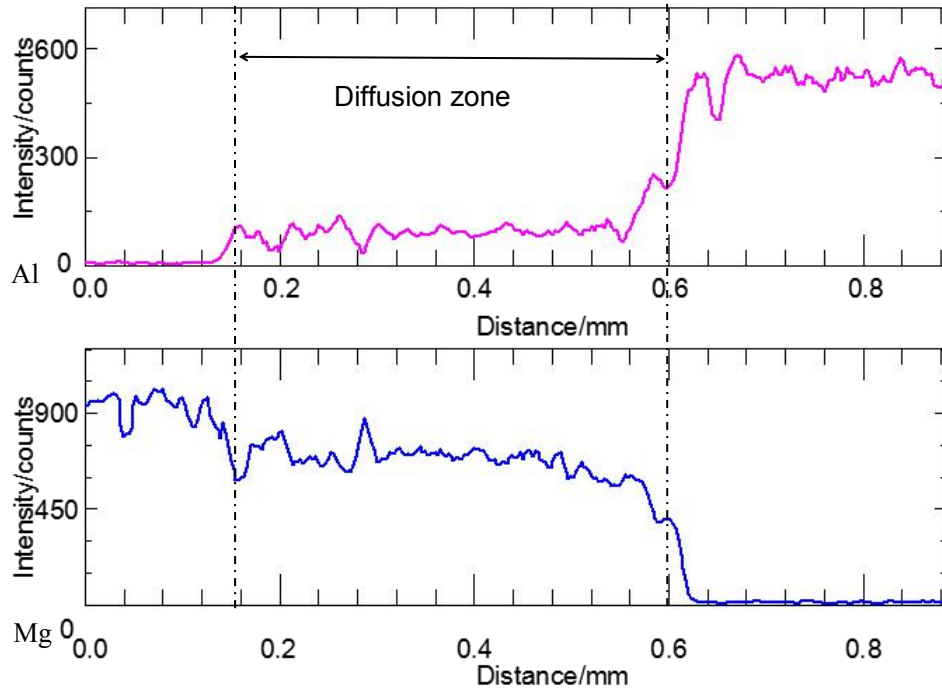
(e)
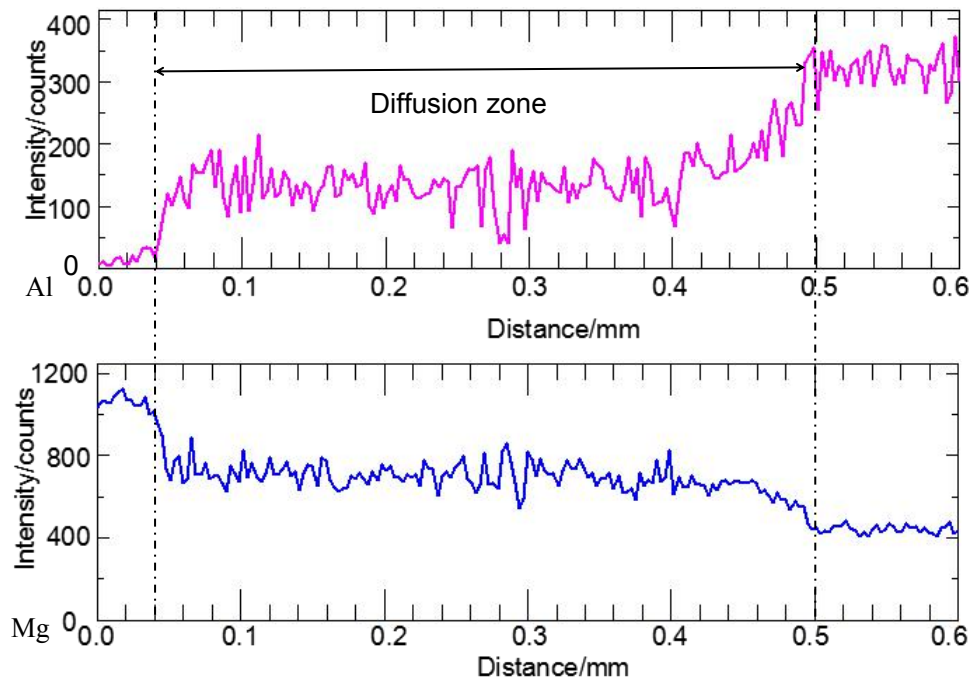
(f)

Fig.2.9 Line scan of element distribution (a) without annealing (b) annealing at 200℃ (c) annealing temperature: 225℃ (d) the specimen annealed at 250℃ (e) under the annealing condition of 275℃ (f) in the case of 300℃

It can be got from the results of scanning for element distribution(from Fig.2.3 to

Fig.2.8) that quantity of elements after annealed at 250℃ are steady. It indicates that the distribution of elements are relatively uniform. That is to say the microstructure is more uniform.

2.6.3 Analysis and identification of crystal structure by XRD

For the purpose of analyzing and identifying the crystal structure about crystal structure, the investigation of the diffusion bonded specimens with the usage of XRD was carried out. The results were shown in the following Figs. Fig.2.10 shows the investigating result of Mg side. The investigating results of the diffusion layers, such as the layer near Mg, the middle layer and the layer near Al were shown in Fig.2.11, Fig.2.12, and Fig.2.13 respectively. In addition, the investigating result of Al side was shown in Fig.2.14. It can be obtained from the results above that the diffraction peak of Mg occurred at the place of 2θ 67.3° and 72.5°. The peak of the diffusion layer which was near Mg was at the place of 2θ 69.7°. The diffraction peaks of the middle diffusion layer appeared at 2θ of 77.5°, 77.8°, and 77.9°. In the case of the diffusion layer near Al, 2θ were 64.5° and 64.7° where the diffraction peaks appeared. In the condition of Al. the locations of peaks were 37.9°, 44.2° and 81°.
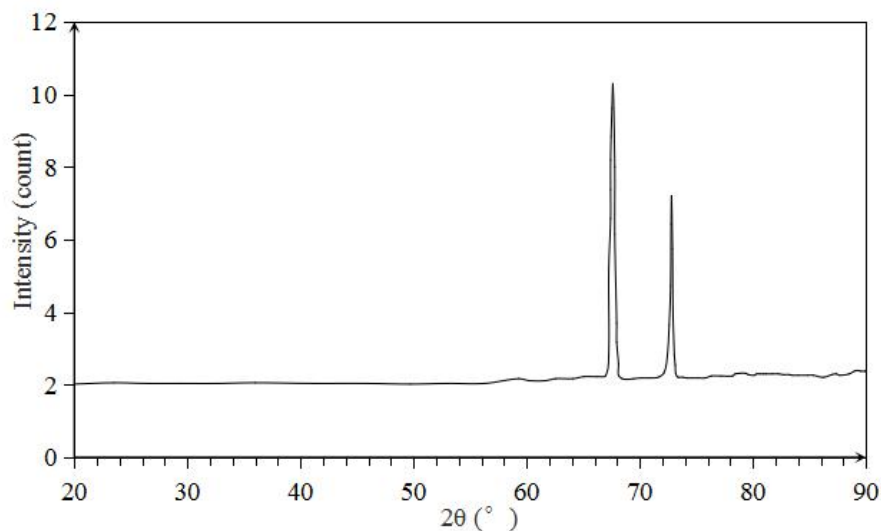
Fig.2.10 The diffraction diagram of Mg side
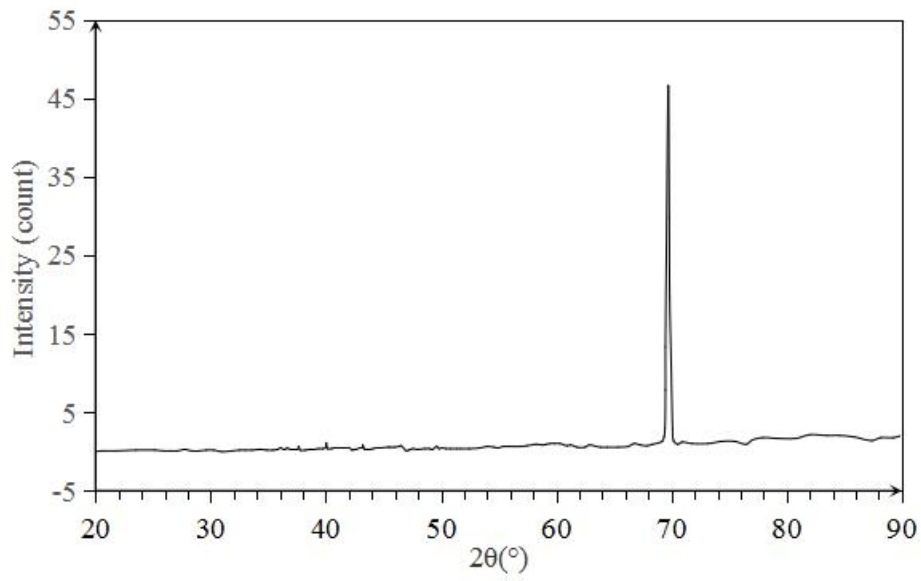
Fig.2.11 The result on XRD of the diffusion layer near Mg side
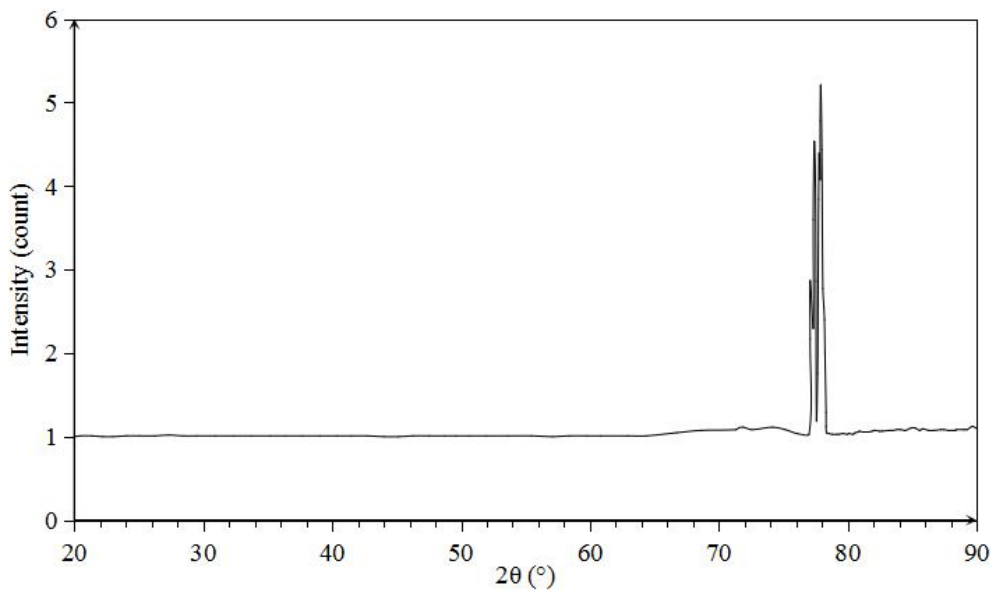
Fig.2.12 The investigation result of the middle diffusion layer
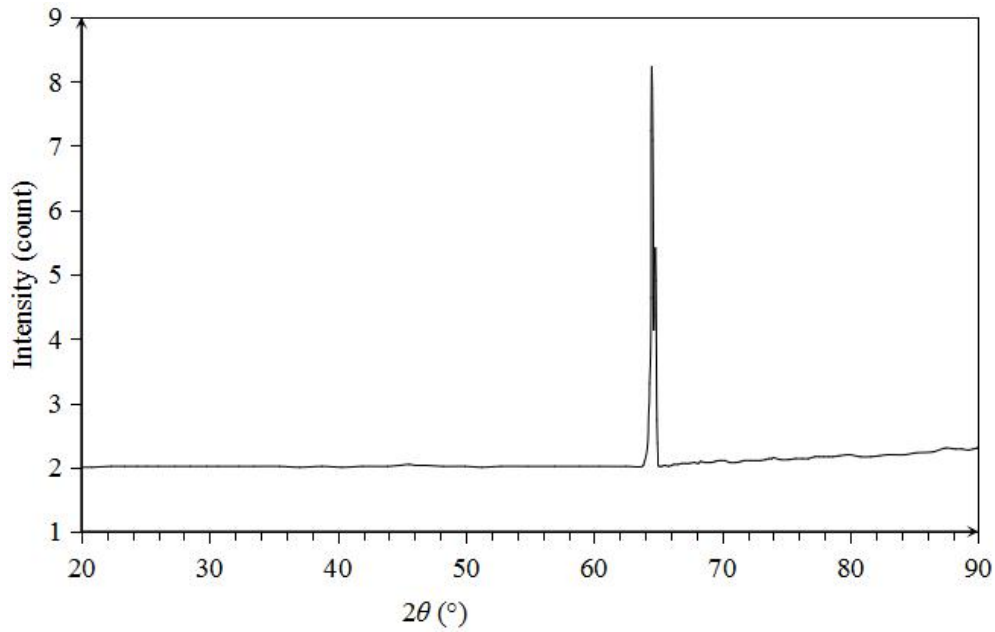
Fig.2.13 The diffraction peak of the diffusion layer near Al side
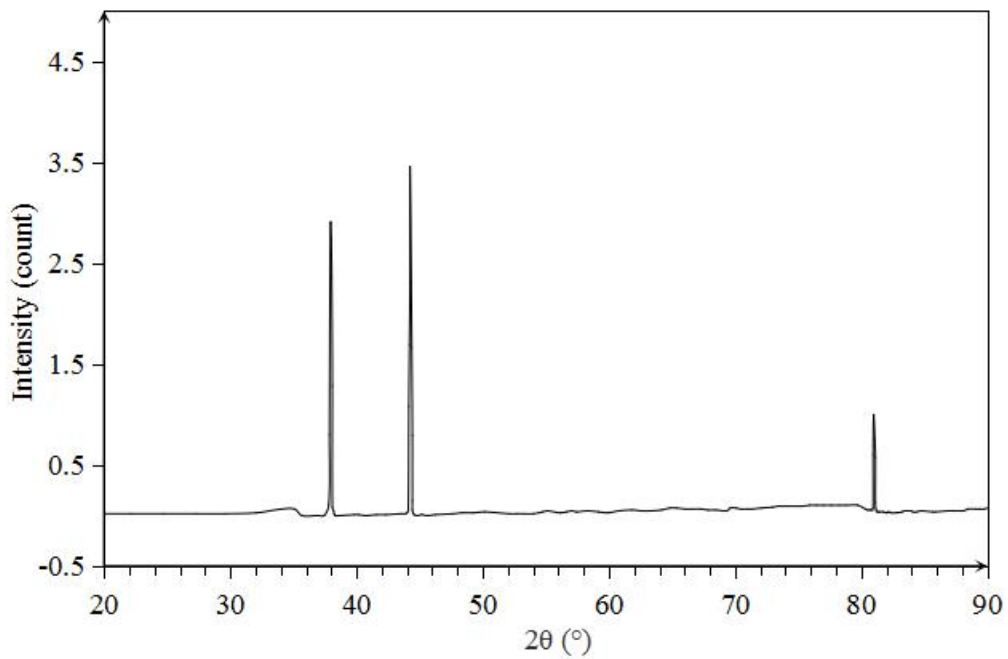
Fig.2.14 The diffraction diagram on Al side of specimen

The results of identification of Al and Mg were shown in Fig.2.15 and 2.16. As the diffraction peaks of Al appeared when 2θ were $37.9°$, $44.2°$, and $81°$, so it can be identified that the planes of Al were (111), (200), and (222).
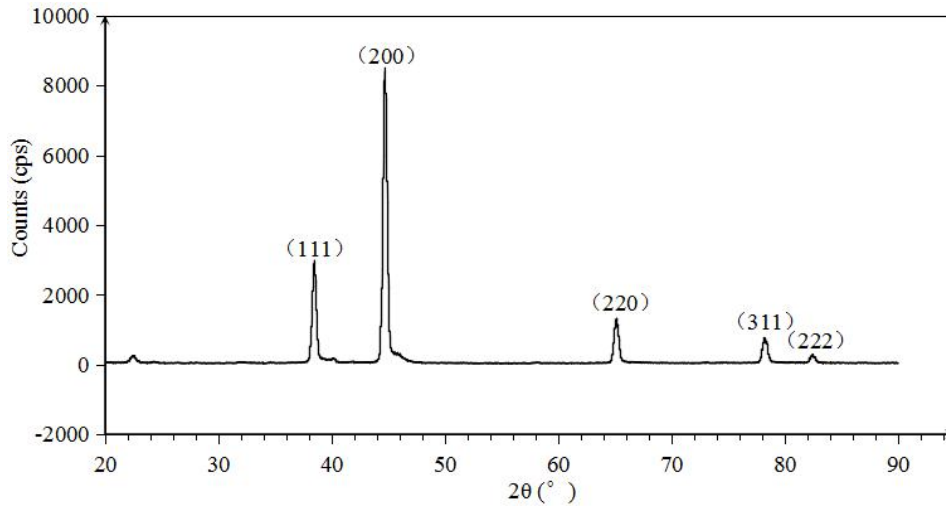
Fig.2.15 The result on x-ray diffraction of Al

In the case of Mg, the diffraction peaks at the place where 2θ were 67° and 72.8° stood for the planes whose plane indexes were (200) and (004).
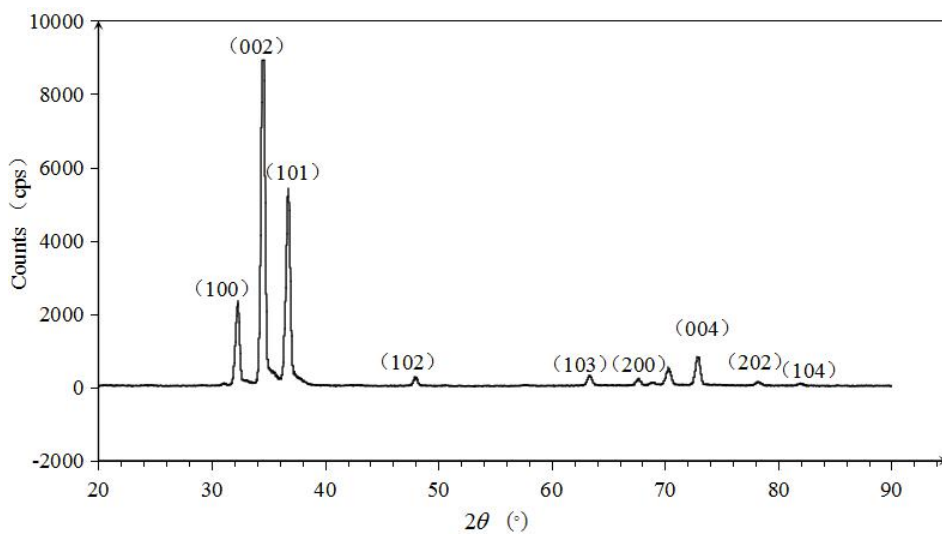
Fig.2.16 The measurement result based on XRD for identification of Mg

2.6.4 Study on crystal structure with the usage of TEM

In this chapter, in order to study the crystal structure of diffusion zone further. The equipment of Transmission Electron Microscope (TEM) was applied. Before the experiment of TEM, the sample for investigation was prepared. At fist, the thickness of the bonded sheet was about 3mm, then the sample was ground to about 10 μm by

using the grinder with abrasive papers, in addition, the sample was processed to about 0.1μm by fine finishing with the application of Focussed Ion Beam Scanning Electron Microscopes (FIB-SEM). The result was shown in Fig.2.17.
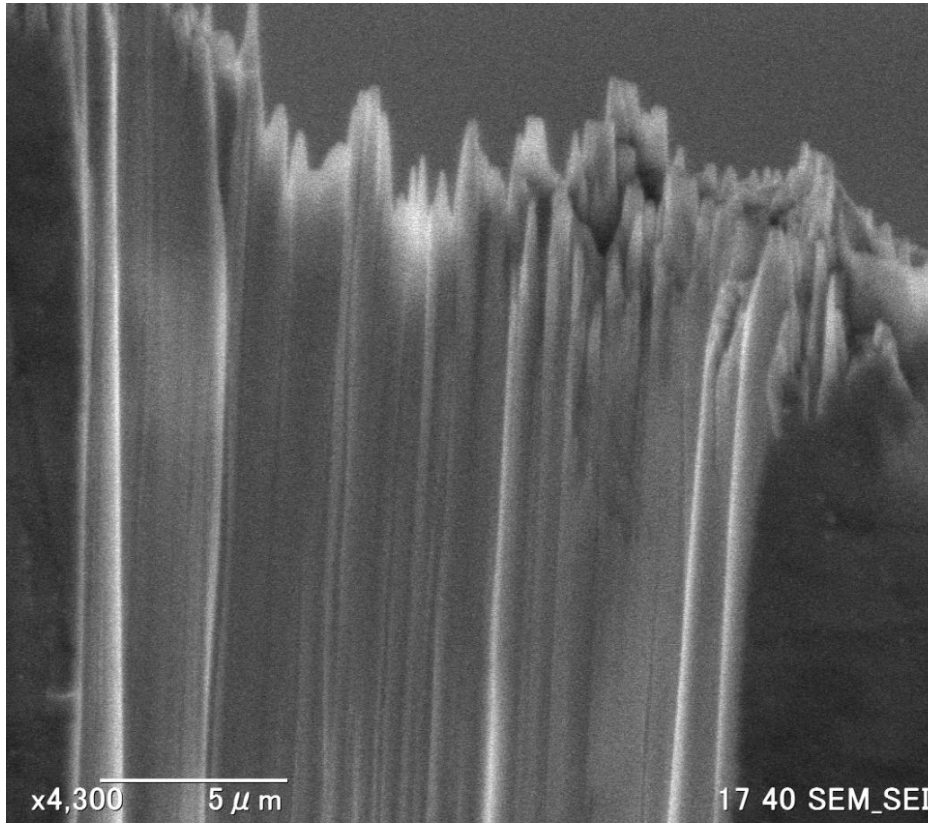
Fig.2.17 The image of the sample after FIB process

It can be seen from Fig.2.17 that the width of the processed section decreased gradually with the increasing number of processes. Actually, the width was 20μm in the fist process, and 6μm in the last process.

After the investigation performed by TEM,The results were shown in following Figs. Fig.2.18 was the microstructure of the investigated location A, and Fig.2.19 and Fig.2.20 were the investigation results of location A. what's more, Fig.2.22 and Fig.2.24 were the results of location B and C. Then the interplanar spacing and plane index and can be identified according to the results of calculation based on the diffraction images obtained with the usage of TEM.
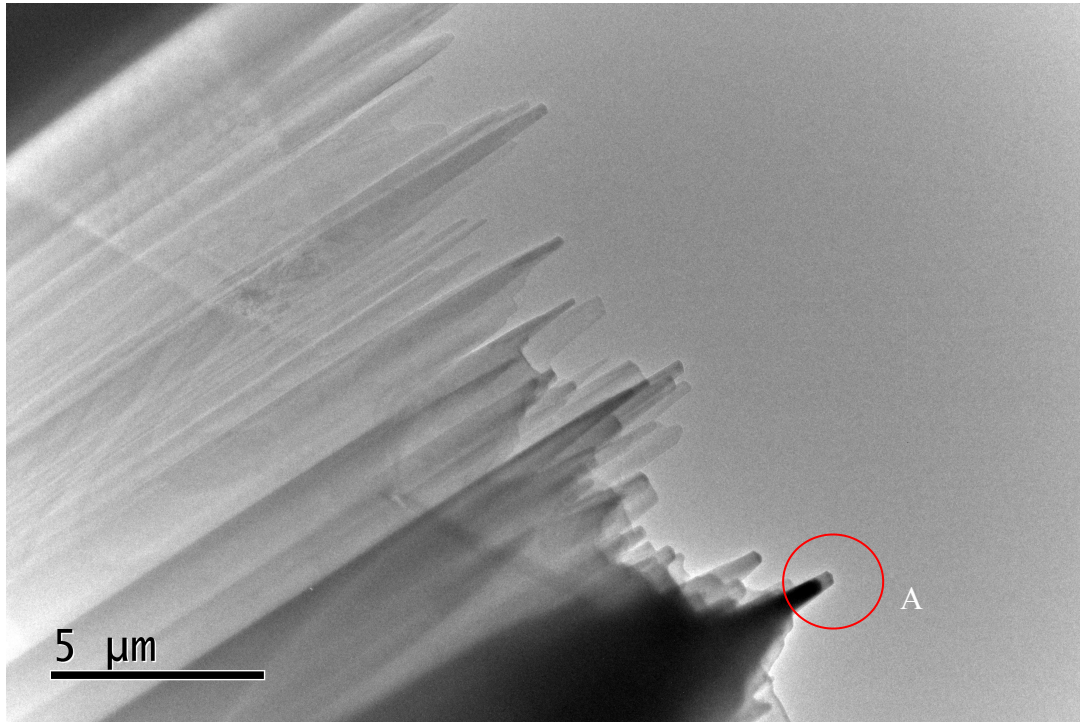
Fig.2.18 The microstructure of workpiece for investigation
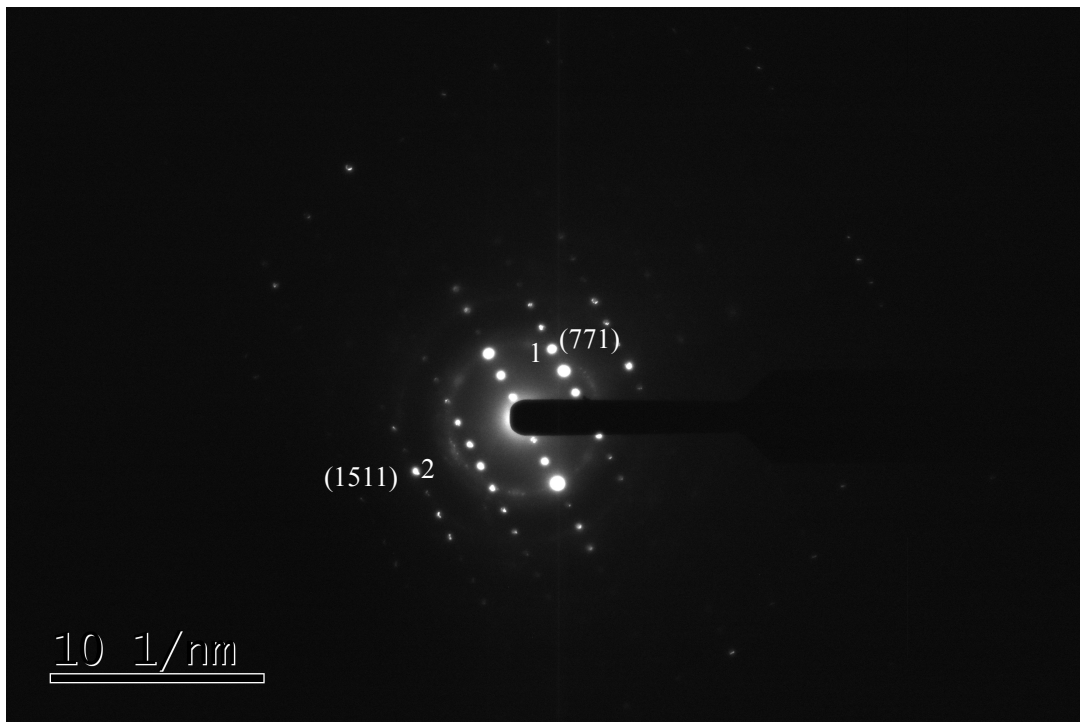
Fig.2.19 The diffraction pattern of specimen

According to the scale in Fig.2.19, and the measurement of the distance to the center, the actual interplanar spacing was calculated, after compared with the database, the

conclusion was obtained that d_1 is 0.283nm, d_2 is 0.187nm. The results indicated the (771) and (1511) planes of Al_3Mg_2.
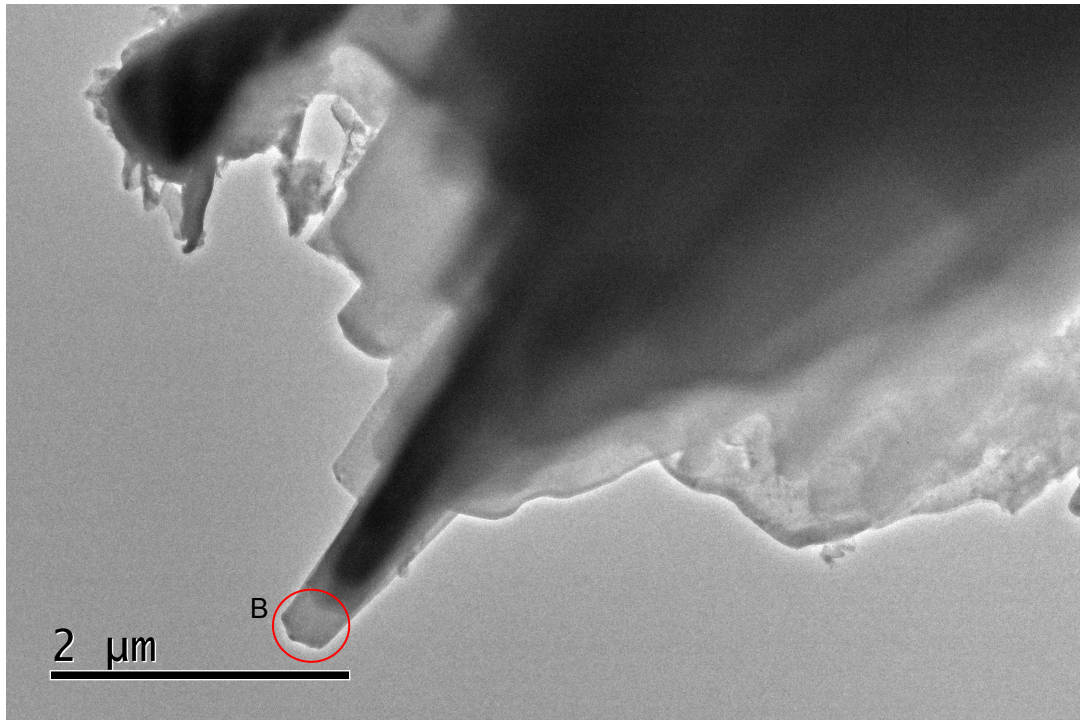
Fig.2.20 Microstructure of the specimen for crystal structure analysis
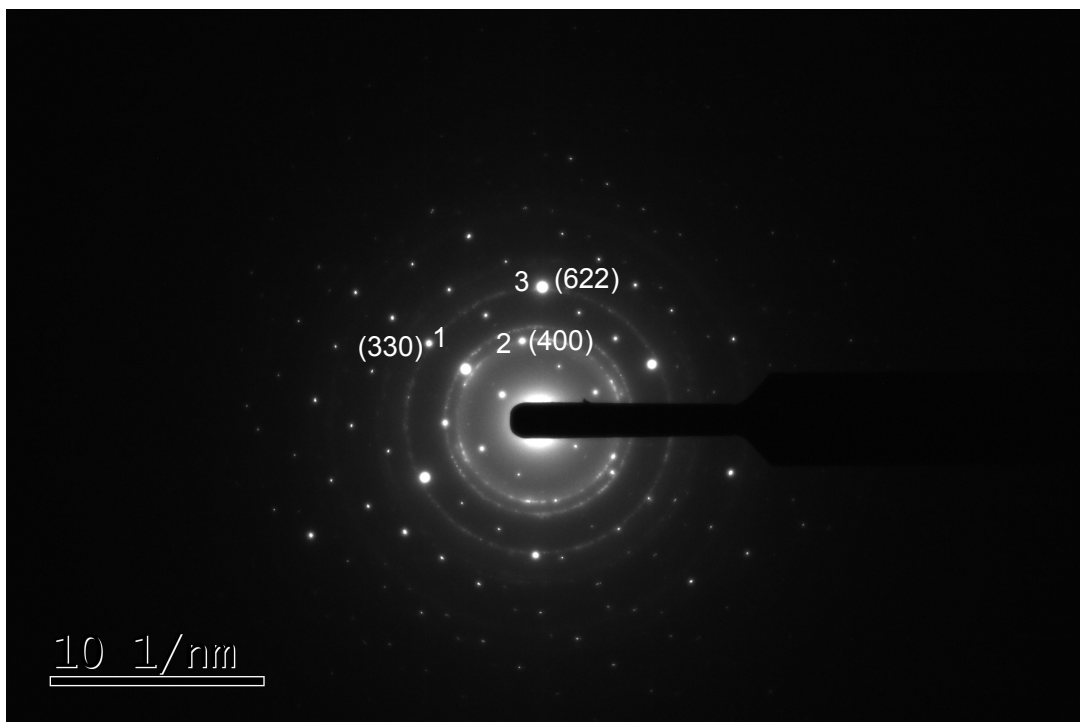
Fig.2.21 The diffraction image obtained from TEM observation

Based on the scale in Fig.2.21, and the distance to the center. The interplanar spacing can be calculated. Therefore, the plane index can be confirmed by referring to the database. The interplanar spacing d_1, d_2 ,d_3 are respectively 0.2480nm, 0.2640nm, 0.1600nm. So the corresponding plane index are (330), (400), and (622) of $Al_{12}Mg_{17}$.
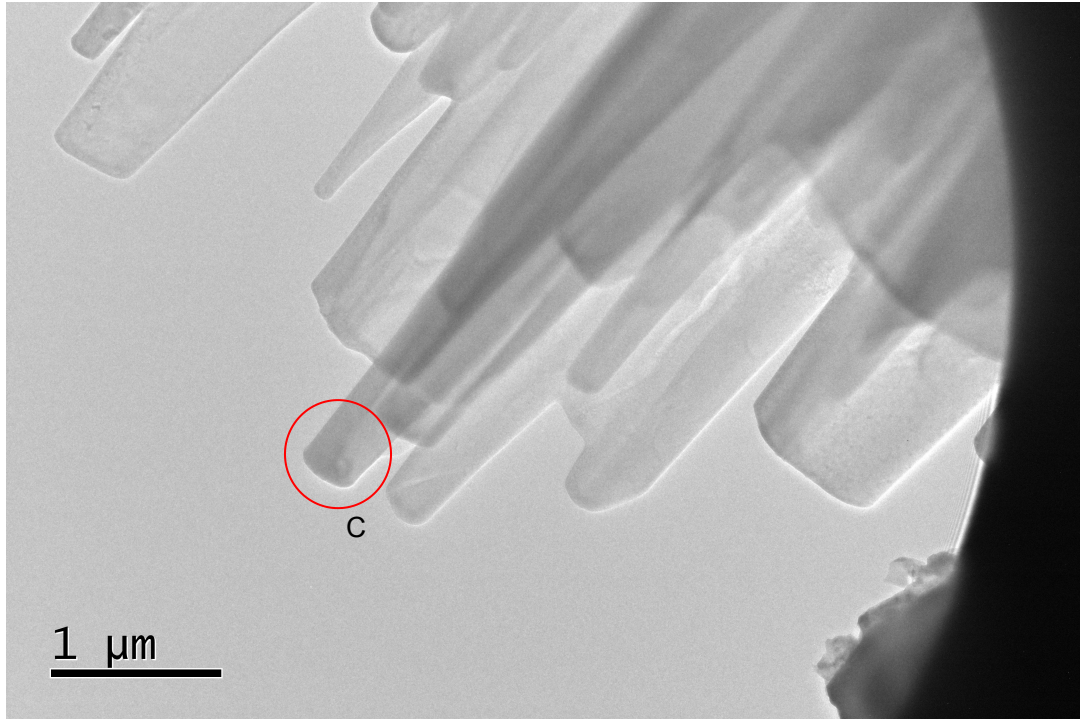
Fig.2.22 The micrograph of the sample for TEM experiment
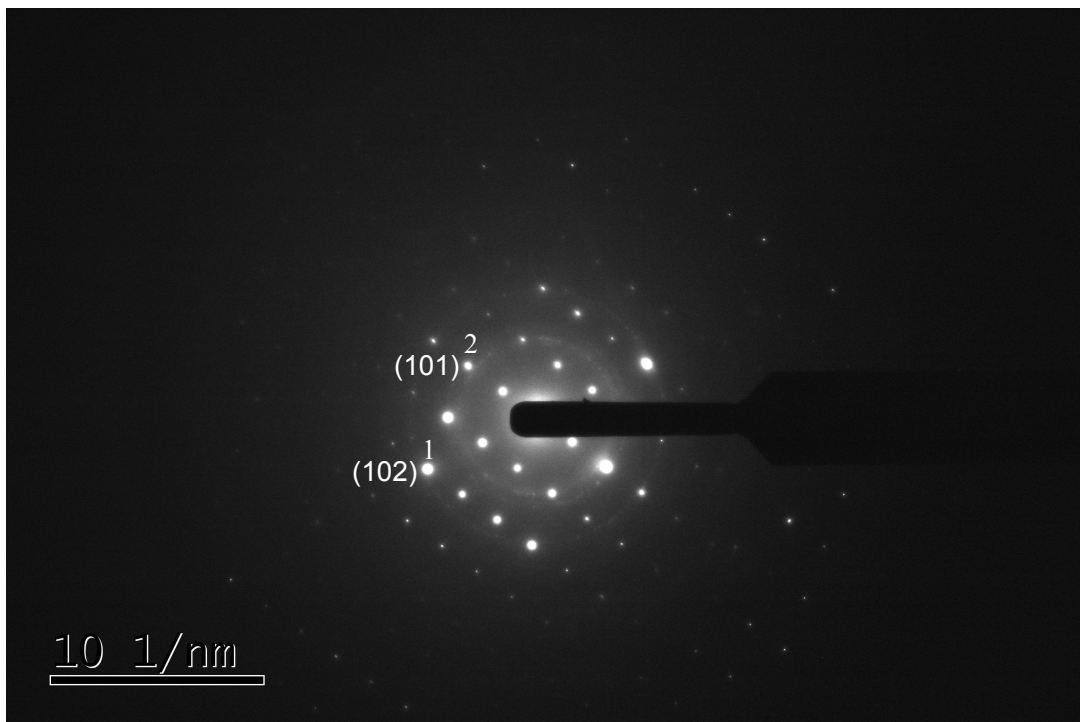
Fig.2.23 The diffraction spots for the analysis of crystal structure

For the analysis of Fig.2.23, according to the distance from the diffraction spots to the center and the scale of Fig.2.23, the interplanar spacing were calculated. After referring to the database, the planes index can be obtained. The interplanar spacing were $d_1=0.1902nm$, $d_2=0.2452nm$, and the corresponding planes index were (102) and (101) of Mg.

2.7 Evaluation on mechanical behaviors of diffusion bonded composite material

2.7.1 Evaluation methods of residual stress

Residual stresses are stresses that remain in a solid material after the original cause of the stresses has been removed. Residual stresses can also be defined as the stresses that remain within a material or body after manufacture and material processing in the absence of external forces or thermal gradients. They can also be produced by service loading, leading to inhomogeneous plastic deformation in the part or specimen [6]. Accordingly, residual stresses are not caused by loads (forces or moments). Residual stress may be desirable or undesirable. For example, laser peening imparts deep beneficial compressive residual stresses into metal components such as turbine engine fan blades, and it is used in toughened glass to allow for large, thin, crack- and scratch-resistant glass displays on smartphones. However, unintended residual stress in a designed structure may cause it to fail prematurely.

Residual stresses can occur through a variety of mechanisms including inelastic (plastic) deformations, temperature gradients or phase transformation. Heat from welding may cause localized expansion, which is taken up during welding by either the molten metal or the placement of parts being welded. When the finished weldment cools, some areas cool and contract more than others, leaving residual stresses. Another example occurs during semiconductor fabrication and

microsystem fabrication [7] when thin film materials with different thermal and

crystalline properties are deposited sequentially under different process conditions. The stress variation through a stack of thin film materials can be very complex and can vary between compressive and tensile stresses from layer to layer.

During the process of usage, residual stress will superimpose with the working stress caused by other loads, and result in secondary deformation and residual stress redistribution of component. Not only will the stiffness and stability of the structure be reduced, but also under the combined action of temperature and medium, it will seriously affect the structural fatigue strength, brittle fracture resistance, resistance to stress corrosion cracking and high temperature creep cracking [8,9].

The effect to stiffness of the structure:

When the stress δ resulted from external load superimposes with the residual stress in some place of the component, and reaches the yield point, The material in this area will have partial plastic deformation，so that the material will lost the ability to bear the further load，and the effective cross-sectional area of the structure will be reduced, the stiffness of the structure will also be reduced. When there are longitudinal and transverse welds in the component, or be treated for flame correction, It is possible to produce residual tensile stress on a larger cross-section. Although the stress distribution in the direction of length is not too large, but they still have a greater impact on the stiffness. For the structures that require higher dimensional accuracy and stability, the effect can not be ignored.

The impact on stability of rod parts:

When the compressive stress that is caused by external load superimposes with residual compressive stress, and reached yield point, this part of the section will lost the ability to withstand more external load. The effective cross-sectional area of the rod is reduced.Then the stiffness will decrease, and the stable bearing capacity will also decrease. So the influence of residual stress on the stable bearing capacity of bar is related to the distribution of residual stress.

Residual stress is an unstable state of stress. When the component is impacted by other factors, such as external force and temperature, due to the interaction between the applied stress and the residual stress, make the parts occur partially plastic

deformation, and the residual stress in the cross-section will redistribute. When the external factors are removed, deformation will occur in the entire component. During the usage of components, the relaxation residual stress will occurs, so the residual stress affects the stability of the components. This is one of the most concerned issues for the engineering department.

The effect of residual stress on the deformation of component includes two aspects: the one is the ability of the component to resist the deformation resulted from static and dynamic load; the other is the ability to recover the deformation after unloading. The effect of residual stresses on the components in these two aspects is significant, so the effective ways to eliminate this effect is studied.

Recent years, there are many methods for investigating the residual stresses have been studied. According to whether the component is destroyed completely or partially, the techniques can be classified as destructive, semi destructive and non-destructive as shown in Table 2.1. The destructive and semi destructive method are also called mechanical method, depending on deducing the original stress, according to the displacement incurred by completely or partially relieving the stress by removing material. These methods rely on the measurement of deformations due to the release of residual stresses upon removal of material from the specimen. Sectioning, contour, hole-drilling, ring-core and deep-hole are the principals destructive and semi destructive techniques used to measure residual stresses in structural members. Non-destructive methods include X-ray or neutron diffraction, ultrasonic methods and magnetic methods. These techniques usually measure some parameter that is related to the stress.

Table 2.1 The techniques for residual stress measurement

Techniques for residual stress measurement		
Non destructive	Semi destructive	Destructive
Barkhausen noise method	Hole-drilling technique	Sectioning
X-ray diffraction method	Ring-core method	technique
Neutron diffraction method	Deep-hole method	Contour
Ultrasonic method		method

Hole-drilling technique

The hole-drilling method is simple; it is one of the most popularly used semi destructive methods for residual stress evaluation which can provide the measurement of residual stress distribution across the thickness in magnitude, direction and sense. The damage caused to the specimen is   limited to the small, drilled hole, and is often tolerable or repairable [10]. Due to drilling the hole, residual stresses can be relieved and the corresponding strains on the surface can be measured [11]. Based on the strains measured around the hole, the residual stresses can be calculated using appropriate calibration constants [12].

The ring-core method

The ring-core method is an "inside-out" variant of the hole-drilling method [13]. The ring core method can measure stress based on measuring the deformation in a central area caused by the cutting of an annular slot in the surrounding material. Compared with the hole-drilling method, the ring-core method has a basic implementation to evaluate in-plane stresses [14,15]. The ring-core method has an advantage over the hole-drilling method that it provides much larger surface strains. However, the ring-core method is less frequently used for the reason of greater specimen damage and less convenient, .

Deep hole method

The deep hole method is also semi destructive methods for residual stress evaluation, and it is a further variant procedure that combines elements of both the hole-drilling

and ring-core methods [16,17]. A hole is first drilled through the workpiece. Then the diameter of the hole can be measured accurately and then a core of material around the hole is taken out, so that the residual stresses in the core is relaxed. Finally the residual stresses can be calculated from the change in diameter of the hole. The the residual stress will be calculated with appropriate calibration constants.

Sectioning technique

The Sectioning technique is a destructive method that relies on measuring the deformation due to the release of residual stress by removing material from the sample [18,19]. It has been widely used to analyze the residual stresses in structural carbon steel, aluminum and stainless steel sections [20-22]. This measurement method includes cutting on the instrumented panel to release residual stresses that is on the cutting line. For this reason, the applied cutting process should not introduce plasticity or heat, so that the original residual stress can be measured without the effect of plasticity on the surface of the cutting plane.

The strain released during the cutting process is generally measured. Usually, the material strips released through the slicing process can exhibit axial deformation and curvature corresponding to the residual stress of membrane and bending (penetrating thickness).

Contour method

The contour method is a new relaxation method for the measurement of residual stress, which makes a 2D residual stress map enable to be evaluated on the plane of interest [23]. Contour methods provide higher spatial resolution, while the sectioning technique is easier to use because it nearly requires no calculations [24-26]. The contour method is better than the traditional relaxation method of measuring residual stress. The theoretical basis of the contour method is a variation of Bueckners elastic superposition principle. [27-29].

X-ray diffraction method

X - ray method is a kind of non-destructive technique for measuring residual stress on the surface of materials. X-ray diffraction technology with the fact that when metal under stress, applied stress or residual stress, elastic strain produced will change the

atomic planes in the metallic crystal structure. X-ray diffraction can directly measure the interplanar atomic spacing. Then the total stress of the metal can be obtained [30-32]. Therefore, X-ray diffraction residual stress measurement is suitable for crystalline, relatively fine-grained materials, and diffraction can be produced on any orientation of the specimen's surface.

Ultrasonic Methods

When material is under stress, the ultrasonic velocity changes can be observed, and these changes provide a measure of the average stress along the wave path. Calibration tests are usually used to calculate the acoustic elastic coefficients, which is required for analysis. Different types of waves can be used, but the commonly used technique is the critical refraction longitudinal wave method. The maximum sensitivity is obtained when the propagation direction of the wave is the same as that of the stress [33].

The basic equation for the stress calculation is shown as follows:

$$V = V_0 + K\sigma \tag{2-22}$$

where V_0 is the velocity of a wave in an unstressed medium, σ is the stress and K is a material parameter that is known as acoustoelastic constant [34].

Neutron Diffraction

The neutron diffraction method is very similar to the X-ray method because it depends on the elastic deformation in the polycrystalline material, which causes spacing change of the lattice plane from the stress-free state. Neutron diffraction is a nondestructive method to determine the residual stress of crystal materials [35].

Neutron diffraction provides the value of elastic strain components parallel to the scattering vector, which can be converted to stress. Neutron diffraction measures the strain components caused by the change in lattice spacing. When the crystal material is exposed to a wavelength of radiation near the interplanar spacing, the radiation is scattered flexibly and coherently, as the different Bragg peaks are usually obtained through the position sensitive detector. The Angle of any given peak can be calculated using the Bragg equation, which is shown as equation (2-23).

$$2d_{hkl} \sin \theta_{hkl} = \lambda \tag{2-23}$$

where λ is the wavelength of the radiation, d_{hkl} is the lattice plane spacing of a family of crystallographic planes (*hkl*) responsible for the Bragg peak and θ_{hkl} is the angular position of this diffraction peak. The peak will be observed at an angle of $2\theta_{hkl}$ from the incident beam. If a specimen is elastically strained, the lattice spacing changes. Therefore any elastic strain will be apparent as a shift in the value of $2\theta_{hkl}$ for a particular reflecting plane illuminated by a fixed wavelength. By differentiating the Bragg's equation, the equation can be written as (2-24):

$$\Delta \theta_{hkl} = -\left(\Delta d / d_0\right) \cdot \tan \theta_0 \tag{2-24}$$

where Δd is the change of lattice spacing, and d_0, the lattice spacing of a stress-free sample of the material. So, the strain in the (hkl) set of planes can be calculated with

$$\varepsilon = \left(\Delta d / d_0\right) = -\Delta \theta \cot \theta_0 \tag{2-25}$$

The direction in which strain is measured is along the scattering vector and is perpendicular to the diffracting planes [36-38].

The advantage of the neutron diffraction method is that it can penetrate deeper. The neutron diffraction technique can penetrate several centimeters inside the material, so it can be widely used to evaluate the internal residual stresses of materials.

2.7.2 Evaluation of residual stress in the bonding layer

In order to investigate the distribution of residual stress of the specimens annealed at different temperatures, residual stress was measured by XRD. Based on residual stress testing principle，and used x-ray whose wavelength was λ. First, radiate the specimen with different incident angles, and obtained the corresponding diffraction angle 2θ, then the slope M of 2θ-$\sin^2\psi$ (generally, ψ was set as 0°、15°、30°、45°) can be calculated. In addition, the relationship between 2θ and $\sin^2\psi$ can be obtained，then residual stress σ can be calculated according to Equation (2-26):

$$\sigma = K \cdot \Delta 2\theta / \Delta sin^2\psi = K \cdot M \tag{2-26}$$

Where K is the stress constant of x-ray diffraction analysis, and expressed as Equation

(2-27):

$$K = -\frac{1}{2} \cdot \cot \theta_0 \cdot \frac{E}{1+\upsilon} \cdot \frac{\pi}{180}$$

(2-27)

Where E is the elastic modulus of material, θ_0 is the diffraction angle without stress, υ is Poisson's ratio [39].

When the side of 6061 Al alloy was measured, 2θ was set as 140˚, stress constant was 163.32MPa/˚, tube type was Cr, wavelength was kα, and the size of collimator was φ0.5mm. While 2θ was set as 155˚, stress constant was -79.14MPa/˚ at the side of AZ31Mg alloy. What's more, tube type, wavelength and the size of collimator were the same with 6061Al alloy. In addition, the 2θ of $Mg_{17}Al_{12}$ and Al_3Mg_2 were set as 150˚ and 145˚, and stress constant were respectively -98.97MPa/˚ and -126.22MPa/˚. Then the results of residual stress were calculated at last.

From the results of the experiment it could be obtained that the diffraction peak of Al emerges in the place where 2θ is near 139˚, and indices of crystal face is (311), while the diffraction peak of Mg occurs when the value of 2θ is near 154.6˚, and indices of crystal face is (104), However, the diffraction peaks of intermetallic compounds near Al and Mg are respectively 154˚ and 154.3˚ [40]. The results of diffraction peak is shown in Fig.2.24.
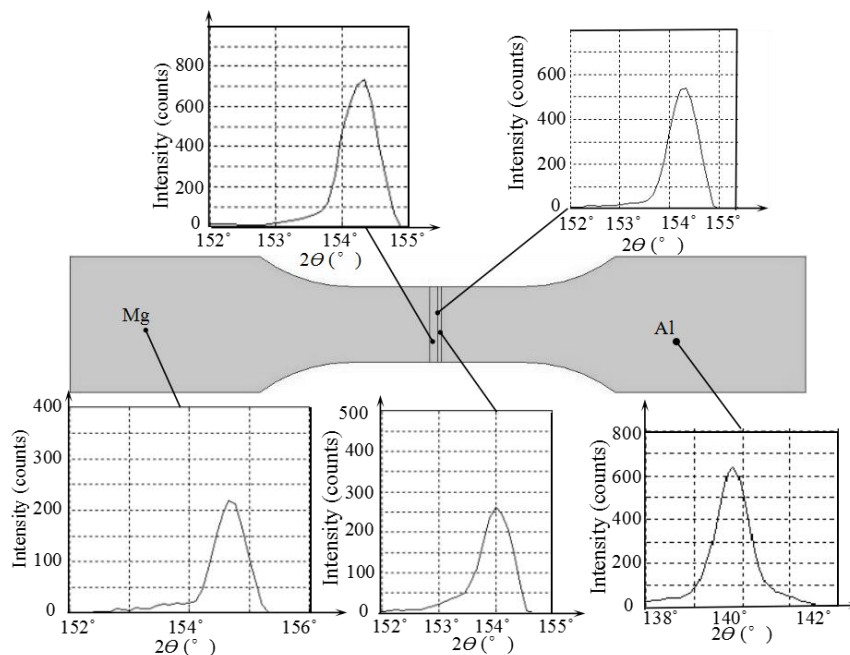
Fig.2.24 The diffraction results on the measurement of residual stress
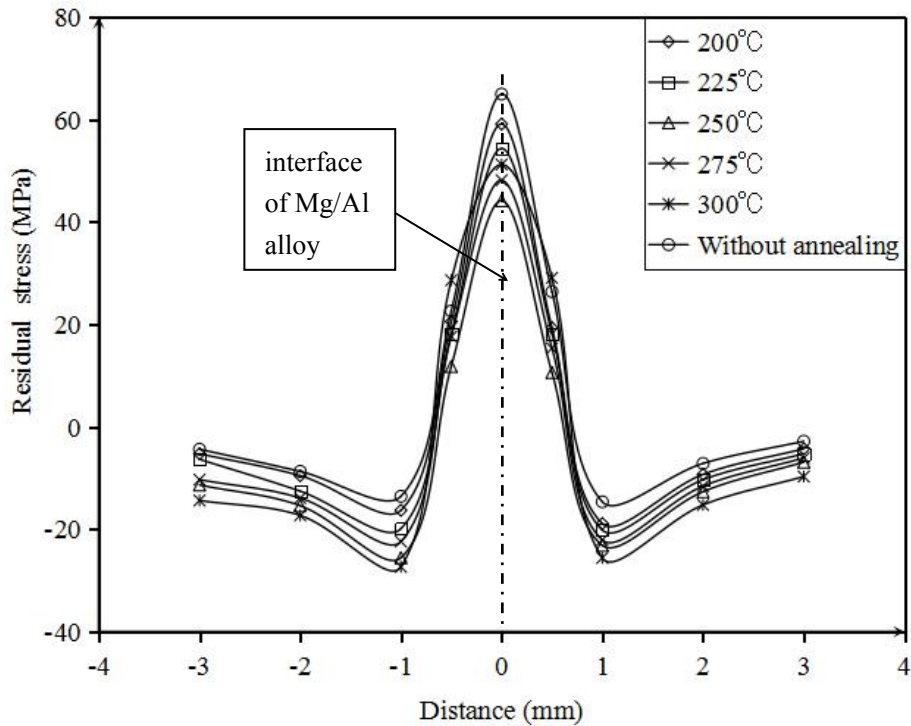
Fig.2.25 Residual stress of specimens treated at different temperatures

The results of residual stress is shown in Fig.2.25. The residual stress is a vector, and in this study, it was axially aligned with the specimens. Under a tensile stress, this value will be positive. In contrast, when the stress is compressive, the residual stress will be negative. It can be inferred from Fig.2.25 that the residual stress at the interface (marked as 0 in Fig.2.25) is tensile stress, and the value is the largest. The stress turns to be lower along with the increasing of the distance from interface. The residual stress nearly turns to be 0MPa in the further place.

The untreated specimen exhibited a stress value of 65MPa. When the samples underwent heat treatment at 300℃, 275℃, 225℃ and 200℃, the stresses were respectively 51Mpa, 48Mpa, 54Mpa and 59MPa. When treated at 250℃, the samples exhibited a stress of approximately 44MPa.

2.7.3 Measurement of Vickers hardness

The Vickers-hardness of diffusion layers annealed at different temperatures was measured in this study, and the load was set as 1kg. The results were shown in the

Figs as follow.
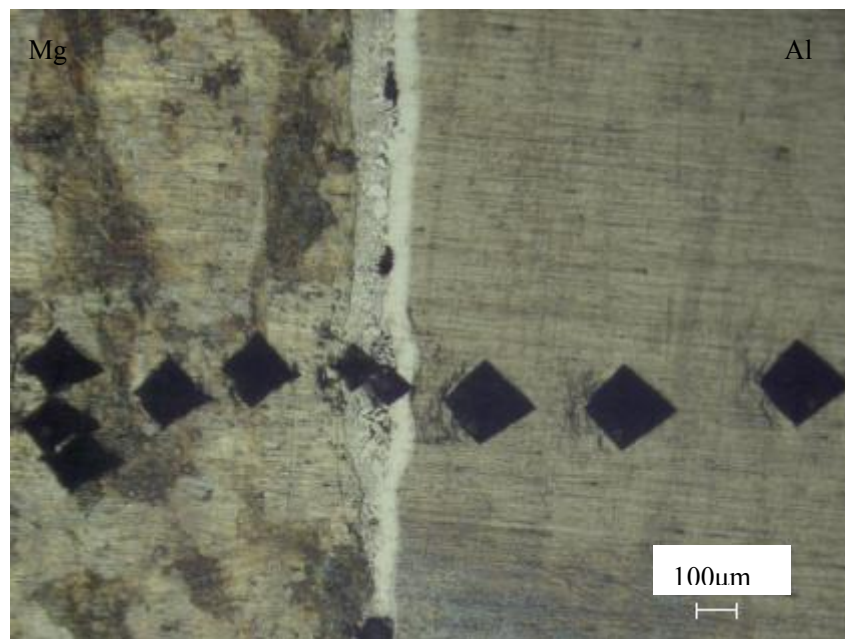
Fig.2.26 The investigation result on Vickers hardness under the condition of annealing absence
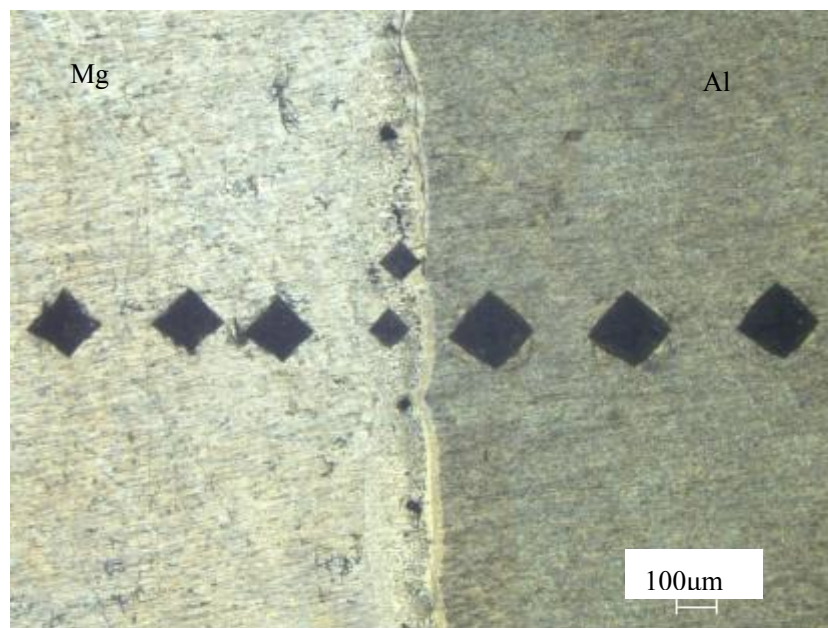
Fig.2.27 The measurement result of Vickers hardness after annealing at 200℃
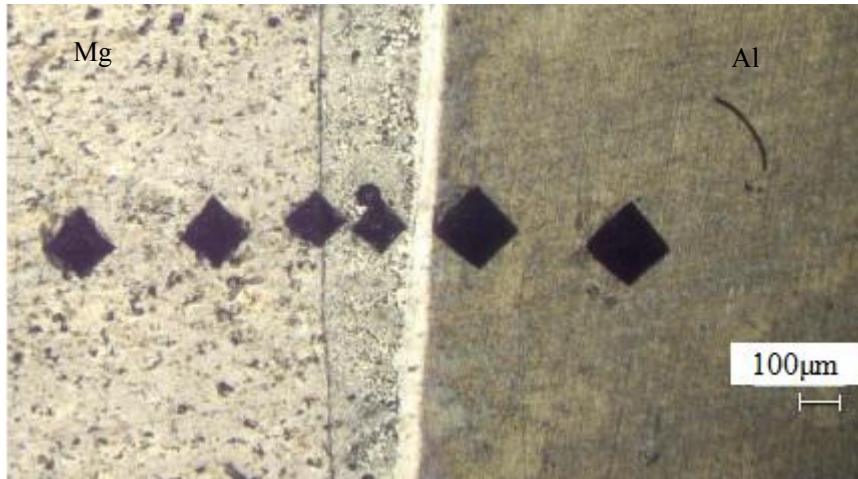
Fig.2.28 Vickers hardness in the case of annealing at 225℃
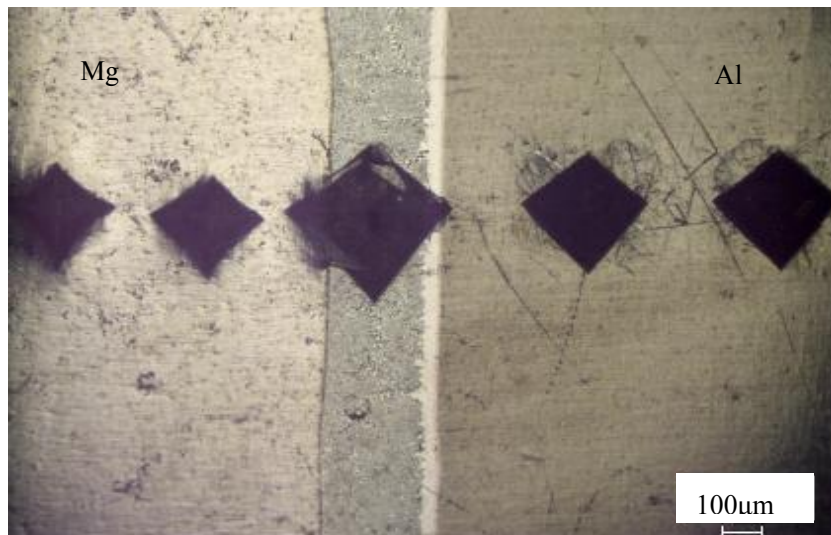
Fig.2.29 Micro-hardness under the annealing condition of 250℃
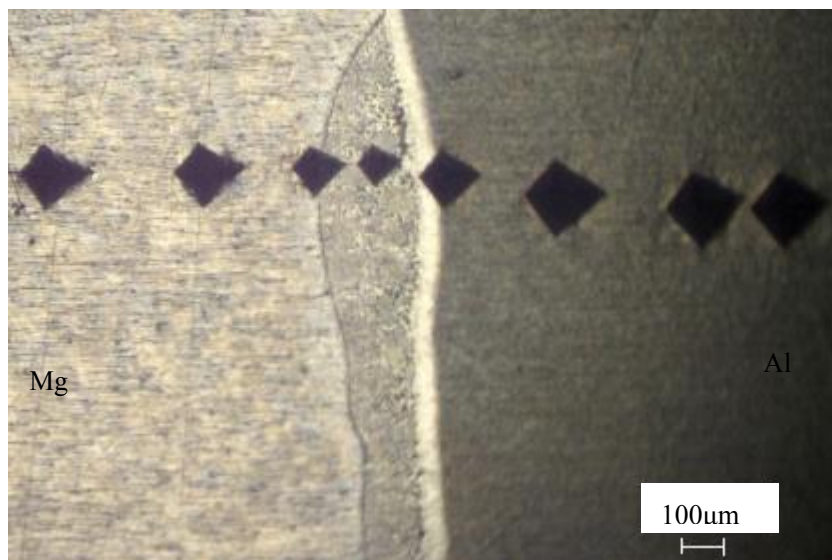
Fig.2.30 The Vickers hardnes of specimen annealed at 275℃

Fig.2.31 The micro-hardness of workpiece annealed at 300℃

The conclusion can be obtained from the results above that the hardness of Mg side were higher than that of Al side. And the hardness in the diffusion zone was higher than other places. Because the size of indentations in the diffusion zone were smaller than other tested locations.
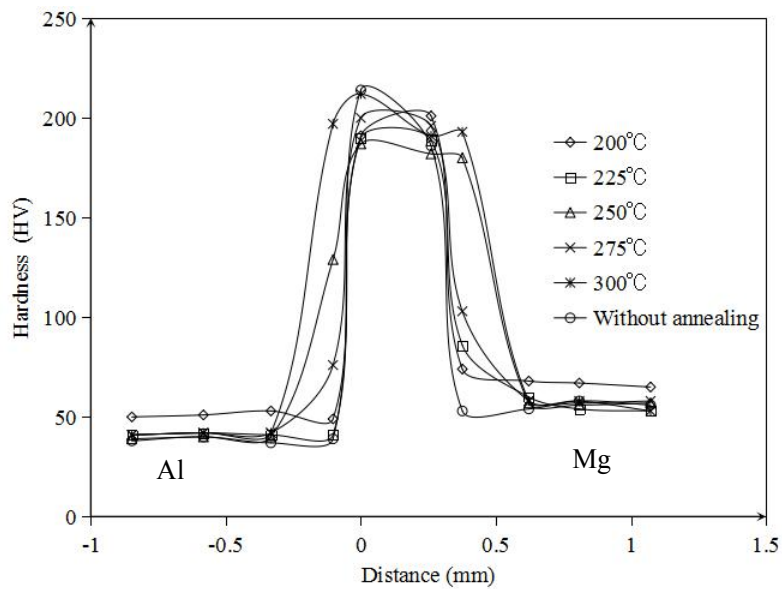
Fig.2.32 Micro-hardness of interfaces annealed at different temperatures

The distributions of hardness of the annealed samples are shown in Fig.2.32. The trends in the hardness distributions are broadly similar in that the hardness of the Mg

side is higher than that of the Al side, and significantly increases in the diffusion zone. After being annealed at 200℃, the hardness of the Mg side was 69 HV, and 51 HV on the Al side, but was 201 HV in the diffusion bonding region. When under the condition of 225℃, the hardness of the Mg side was 60 HV, and 41 HV on the Al side, while the hardness was 190 HV in the diffusion zone. In case of 275℃, the hardness was 58 HV on the Mg side, and 42 HV on the Al side. But was 200 HV in the diffusion zone. When the specimen was treated at 250℃, the hardness of the Mg and Al sides was respectively 57 HV and 40 HV. The interface had a hardness of 187 HV. When the sample underwent heat treatment at 300℃, the hardness of the Mg side was 58 HV and was 42 HV in the Al side. The hardness was 212HV in the bonded zone. When the sample did not undergo annealing, the hardness of the Mg and Al sides was respectively 55 HV and 39 HV, and the hardness of interface was about 214 HV. The hardness in the diffusion layer near the Al substrate was higher than that of the region near the Mg substrate. Thus, the variation in hardness is a result of the intermetallic compounds formed in varying locations in the diffusion zone.

So the conclusion can be obtained that the different hardness result from different intermetallic compounds in different locations of diffusion zone, the fundamental factor controlling hardness is the annealing temperatures. when annealing temperature is 250℃, the hardness of diffusion layers are the lest of all.

2.7.4 Measurement of tensile strength

The results of tensile strengths at different annealing treatment temperatures were as follows. When the annealing temperature is 250℃, the tensile strength is the strongest, which is about 45MPa. While annealed at 200℃, 225℃, 275℃ and 300℃, the tensile strength are approximately 30MPa, 35MPa, 40MPa and 28MPa. The specimens without annealing treatment represented a tensile strength of 29MPa. As the processing of annealing in this study, the strength turns to be stronger.
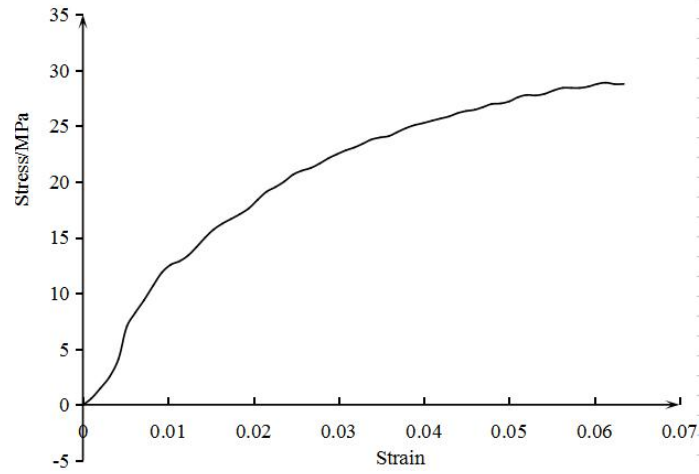
Fig.2.33 Tensile curve of the workpiece without annealing
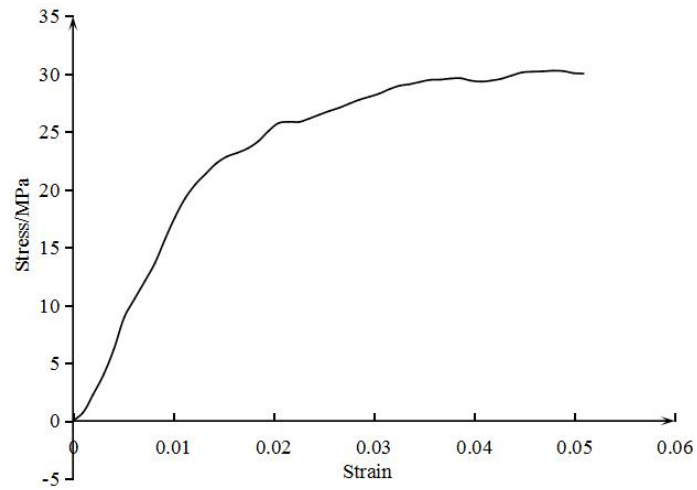
Fig.2.34 The tensile curve of specimen after annealing at 200℃
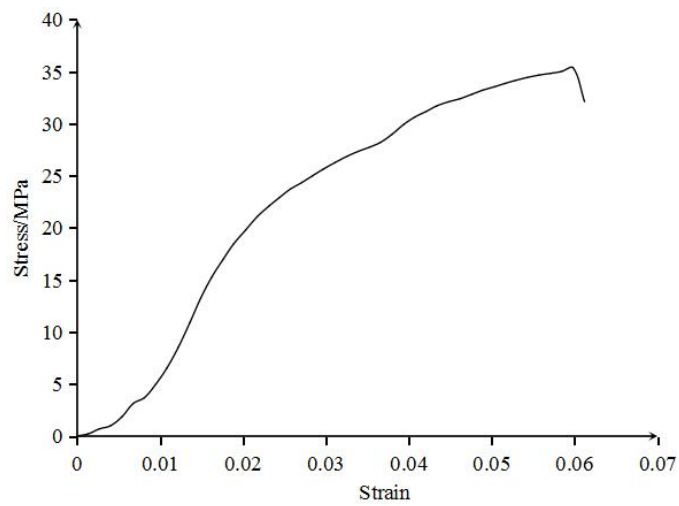
Fig.2.35 Tensile strength in the context of annealing at 225℃
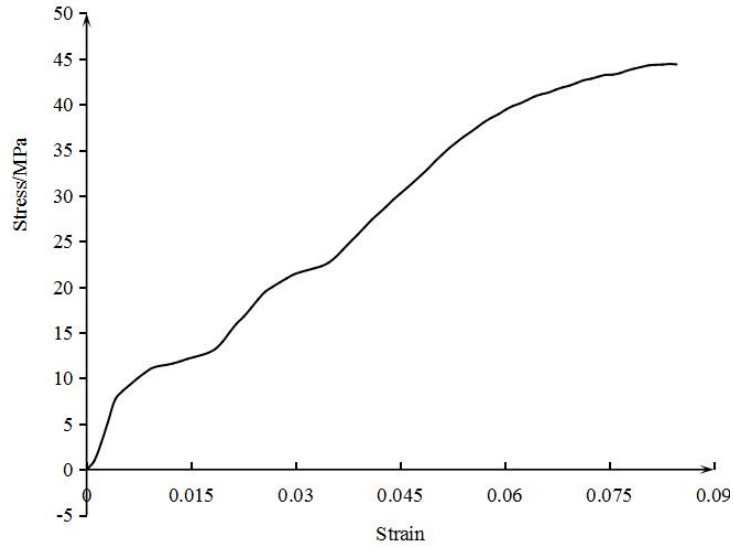
Fig.2.36 The tensile strength in the case of annealing at 250℃
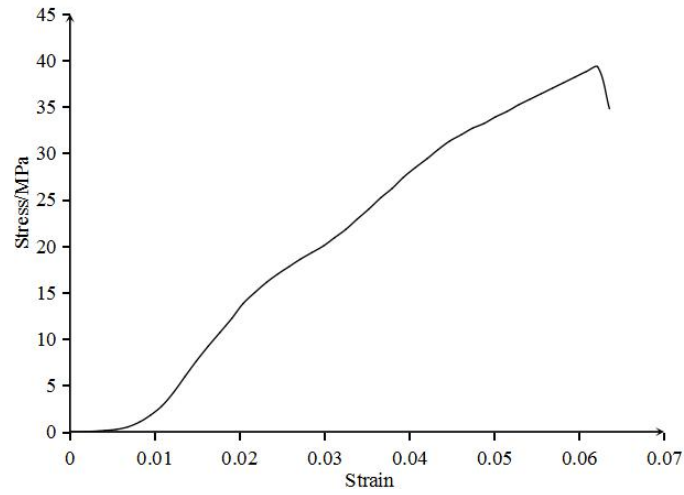
Fig.2.37 Tensile strength under the annealing condition of 275℃
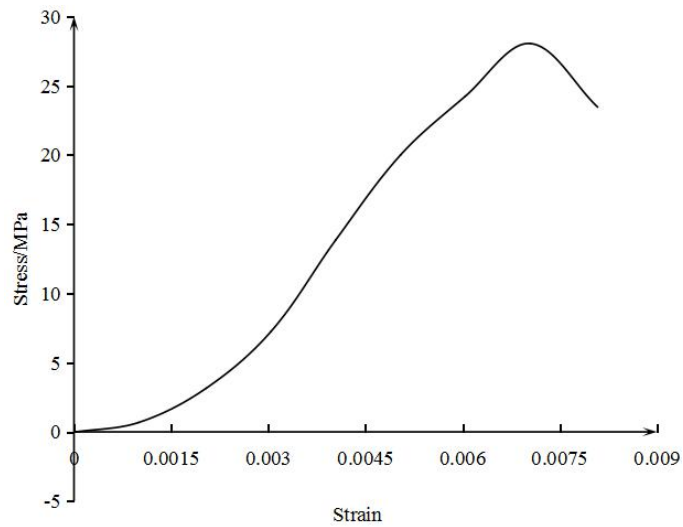
Fig.2.38 Tensile strength after annealing at 300℃

Concluding remarks

For the purpose of refining the microstructure of diffusion zone of Mg/Al alloy, and study the effect of annealing temperatures on microstructure and mechanical behavior, annealing process has been applied in this chapter. According to the results of analysis on microstructure, element distribution and tensile strength, the conclusions can be described as follows:

1. It was difficult to obtain enough quality of bonding strength just by diffusion bonding between magnesium and aluminum alloy sheets due to the formation of intermetallic compound layer. In this study, the application of annealing treatment makes it possible.

2. The width of diffusion layers increases with the rise of annealing temperature, because diffusion rate turns faster with the increasing temperature.

3. Annealing temperatures have a great effect on microstructures and mechanical character. The microstructure can be refined by annealing treatment. Such as, the element distribution of the annealed specimens is more uniform than the one without annealing. And the hardness of diffusion layers can also be decreased, it's 187 HV in interface after the specimen is treated at 250℃. In addition, When the annealing temperature is 250℃, the tensile strength is the strongest, which is about 56MPa.

4. 250℃ is the most advisable annealing temperature for the diffusion zone of AZ31B magnesium alloy and 6061 aluminum alloy.

References

[1] Shoucheng Li, Shun Zhang, Magnesium alloy heat treatment method. Inner mongolia petrochemical industry. (2012) 1006-7981-0068-01.

[2] Yanlong Ma, Jin Zhang, New progress in AZ91D magnesium alloy research[J]. Hot Working Technology. 36 (16) (2007) pp.73-76

[3] Wenchao Dong, Chaohun Wang, Yonglin Kang, Effect of T61 heat treatment and superheat on microstructure and mechanical properties of AM60 magnesium alloy. Automobile Technology & Material. 7 (2004) pp.26-28.

[4] Ryuji Mukai, Study on the control method of internal structure and residual stress /deformation hybrid during quenching process. Doctor thesis at Saitama Institute of Technology Graduate School of Engineering. (2004).

[5] Inoue, Inelastic constitutive models under plasticity-creep interaction condition theories and evaluations, The Japan Society of Mechanical Engineers. Series Ⅰ，31/4 (1998).

[6] N.S. Rossini, M. Dassisti, K.Y. Benyounis, A.G. Olabi, Methods of measuring residual stresses in components, Review. Materials and Design. 35 (2012) pp.572–588.

[7] Schiavone, G., Murray, J., Smith, S.,Desmulliez, M. P. Y., Mount, A. R., Walton,A. J, "A wafer mapping technique for residual stress in surface micromachined films". Journal of Micromechanics and Microengineering. 26 (9) (2016).

[8] Y.C.LamK.S.Lian, The effect of residual stress and its redistribution of fatigue crack growth. Theoretical and Applied Fracture Mechanics. 12/1 October (1989) pp.59-66.

[9] C.D.M.Liljedahl, O.Zanellato, M.E.Fitzpatrick, J.Lin, L.Edwards, The effect of weld residual stresses and their re-distribution with crack growth during fatigue under constant amplitude loading. International Journal of Fatigue. 32/4 April (2010) pp.735-743.

[10] M. Steinzig, E. Ponslet, Residual stress measurement using the hole drilling

method and laser speckle interferometry part1. 27/3 May (2003) pp.43–46.

[11] Olabi AG, Hashmi MSJ, Stress relief procedures for low carbon steel (1020) welded components. J Mater Process Technol. 56 (1996) pp.552–562.

[12] Kandil FA, Lord JD, A review of residual stress measurement methods, a guide to technique selection. NPL Report MAT(A)04. (2001).

[13] Milbradt KP, Ring-method determination of residual stresses. Proc SESA. 9(1) (1951) pp.63–74.

[14] Kiel S, Experimental determination of residual stresses with the ring-core method and an on-line measuring system. Exp Tech. 16(5) (1992) pp.17–24.

[15] Ajovalasit A, Petrucci G, Zuccarello B, Determination of non-uniform residual stresses using the ring-core method. J Mater Process Technol. 118(2) (1996) pp.224–228.

[16] Leggatt RH, Smith DJ, Smith SD, Faure F, Development and experimental validation of the deep hole method for residual stress measurement. J Strain Anal. 31(3) (1996) pp.177–186.

[17] DeWald AT, Hill MR, Improved data reduction for the deep hole method of residual stress measurement. J Strain Anal. 38(1) (2003) pp.65–78.

[18] Shadley JR, Rybicki EF, Shealy WS, Application guidelines for the parting out in a through thickness residual stress measurement procedure. Strain. 23 (1987) pp.157–166.

[19] Tebedge N, Alpsten G, Tall L, Residual-stress measurement by the sectioning method. Exp Mech. 13(2) (1973) pp.88–96.

[20] Mazzolani FM, Aluminium alloy structures. 2nd ed. E&FN Spon, An imprint of Chapman and Hal. ISBN: 978-0419177708. (1995).

[21] Lagerqvist O, Olsson A, Residual stresses in welded I-girders made of stainless steel and structural steel. In: Helsinki: Proceedings of the ninth nordic steel construction conference. (2001) pp.737–744.

[22] Young B, Lui WM, Behavior of Cold-formed high strength stainless steel sections. J Struct Eng, ASCE. 131(11) (2005) pp.1738–1745.

[23] Prime MB, Gonzales AR. In: Proceedings of the sixth international conference on

residual stresses. Oxford, UK: IOM Communications Ltd. (2000) pp.617–624.

[24] Prime MB, Hughes DJ, Webster PJ, In: Proceedings of 2001 SEM annual conference on experimental and applied mechanics. Portland, OR. (2001) pp.608–611.

[25] Murugan N, Narayanan R, Finite element simulation of residual stresses and their measurement by contour method. Mater Design. 30(6) (2009) pp.2067–2071.

[26] Prime MB, Martineau RL, Mapping residual stresses after foreign object damage using the contour method. Mater Sci Forum. 404–407 (2002) pp.521–5216.

[27] Zhang Y, Fitzpatrick ME, Edwards L, Measurement of the residual stresses around a cold expanded hole in an EN8 steel plate using the contour method. Mater Sci Forum. 404–407 (2002) pp.527–534.

[28] Prime MB, Cross-Sectional Mapping of residual stresses by measuring the surface contour after a cut. J Eng Mater Technol. 123(2) (2001) pp.162–168.

[29] Bueckner HF, The propagation of cracks and the energy of elastic deformation. Trans ASME. 80 (1958) pp.1225–1230.

[30] Norton JH, Rosenthal D, Stress measurement by x-ray diffraction. Proc Soc Exp Stress Anal. 1(2) (1944) pp.73–76.

[31] Norton JH, Rosenthal D, Application of the x-ray method of stress measurement to problems involving residual stress in metals. Proc Soc Exp Stress Anal. 1(2) (1944) pp.81–90.

[32] Ruud CO, A review of selected non-destructive methods for residual stress measurement. NDT Int. 15(1) (1982) pp.15–23.

[33] Withers PJ, Bhadeshia HKDH, Overview: Residual Stress, Part 1—Measurement Techniques. Materials Science and Technology. 17 (2000) p.355.

[34] James M, Lu J, Roy G, Handbook of Measurement of Residual Stress. Englewood Cliffs, NJ: Prentice Hall. (1996).

[35] A.J. Allen, M.T. Hutchings, C.G. Windsor &C, Andreani. Neutron diffraction methods for the study of residual stress fields. Advances in Physics. 34/4 (1985).

[36] Noyan IC, Cohen JB, Residual Stress Measurement by Diffraction and Interpretation, New York: Springer-Verlag. (1987).

[37] M Vrána, P Mikula, P Lukáš, J Šaroun, P Strunz, High resolution neutron diffraction techniques for strain/stress measurements at a steady state reactor. Acta Physica Hungarica. 75 (1994) 305-310.

[38] Seok-Hoon Kim, Jong-Bum Kim, Won-Jae Lee, Numerical prediction and neutron diffraction measurement of the residual stresses for a modified 9Cr-1Mo steel weld. J Mater Process Technol. 209(8) (2009) pp.3905–3913.

[39] ZhANG Dingquan, He Jiawen, Residual stress Analysis by x-ray diffraction and It's Functions [M]. 1st ed. Xi'an: Xi'An Jiao Tong University, China. (1999).

[40] WANG Jiangang, Ju Dongying, Study on evolution technology of anisotropic mechanical properties and microstructures evolution of metal thin plate under complex stress condition [D]. Saitama Institute of Technology. Japan. (2011).

Chapter 3 Simulations based on heat conduction theory and constitutive equation of thermal-elastoplasticity

3.1 Introduction

Heat transmits from one part of the system to another part or from one system to another system is called heat transfer. Heat conduction is one of three heat transfer modes (heat conduction, convection, radiation). It is the main mode of heat transfer in solid objects and is transported in layers of non-flowing liquid or gas layers, and heat conduction often happens simultaneously with convection under the flowing conditions.

The temperature difference within an object or system is a necessary condition for heat conduction [1][2]. In another word, as long as there is a temperature difference in the media or between the media, it is certainly that the heat transfer will occur. The rate of heat conduction depends on the distribution of the temperature field inside the object.

The essence of heat conduction is that a large number of molecules in the material collide with each other due to the thermal motion, so that the energy is transferred from the high temperature part of the object to the low temperature part or from the high temperature object to the low temperature object [3][4]. In solids, the microscopic process of heat conduction is: in the high temperature parts of the crystal, the vibration energy of the particles on the nodes is larger. In the low temperature parts, the vibration energy of the particles is smaller. Due to the vibration of the particles interact with each other, the thermal energy in the crystal is transferred from the parts having a larger kinetic energy to the sections having a smaller kinetic energy. The heat conduction in a solid object is the transfer of energy.

In the conductor, due to the existence of a large number of free electrons, and the free electrons carry out a continuous and random heat movement. In general, the energy of lattice vibration is small, and free electrons play a major role in the conduction of heat in metal crystals. So the general electrical conductor is also a good conductor of heat.

The heat conduction in the liquid is as follows: the liquid molecules carry out strong thermal movement in the high temperature region. Due to the interactions between the liquid molecules, the energy of the thermal movement will gradually be transmitted to the surrounding layers, and cause the heat conduction phenomenon. Due to its small thermal conductivity and slow conduction, it is similar to solid. Unlike liquid, the distance between gas molecules is relatively large. Gas relies on random thermal motion of molecules and collisions between molecules to generate energy migrations within the gas and form a macro heat transfer.

The constitutive equation of thermal and elastoplastic dynamics is a theoretical system for analyzing the relationships between temperature, microstructure, stress and strain. And it has been the theoretical basis for heat treatment. During the processes of duffusion bonding and annealing, the variety of temperature throughout all the processes. So it is significant to study the heat conduction, diffusion, thermal and elastoplastic dynamics for researching the effect of temperature on heat, microstructure, stress and strain. What's more, basing on the study about the relationships between temperature, microstructure, stress and strain, it will contribute to control the processes of diffusion bonding and heat treatment for obtaining microstructure and mechanical behaviors.

Based on the theory above, and along with the recent advances in numerical analysis technology and computers, the finite elements method is being applied in more and more research and production areas. Application of the finite elements method contains many fields of contemporary industry and also modern technologies supported by computers [5-10]. This method is presently the most popular and the fastest developing numerical methods which are used in aircraft, ballistic rocket, automotive, shipbuilding, machine and electrotechnics industry and also contains these fields such as bio-mechanical, medicine, mechatronic, and in materials technology. Computer methods using in design processes serves mainly to optimization of these processes [11-14].

The finite elements method is also used in plastic forming and its application makes it possible to perform simulation of aluminum press forming by selection of appropriate

forming parameters for given material such as pressure force and falling speed of punch on material [15].

In this work, for the purpose of improving the tensile strength, simulations on annealing treatment were applied to search for the apposite annealing temperature. This chapter mainly describes simulations about the effect of heat treatment temperature on properties of diffusion bonded Mg/Al joints.

During the diffusion bonding process and heat treatment process, the structure of the bonding layer changes with varieties of conditions, such as heating rate, cooling rate, holding time and annealing temperatures. That is to say, if the bonding conditions and heat treatment conditions change, the material performance parameters, such as bonding strength, diffusion layers' hardness and residual stress will also vary. So it is important to confirm the optimum bonding conditions and heat treatment conditions. Furthermore, it is important to predict the thermal-mechanical behavior such as heat conduction and inelastic deformation generated in the heat treated material.

3.2 Thermal conduction analysis

If the internal energy of the object is represented as $e = g + T\eta + tr(\sigma\varepsilon^e)$, then the first law of thermodynamics can be displayed as the following equation:

$$\rho\dot{e} - tr(\boldsymbol{\sigma}\dot{\boldsymbol{\varepsilon}}) + div\mathbf{h} = 0 \tag{3-1}$$

Using Fourier law ($\mathbf{h} = kgradT$), if do not consider latent heat due to plastic work and phase transformation, and the terms relating to elastic strain and curing parameters are omitted, the equation (3-1) can be rewritten as equation (3-2):

$$\rho c\dot{T} - kdiv(gradT) = 0 \tag{3-2}$$

Where ρ is the density, c is the specific heat, k is the thermal conductivity. Thermal conduction boundary condition: if the temperature and thermal conductivity coefficient of the fluid in contact with the object are specified, boundary conditions are indicated as follows.

$$-kgradT \cdot \mathbf{n} = h(T)(T - T_w) \tag{3-3}$$

Where **n** is outward unit normal vector on object surface, T_w is the temperature around the boundary [16]. Also, $h(T)$ is the heat transfer coefficient between the object and the external environment. In general, the heat transfer coefficient is a function of the temperature T obtained from the experimental value of the cooling curve [17]. What's more, temperature T is a function of time.

3.3 Constitutive equation of thermal-elastoplasticity

For the plastic material, elastic deformation will occur when load is applied. In addation, when the sress resulted from the applied load exceeds the elastic limit, then plastic deformation will be caused. What's more, the temperature changes of materials will cause thermal stress and strain. For the three-dimensional stress and strain, the generalized Hooke's law can be applied. Then the equation (3-4) can be obtained.

$$\dot{\varepsilon}_{ij} = \dot{\varepsilon}_{ij}^{\,e} + \dot{\varepsilon}_{ij}^{\,p} + \dot{\varepsilon}_{ij}^{\,T} \tag{3-4}$$

whre $\dot{\varepsilon}_{ij}$ is the total strain rate, $\dot{\varepsilon}_{ij}^{\,e}$ is the elastic strain rate，$\dot{\varepsilon}_{ij}^{\,p}$ and $\dot{\varepsilon}_{ij}^{\,T}$ are plastic strain rate and thermal strain rate respectively. the elastic strain rate $\dot{\varepsilon}_{ij}^{\,e}$ and the thermal strain rate $\dot{\varepsilon}_{ij}^{\,T}$ can be represented as equation (3-5). α is the linear expansion coefficient, G is the shear elastic modulus, v is the Poisson's ratio, and the ΔT, standing for the difference of temperature, is expressed as $\Delta T = T - T_0$ [18][19].

$$\begin{cases} \dot{\varepsilon}_{ij}^{\,e} + \dot{\varepsilon}_{ij}^{\,T} = E_{ijkl}^{e} \, \dot{\sigma}_{kl} + \beta_{ij} \, \dot{T} \\ \beta_{ij} = \dfrac{\partial E_{ijkl}^{e}}{\partial T} \sigma_{kl} + \alpha_{ij} \dfrac{\partial \alpha_{ij}}{\partial T} \Delta T \end{cases} \tag{3-5}$$

Where E_{ijkl}^{e} is the Young's modulus of elasticity, which can be displayed as the equation (3-6):

$$E_{ijkl}^{e} = \frac{1}{2G} \left\{ (\delta_{ik}\delta_{jl} + \delta_{il}\delta_{jk}) - \frac{v}{1+v} \delta_{ij}\delta_{kl} \right\} \tag{3-6}$$

The plastic strain rate $\dot{\varepsilon}_{ij}^{p}$ can be represented as equation (3-7), F is the yield function.

$$\begin{cases} F = F(\sigma, T, \xi) \\ \\ \dot{\varepsilon}_{ij}^{p} = \frac{1}{\hat{G}}(\frac{\partial F}{\partial \sigma_{mn}}\dot{\sigma}_{mn} + \frac{\partial F}{\partial T}\dot{T})\frac{\partial F}{\partial \sigma_{ij}} \\ \frac{1}{\hat{G}} = -\frac{1}{\dfrac{\partial F}{\partial \kappa}\dfrac{\partial F}{\partial \sigma_{kl}}\sigma_{kl}} \end{cases}$$
(3-7)

3.4 Concept of mixture and mixture law

$Mg_{17}Al_{12}$ and Mg_2Al_3 formed during the diffusion process are intermetallic compounds of magnesium alloy and aluminum alloy. When the microstructure is viewed from a macroscopic point, it is thought that several compositions are mixed. In order to represent it, an arbitrary substance point in the object is composed of a mixture of N phases, and every phase has a volume fraction $\xi_I(I = 1, 2, \cdots\cdots, N)$. Since all the volume fractions collected are 1, so the equation (3-8) is established.

$$\sum_{I=1}^{N}\xi_I = 1$$
(3-8)

If the characteristic of the I th component is definited as χ_I, the properties χ of the material or its mechanical and physical propertiesis χ is represented by the properties of N components $\chi_I(I = 1, 2, \cdots\cdots N)$, which is shown in equation (3-9):

$$\chi = \sum_{I=1}^{N}\chi_I\xi_I$$
(3-9)

and this is called mixture law. In order to calculate the parameters related to the properties of the intermetallic compound of the magnesium alloy and aluminum, the expression of the material constant by the mixing rule is as follows [20].

Density: $$\rho = \sum_{I=1}^{N}\rho_I\xi_I$$
(3-10)

Specific　heat：
$$C = \sum_{I=1}^{N} C_I \xi_I \tag{3-11}$$

Thermal conductivity：
$$k = \sum_{I=1}^{N} k_I \xi_I \tag{3-12}$$

Coefficient of linear expansion：
$$\alpha = \sum_{I=1}^{N} \alpha_I \xi_I \tag{3-13}$$

Longitudinal elastic modulus (Young's modulus):
$$E = \frac{1}{\sum_{I=1}^{N} \left(\xi_I / E_I \right)} \tag{3-14}$$

Poisson's ratio：
$$v = \frac{\sum_{I=1}^{N} \left(v_I \xi_I / E_I \right)}{\sum_{I=1}^{N} \left(\xi_I / E_I \right)} \tag{3-15}$$

Yield stress：
$$\sigma_s = \sum_{I=1}^{N} \sigma_{sI} \xi_I \tag{3-16}$$

3.5 Heat conduction analysis by finite element method

For the formulation of heat conduction analysis by finite element method, at first, the region V is divided into a finite number of elements. As shown below,　The temperature T at any time t in each element is assumed as the product of the shape function $[N]$ and the node temperature $\{T\}^e$.

$$T = [N]\{T\}^e \tag{3-17}$$

By using the principle of the weighted residual method, the residual errors of the temperature approximated by the above equation and the true solution are made to be zero in average to determine the temperatures of the nodes in the region. That is to say, if the weight function and the residual error are orthogonalized, then can be represented as the following equation.

$$\int_V W_i \left\{ \rho c \dot{T} - div\left(kgradT\right) + \rho \gamma_a - \rho \gamma \right\} dV$$
$$+ \int_{S_h} W_i \left\{ kgradT \bullet n + h\left(T\right)\left(T - T_w\right) \right\} ds = 0 \tag{3-18}$$

Where the Galerkin method is applied to the above equation, That is to say, a shape function N_i is used as the weight function W_i. And furthermore, if the equation (3-17) is substituted and the temperature at the node is expressed as $C_j \left(j = 1 \cdots\cdots n \right)$, then the equation as follows can be obtained.

$$\sum_{j=1}^{N} \left\{ \left(\int_V kgradN_i \bullet gradN_j dV + \int_{S_h} N_i h \left(T \right) N_j dV \right) T_j + \int_V N_i \rho c N_j dV \, \dot{T_i} \right\}$$
$$- \int_V \rho \left(\gamma_a - \gamma \right) N_i dV - \int_{S_h} N_i h \left(T \right) T_w ds = 0 \tag{3-19}$$

When this formula is rewritten in matrix form, it becomes a simplified form as follows:

$$[H]\{T\} + [P]\left\{ \dot{T} \right\} + \{Q\} + \{F\} = \{0\} \tag{3-20}$$

Where the matrix and vector are represented as follows:

$$[H] = \sum [H]^e, \ [P] = \sum [P]^e, \ \{Q\} = \sum \{Q\}^e, \ \{F\} = \sum \{F\}^e \tag{3-21}$$

As the above, the heat conduction equation shown in (3-20) for the entire region is obtained. The thermal conductivity k, the density ρ, and the specific heat c included in this equation is dependent on the temperature. Therefore, the matrix $[H]$, $[P]$, $\{Q\}$ are the function of temperature. Therefore, using the difference approximation method, equation (3-20) can be applied as follows. At first, Assuming that the change of temperature T from time $t - \Delta t$ to t matches the primary function relationship, the following equation is obtained [21].

$$\left\{ \dot{T} \right\}_t = \frac{\{T\}_t - \{T\}_{t-\Delta t}}{\Delta t} \tag{3-22}$$

So the equation (3-22) can be represented as follows:

$$\left([H] + \frac{[P]}{\Delta t} \right) \{T\}_t = \frac{[P]}{\Delta t} \{T\}_{t-\Delta T} - \{F\} - \{Q\} \tag{3-23}$$

Where $\{T\}$ represents the vector of temperature at time t. If the matrix $[H]$, $[P]$, $\{F\}$ and $\{Q\}$ approximately do not change from time $t - \Delta t$ to t, the results at

time $t - \Delta t$ are $[H]_{t-\Delta t}$, $[P]_{t-\Delta t}$, $\{F\}_{t-\Delta t}$ and $\{Q\}_{t-\Delta t}$. So the equation (3-23) and be rewritten as follows:

$$\left([H]_{t-\Delta t} + \frac{[P]_{t-\Delta t}}{\Delta t} \right) \{T\}_t = \frac{[P]_{t-\Delta t}}{\Delta t} \{T\}_{t-\Delta T} - \{F\}_{t-\Delta t} - \{Q\}_{t-\Delta t} \tag{3-24}$$

Therefore, if $\{T\}$, $[H]$, $\{F\}$, $[P]$ and $\{Q\}$ at the previous time step are already known, it is possible to obtain $\{T\}$ at the subsequent stage from the above equation.

3.6 Analysis of thermo-elastoplasticity by finite element method

When the stress analysis of a structure is carried out by the finite element method, the variational principle, including the virtual work principle and minimum potential energy principle, is used as the basic principle. Here, finite element formula for the analysis of elasto-plastic stress is performed based on the principle of virtual work. First, the Mises kinematic hardening yield function is applied as F shown in following equation:

$$F = \left(\frac{3trs'^2}{2} \right)^{1/2} - \sigma_0 (T, \kappa, \xi_I) \tag{3-25}$$

However, σ_0 is the Initial yield function of materials [24], and s' is represented as the equation (3-26):

$$S' = \left\{ \sigma - \frac{1}{3}(tr\sigma) \right\} - \left\{ \alpha - \frac{1}{3}(tr\alpha) \right\} \tag{3-26}$$

Besides, the following equation can be obtained from strain rate and thermal conduction equation:

$$\overset{\wedge}{\Lambda} = G \left\{ \left(\frac{3}{2trs'^2} \right)^{1/2} tr\left(s' \overset{\cdot}{\sigma} \right) - \frac{\partial \sigma_0}{\partial T} \overset{\cdot}{T} \right\} \tag{3-27}$$

$$\hat{G} = \frac{2}{3a} \tag{3-28}$$

Combining the combination hardening law with equation (3-27) and (3-28), plastic strain rate can be written as follows:

$$\dot{\varepsilon}_p = \frac{1}{a\sigma_0}\left\{\frac{3}{2\sigma_0}tr\left(s'\sigma\right) - \frac{\partial\sigma_0}{\partial T}\dot{T}\right\}$$ (3-29)

Strain Increment and equation (2-27) can be expressed in matrix style based on the Cartesian coordinate system.

$$\{d\varepsilon\} = \{d\varepsilon^e\} + \{d\varepsilon^p\} + \{d\varepsilon'\}$$ (3-30)

$$\{d\varepsilon^e\} = [D^e]^{-1}\{d\sigma\} + \left(\frac{\partial}{\partial T}[D^e]^{-1}\{\sigma\} + \{\alpha\}\right)dT$$ (3-31)

In addition, the elastoplastic matrix $[D]$ is written as follows:

$$[D] = [D^e] - \frac{1}{S_0}[D^e]\{S'\}\{S'\}^T[D^e]$$ (3-32)

$$S_0 = \frac{3}{2a\sigma_0^2} + \{S'\}^T[D^e]\{S'\}$$ (3-33)

Where the elastoplastic matrix $[D]$ can be represented as follows:

$$[D] = [D^e] - C_f \begin{bmatrix} S_x'^2 & & & & & \\ S_x'S_y' & S_y'^2 & & & & \\ S_x'S_z' & S_y'S_z' & S_z'^2 & & sym & \\ S_x'S_{xy}' & S_y'S_{xy}' & S_z'S_{xy}' & S_{xy}'^2 & & \\ S_x'S_{yz}' & S_y'S_{yz}' & S_z'S_{yz}' & S_{xy}'S_{yz}' & S_{yz}'^2 & \\ S_x'S_{zx}' & S_y'S_{zx}' & S_z'S_{zx}' & S_{xy}'S_{zx}' & S_{yz}'S_{zx}' & S_{zx}'^2 \end{bmatrix}$$ (3-34)

3.7 Calculation on thermo-elastoplastic performance parameters of intermetallic compounds based on the mixture law

As the parameters of intermetallic compounds of Mg/Al alloy were necessary for simulation on diffusion and annealing, the thermo-elastoplastic performance parameters were calculated based on the mixture law related above. And the necessary parameters were shown from Fig.3.1 to Fig.3.3 and Table 3.1.

Fig.3.1 The thermal conductivity

Fig.3.2 Variation of yield strength with temperatures
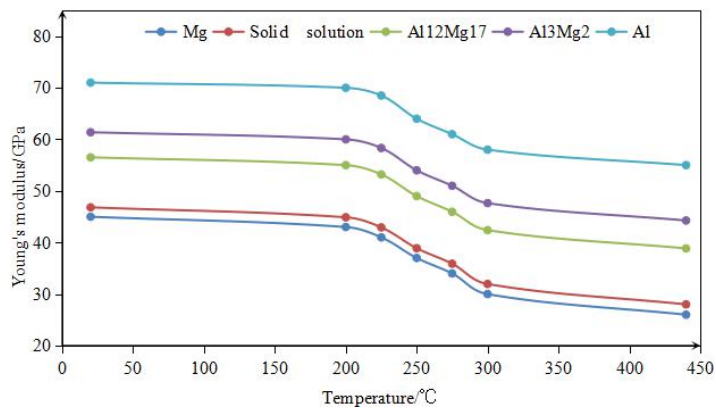
Fig.3.3 The changes of young's modulus with temperatures

Table 3.1 The parameters for simulation

	Mg	Solid solution	Al12Mg17	Al3Mg2	Al
Density(g/cm3)	1820	1882	2210	2374	2700
Poisson's ratio	0.3	0.3	0.32	0.33	0.34
Linear expansion coefficient（10-6/k）	26	25.83	24.94	24.49	23.6
Specific heat capacity(J/Kg℃)	1016	1006	955	930	880

3.8 Simulations on diffusion bonding and annealing

3.8.1 Selection of coupling field and element type

According to the maxing rule, the coefficients of AZ31 magnesium alloy and 6061 aluminum alloy, and all the coefficients that relate the intermetallic compounds of Mg and Al are calculated. For the simulation, thermal stress coupling field of ANSYS was applied, and the element type is "Coupled Field, Vector Quad 13". Material model is "Structural" and "Thermal".

According to the size of the specimens，the model was created using the modeling function module. At first, the key points were created by the coordinate which were calculated according to the size of specimens. Based on the key points, lines were created . Then the area was created by the lines (shown in Fig.3.4).
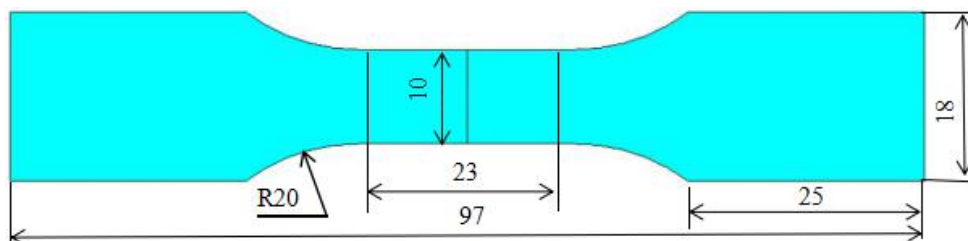
Fig.3.4 Size of model for simulation

3.8.2 Setting of simulation conditions for diffusion bonding and annealing treatment

At fist, the material properties were distributed to the different parts of the model. then set up the size of elements for the mesh of the finite elements. The element mesh is shown in Fig.3.5.
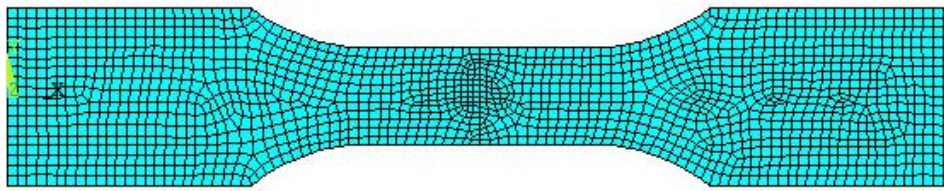
Fig.3.5 Mesh of the finite elements

The number of the node is 15437, and the number of the elements is 15178. The nest step is to set up the conditions for calculation according to the parameters of magnesium alloy and aluminium alloy. The heating speed was set at 10℃/min, the temperature increases from the room temperature 20℃ to the eutectic temperature 440℃. For the process of annealing, the temperature loads were set at 200℃, 225℃, 250℃, 275℃ and 300℃. In addition, the restrictions were set to the model. It is thought that the end faces can't move during the diffusion process. Therefore, restrict was only applied to the end faces, so that it can't move to any directions. Temperature load was applied to the model, then the solution begins. (the model with temperature load is shown in Fig.3.6).
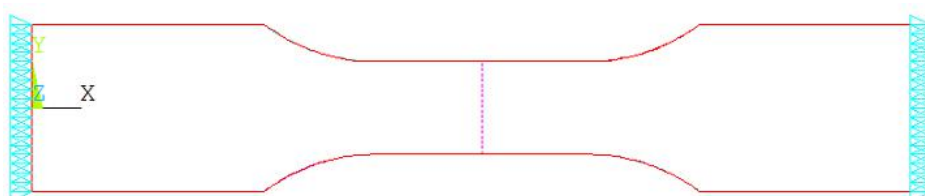
Fig.3.6 Model with load and restrictions

3.8.3 Results and discussion of simulations

When the simulations were completed, data processing was carried out. The stress distribution in the heating process at different conditions were shown from Fig.3.7 to Fig.3.11. Along the measuring line, the stress at the place of the node on the line can be gotten, then based on the value of stress and the distance between nodes, the graph showing the stress distribution along the measuring line can be obtained. The graph is shown in Fig.3.12.

-.959E+08   -.769E+08   -.578E+08   -.388E+08   -.197E+08
    -.864E+08   -.673E+08   -.483E+08   -.292E+08   -.102E+08
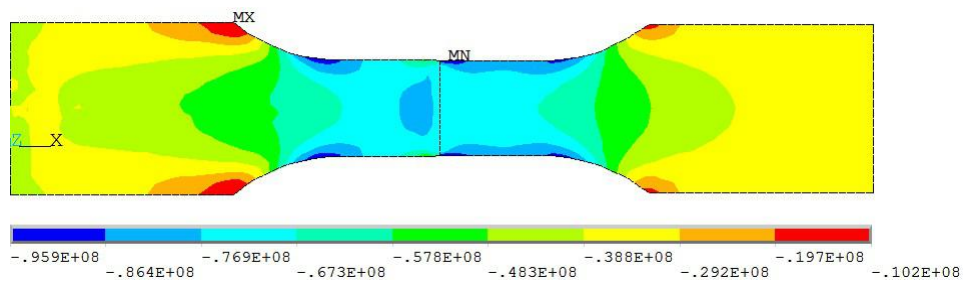
Fig.3.7 Distribution of stress in x-axis direction during heating process (200℃)

-.102E+09   -.818E+08   -.618E+08   -.418E+08   -.219E+08
    -.918E+08   -.718E+08   -.518E+08   -.319E+08   -.119E+08
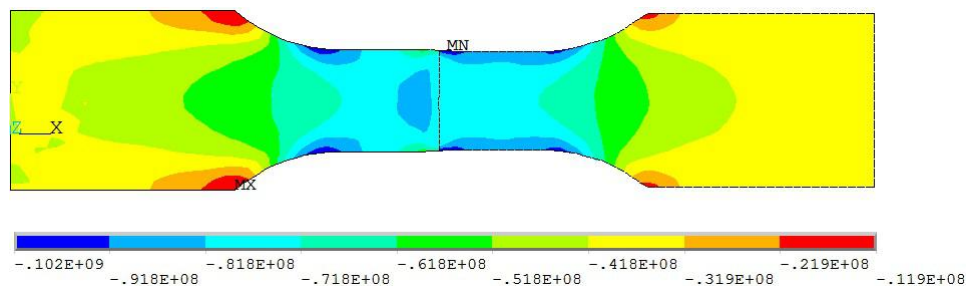
Fig.3.8 Stress in x-axis direction during heating process (225℃)

-.130E+09   -.102E+09   -.744E+08   -.465E+08   -.185E+08
    -.116E+09   -.884E+08   -.604E+08   -.325E+08   -.449E+07
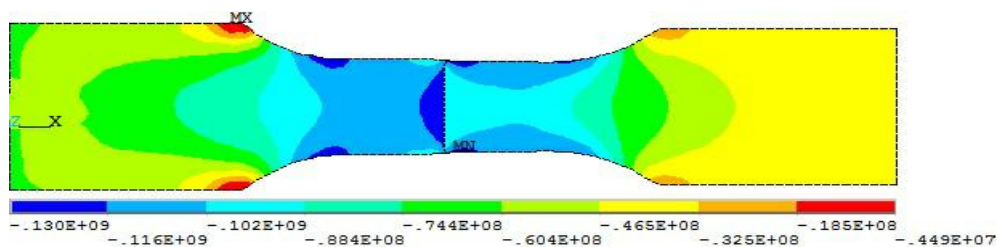
Fig.3.9 X-axis stress of specimen after being heated to 250℃
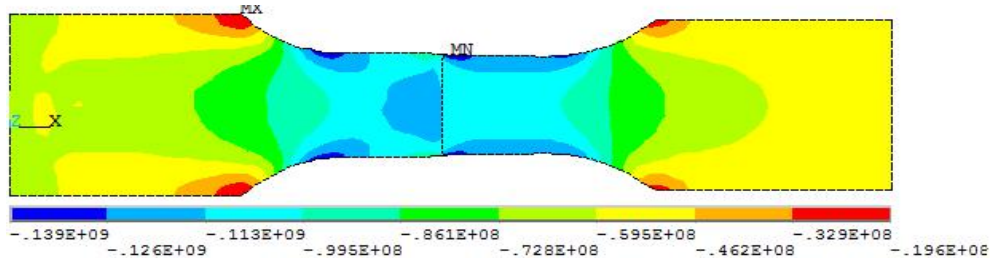
Fig.3.10 X-axis stress during the process of heating (275℃)
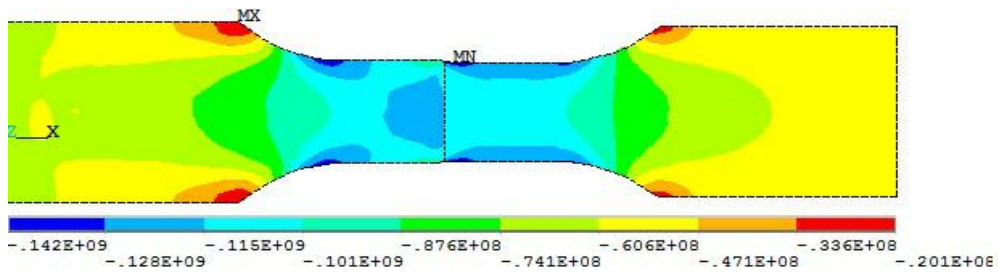
Fig.3.11 Simulation result of x-axis stress in the heating process (300℃)
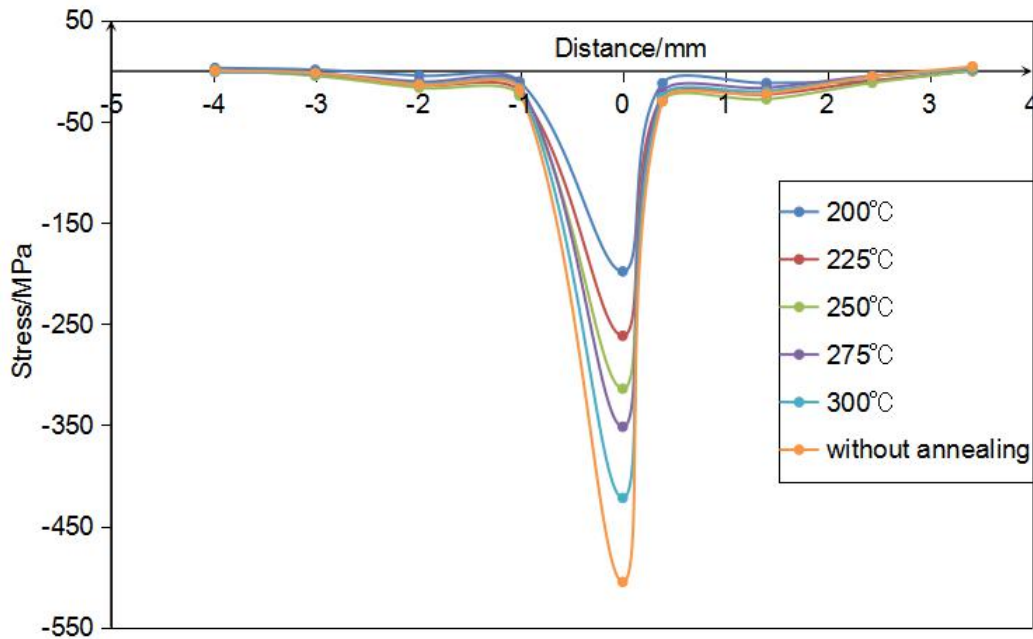
Fig.3.12 Stress distribution of x-axis after the heating process

According to the simulation results of heating process above, it can be depicted that the residual stress occurred as compressive one. The maximum residual stress in every conditions occurred in the diffusion zone, the values are -225Mpa, -238Mpa, -314Mpa, -351Mpa and -422Mpa. So it's thought that the stress in the diffusion zone

is bigger than the one far from the interface. In addition, at the place where is away from the diffusion zone, stress turn to be 0MPa.

The distribution of stress during the holding process can be shown from Fig. 3.13 to Fig.3.17.

-.132E+09   -.104E+09   -.762E+08   -.481E+08   -.201E+08
        -.118E+09   -.902E+08   -.622E+08   -.341E+08   -.603E+07
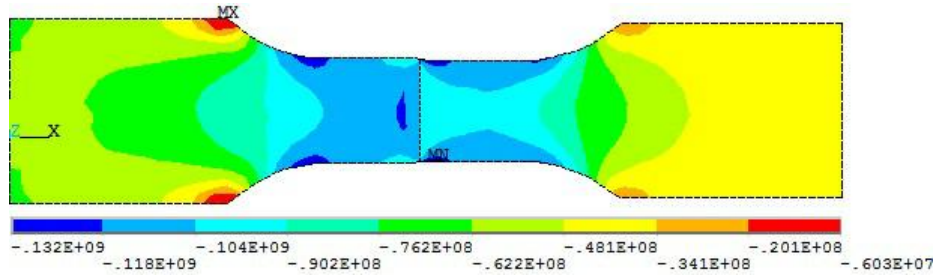
Fig.3.13 Stress distribution in x-axis direction after holding process at 200℃

-.139E+09   -.113E+09   -.870E+08   -.607E+08   -.345E+08
        -.126E+09   -.100E+09   -.738E+08   -.476E+08   -.214E+08
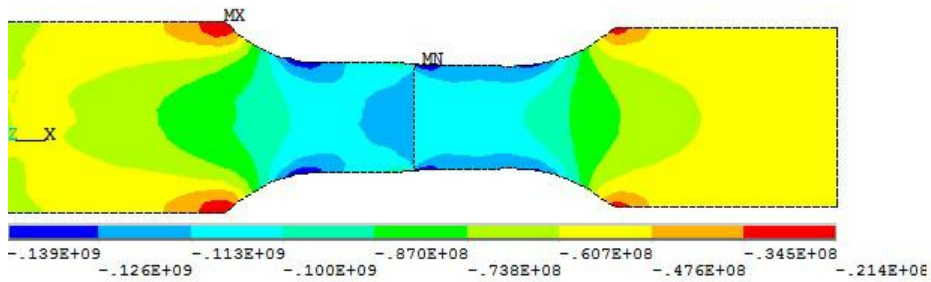
Fig.3.14 Distribution of x-axis stress after the holding process (225℃)

-.142E+09   -.115E+09   -.884E+08   -.618E+08   -.352E+08
        -.128E+09   -.102E+09   -.751E+08   -.485E+08   -.219E+08
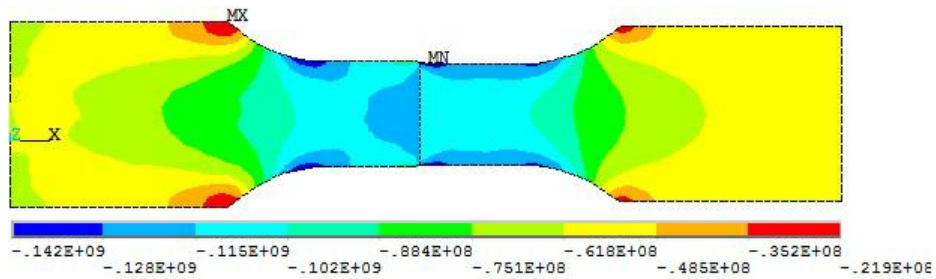
Fig.3.15 X-axis stress of specimens after holding at 250℃

-.409E+09   -.334E+09   -.258E+09   -.183E+09   -.108E+09
        -.372E+09   -.296E+09   -.221E+09   -.145E+09   -.698E+08
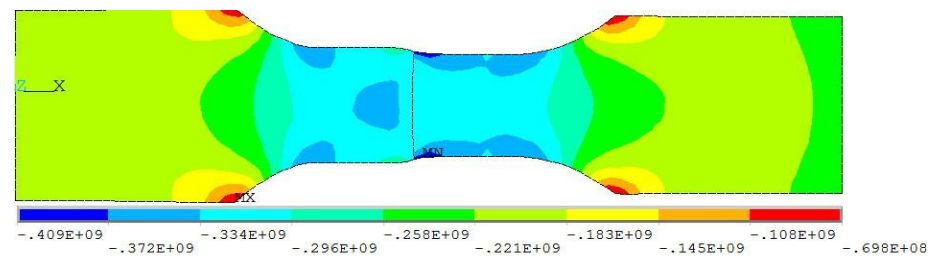
Fig.3.16 Stress of x-axis in the end of holding process (275℃)
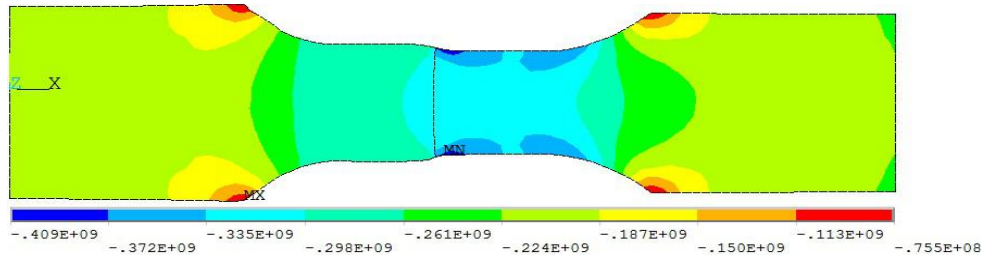
Fig.3.17 Simulation result on x-axis stress after the process holding (300℃)
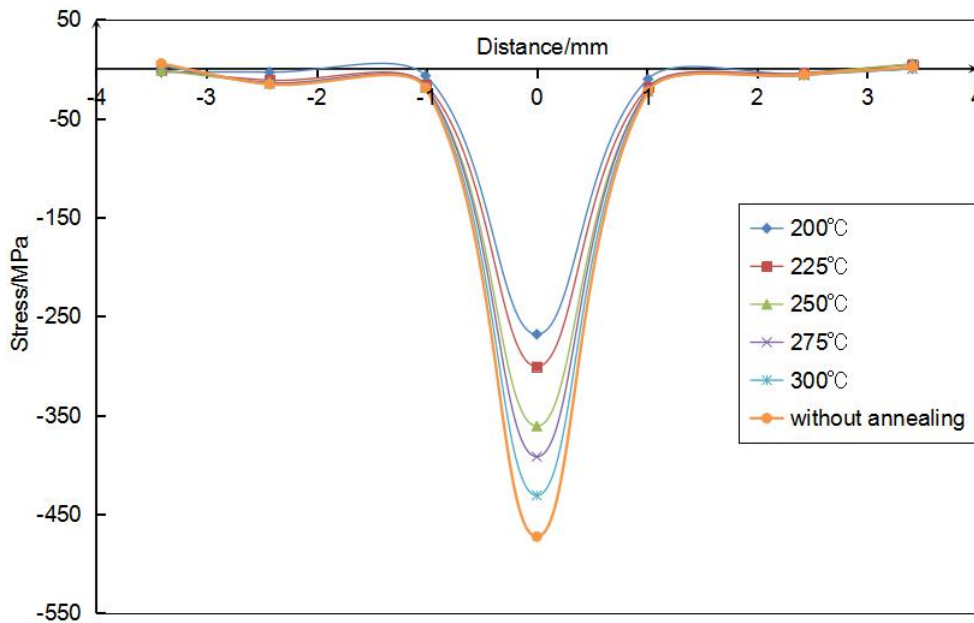
Fig 3.18 X-axis stress of specimens after the holding process

According to the simulation results of holding process above, and compare with the results of heating process, it can be described that with the holding process carried out, the stress increased (shown in Fig.3.18), and the distribution is nearly the same with the one of heating process. In the case of 200℃, 225℃, 250℃, 275℃ and 300℃, the maximum stress increased to -260Mpa, -300Mpa, -360Mpa, -392Mpa and -431Mpa. And it can be thought that the phenomenon is in line with the heat treatment theory.

The final results of simulations were shown in Fig.3.19 a, b, c, d, e and f. The distributions of residual stress obtained by simulations at different temperatures were nearly the same, but the stress values were different from each other. Because of the phenomenon of stress concentration emerges at the edge of interface, in another words,

the place will fracture easily. In this paper, stress distribution along the line crossing the edge of interface was investigated. Based on the stress values at the places of nodes and the distance between nodes, Fig.3.20 was obtained.
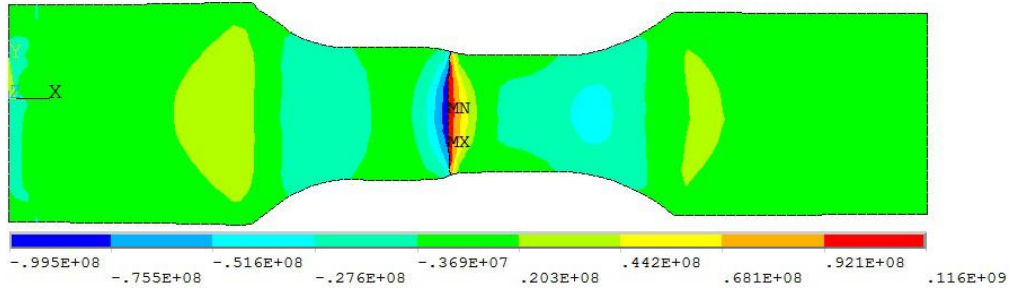
(a)　Without annealing
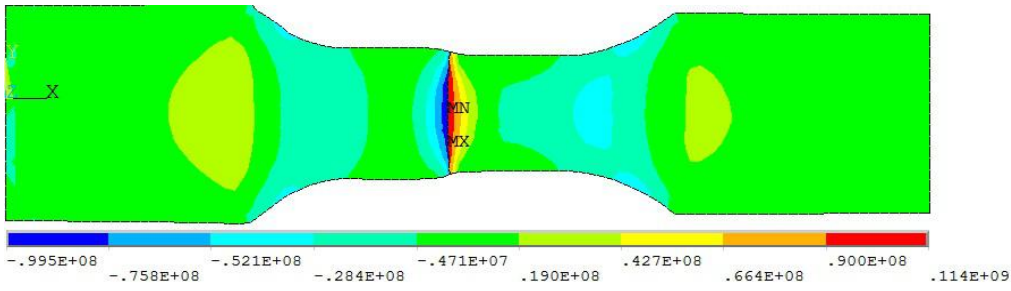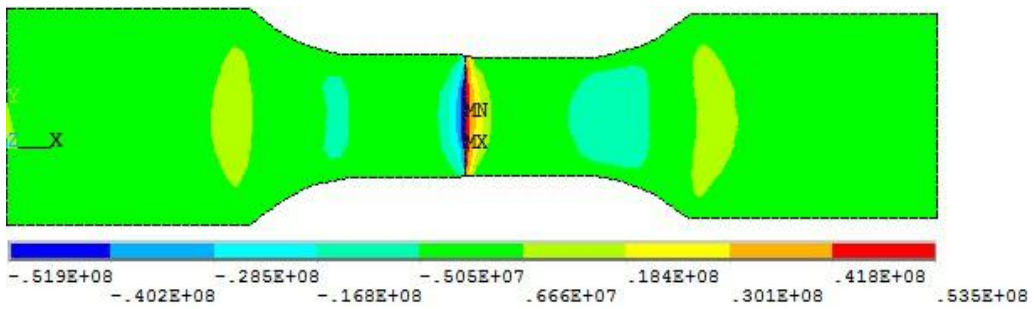
(b)　Annealing at 200℃
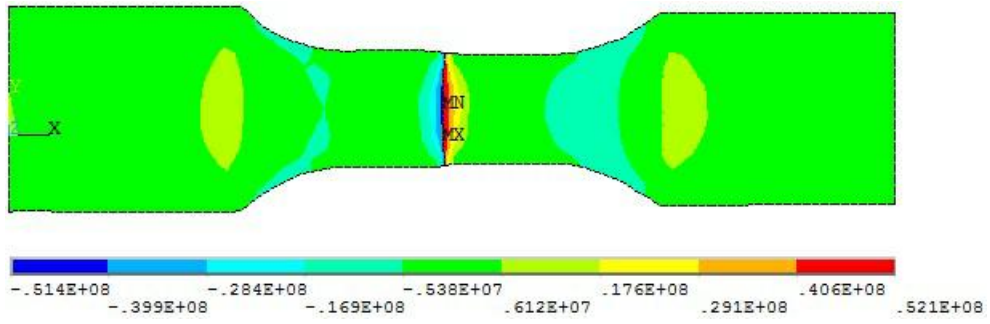
(c)　Annealing at 225℃
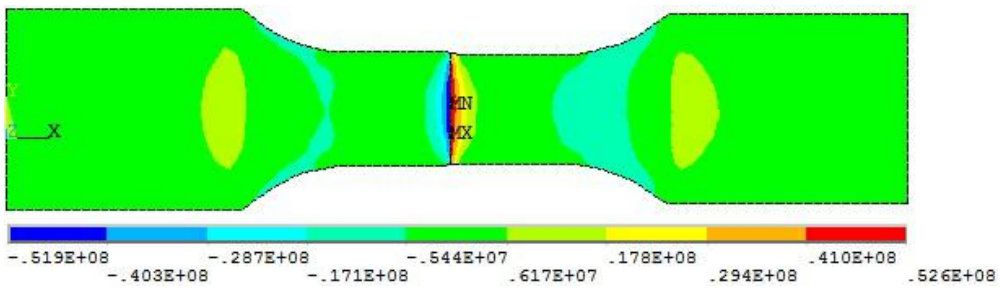
(d) Annealing at 250℃
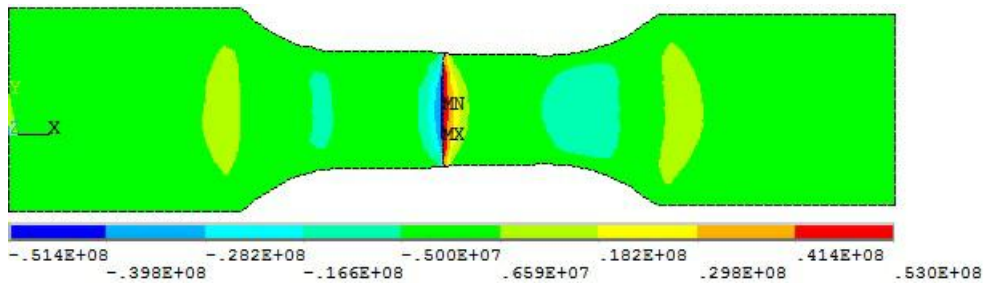
(e) Annealing at 275℃

(f) Annealing at 300℃

Fig.3.19 Final results of simulations on annealing
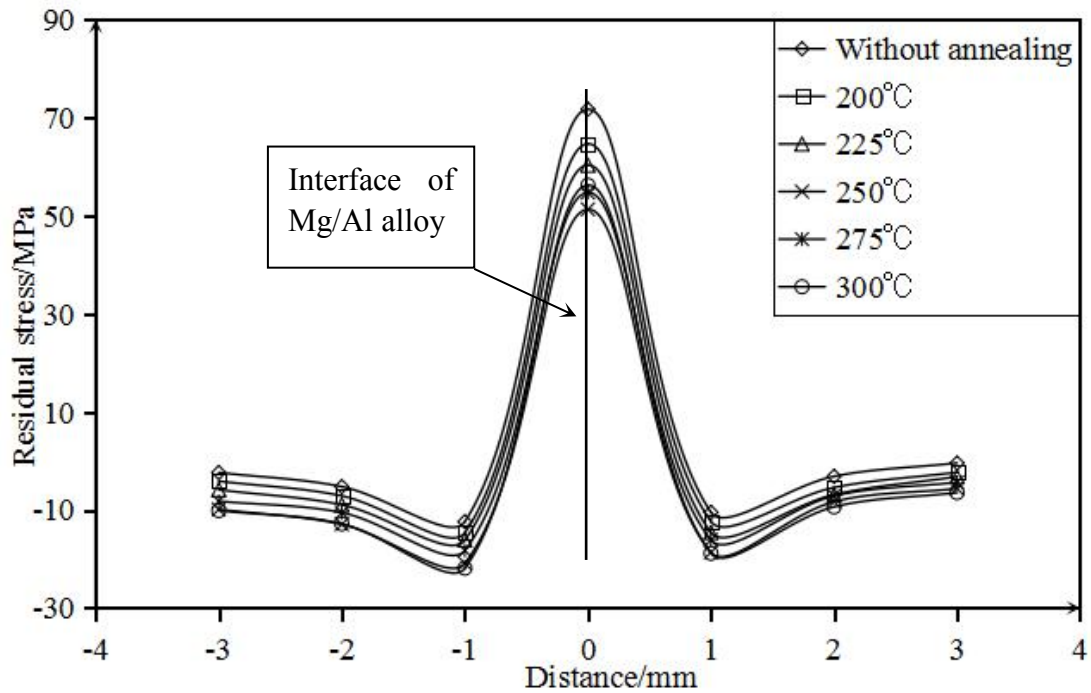
Fig.3.20 Distribution of residual stress obtained from simulation

Residual stress is a vector, and in this study, the direction is axial along the specimens. As it is defined in material mechanics that tensile stress is positive while compress stress is negative. Therefore, it can be known from Fig.3.20 that the value of stress near interface is positive, so it is tensile stress, and the value is the largest. The stresses near interface at the treated conditions 200℃, 225℃, 250℃, 275℃ and 300℃ are respectively 65MPa, 60MPa , 51MPa, 54MPa and 56MPa. When without annealing, the stress is about 72MPa. However, the stress turns to be smaller along with the increasing distance from interface. In another words, The further from interface the smaller it will be. What's more, the stress turns to be negative, so stress becomes compressive stress. In addition, the residual stress nearly to be 0MPa in the further place.

Concluding remarks

In this chapter, based on the analysis of diffusion, heat conduction, constitutive equation of thermal-elastoplastic, and the finite element method, the simulations was carried out to study the effect of annealing temperatures on the distribution of residual

stress in the bonded sheets of Mg/Al alloy. The conclusions can be generalized as follows:

1. During the heating process, the residual stress occurred as compressive one. And the stress in the diffusion zone is bigger than the one far from the interface. In addition, at the place where is away from the diffusion zone, stress turn to be 0MPa.

2. With the holding process carried out, the stress increased, and the distribution is nearly the same with the one of heating process. The phenomenon is in line with the heat treatment theory.

3. The value of stress near the interface are positive, thus tensile one, and the value is the largest. As the distance from the interface increases, the value of stress decrease, the stress turn to be negative one, and become 0MPa in the further place.

4. Annealing temperatures have a great effect on the residual stress. And 250℃ is the most advisable annealing temperature for the diffusion bonded Mg/Al alloy, which was in accord with the results of experiments in chapter 2.

References

[1] Abbott, J.M., Smith, H.C., Van Ness, M.M, Introduction to Chemical Engineering Thermodynamics (7[th]ed.). Boston, Montreal: McGraw-Hill. ISBN 0-07-310445-0. (2005).

[2] Wang Xiang pu, Dictionary of hygiene [M]. Qingdao Publishing House. (2000).

[3] F.P.Incropera, Ge Xin shi, Ye Hong, Fundamentals of heat and mass transfer．Beijing: Chemical Industry Press. (2007).

[4] Lin Chongde, China adult education encyclopedia [M]. Nanhai Publishing House. (1992).

[5] W. Walke, Z. Paszenda, Numerical analysis of three-layer vessel stent made from Cr-Ni-Mo steel and tantalum international. Journal of Computational Materials Science and Surface Engineering. 1/1(2007) pp.129-139.

[6] T. Da SilvaBotelho, E. Bayraktar, Experimental and finite element analysis of spring back in sheet metal forming. International Journal of Computational Materials Science and Surface Engineering. 1/2 (2007) pp.197-213.

[7] A.V. Benin, A.S. Semenov, S.G. Semenov, Modelling of fracture process in concrete reinforced structures under steel corrosion. Journal of Achievements in Materials and Manufacturing Engineering. 39/2 (2010) pp.168-175.

[8] S. Thipprakmas, M. Jin, K. Tomokazu, Y. Katsuhiro, M. Murakawa, Prediction of Fineblanked surface characteristics using the finite element method (FEM). Journal of Materials Processing Technology. 198/1 (2008) pp.391-398.

[9] Y. Kim, S. Yaang, D. Shan, S. Choi, S. Lee, B. You, Three-dimensional rigid-plastic FEM simulation of metal forming processes. Journal of Materials Engineering and Performance. 15 (2006) pp.275-279.

[10] K. Lenik, D. Wójcicka-Migasiuk, FEM applications to the analysis of passive solar wall elements. Journal of Achievements in Materials and Manufacturing Engineering. 43/1 (2010) pp.333-340.

[11] J. Okrajni, W. Essler, Computer models of steam pipeline components in the evaluation of their local strength. Journal of Achievements in Materials and

Manufacturing Engineering. 39/1 (2010) pp.71-78.

[12] J. Bouzakis, G. Maliaris, A. Tsouknidas, FEM supported semi-solid high pressure die casting process optimization based on rheological properties by isothermal compression tests at thixo temperatures extracted. Computational Materials Science. 59 (2012) pp.133-139.

[13] B. Regener, C. Krempaszky, E. Werner, M. Stockinger, Modelling the micromorphology of heat treated Ti6Al4V forgings by means of spatial tessellations feasible for FEM analyses of microscale residual stresses. Computational Materials Science. 52/1 (2012) pp.77-81.

[14] Z. Shiping, K. Rooh A. Khurram, G.Habashi, FEM analysis of in-flight ice break-up. Finite Elements in Analysis and Design. 57 (2012) pp.55-66.

[15] U. E. Ozturk, G. Anlas, Finite element analysis of Expanded polystyrene foam under multiple compressive loading and unloading. Materials and Design. 32/2 (2011) pp.773-780.

[16] Ryuji Mukai, study on the control method of internal structure and residual stress /deformation hybrid during quenching process. Doctor thesis at Saitama Institute of Technology Graduate School of Engineering. (2004).

[17] Inoue Tatsuo, Foundations of elastic mechanics，1st edition，NO.13 print issue. (1997).

[28] Inoue Tatsuo, Tanaka Kikuhisa, Masato AOKI, A theoretical investigation on the thermal ratcheting. 22 (1973) pp.224-228.

[19] Tatsuo Inoue, Transformation Plasticity. Journal of the Society of Materials Science, Japan. 64/4 Apr. (2015) pp.247-257.

[20] Dong-Ying Ju, Actuality and Scope on Simulation of Heat Treatment III: Simulation of Carburized and Nitrided Quenching Process, Journal of The Society of Materials Science, Japan. 7, (2006).

[21] Inoue, Inelastic constitutive models under plasticity-creep interaction condition theories and evaluatio, The Japan Society of Mechanical Engineers, Series I. 31/4 (1998).

[22] Zhi-Gang WANG and Tatsuo INOUE, Analyses of temperature, structure and

stress during quenching of steel with consideration for stress dependence of transformation kinetics. Journal of the Society of Materials Science. (1982) pp.991-996.

Chapter 4 Effect of prior rolling on microstructure and property of diffusion bonded Mg/Al alloy

4.1 Introduction

Among the metalworking, rolling is a metal forming process in which metal material is rolled and passed through one or more pairs of rolls to reduce the thickness and to make the thickness uniform. Rolling is classified into two categories according to the rolling temperature. Hot rolling is the process of rolling the metal materials at a high temperature. These extreme temperatures are higher than the material's recrystallisation temperature, meaning it can be shaped and formed more easily. If the rolling temperature is above its recrystallization temperature of the metal which is rolled, then the process is known as hot rolling. If the temperature is below its recrystallization temperature, the process is known as cold rolling. In terms of usage, hot rolling processes more tonnage than any other manufacturing process, and cold rolling processes the most tonnage out of all cold working processes [1]. Roll stands holding pairs of rolls are grouped together into rolling mills that can quickly process metal into products.

Hot rolling is a metalworking process that occurs above the recrystallization temperature of the material. After the grains deform during processing, they recrystallize, which maintains an equiaxed microstructure and prevents the metal from work hardening. The starting material is usually large pieces of metal, like semi-finished casting products, such as slabs, blooms, and billets. If these products came from a continuous casting operation the products are usually fed directly into the rolling mills at the proper temperature. In smaller operations the material starts at room temperature and must be heated. This is done in a gas- or oil-fired soaking pit for larger work-pieces and for smaller work-pieces induction heating is used. As the material is worked the temperature must be monitored to make sure it remains above the recrystallization temperature. To maintain a safety factor a finishing temperature is defined above the recrystallization temperature; this is usually 50 to 100°C (90 to

180 °F) above the recrystallization temperature. If the temperature does drop below this temperature the material must be re-heated before more hot rolling.

Hot rolled metals generally have little directionality in their mechanical properties and deformation induced residual stresses. However, in certain instances non-metallic inclusions will impart some directionality and workpieces less than 20mm (0.79in) thick often have some directional properties. Also, non-uniform cooling will induce a lot of residual stresses, which usually occurs in shapes that have a non-uniform cross-section, such as I-beams. While the finished product is of good quality, the surface is covered in mill scale, which is an oxide that forms at high temperatures. It is usually removed via pickling or the smooth clean surface process, which reveals a smooth surface. Dimensional tolerances are usually 2 to 5% of the overall dimension. Also for similar metals, hot rolled products seem to be less costly than cold-rolled ones.

Hot rolling is used mainly to produce sheet metal or simple cross sections, such as rail tracks. Other typical uses for hot rolled metal includes truck frames, automotive wheels, pipe and tubular, water heaters, agriculture equipment, strapping, stamping, compressor shells, railcar components, wheel rims, metal buildings, railroad hopper cars, doors, shelving, discs, guard rails, automotive clutch plates.

Cold rolling occurs with the metal below its recrystallization temperature (usually at room temperature), which increases the strength via strain hardening up to 20%. Furthermore, cold rolling during which severe plastic deformation can be generated, is an effective way to refine the grain structure, and the grain size decreases with increasing cold rolling reduction [2-5]. It also improves the surface finish and holds tighter tolerances. Commonly cold-rolled products include sheets, strips, bars, and rods; these products are usually smaller than the same products that are hot rolled. Because of the smaller size of the work-pieces and their greater strength, as compared to hot rolled material, four-high or cluster mills are used. Cold rolling cannot reduce the thickness of a work-piece as much as hot rolling in a single pass.

Cold-rolled sheets and strips come in various conditions: full-hard, half-hard, quarter-hard, and skin-rolled. Full-hard rolling reduces the thickness by 50%, while

the others involve less of a reduction. Skin-rolling, also known as a skin-pass, involves the least amount of reduction: 0.5-1%. It is used to produce a smooth surface, a uniform thickness, and reduce the yield point phenomenon (by preventing Lüders bands from forming in later processing). It locks dislocations at the surface and thereby reduces the possibility of formation of Lüders bands. To avoid the formation of Lüders bands it is necessary to create substantial density of unpinned dislocations in ferrite matrix. It is also used to break up the spangles in galvanized steel. Skin-rolled material is usually used in subsequent cold-working processes where good ductility is required.

Other shapes can be cold-rolled if the cross-section is relatively uniform and the transverse dimension is relatively small. Cold rolling shapes requires a series of shaping operations, usually along the lines of sizing, breakdown, roughing, semi-roughing, semi-finishing, and finishing.

If processed by a blacksmith, the smoother, the more consistent, and lower levels of carbon encapsulated in the steel makes it easier to process, but the cost will be more expensive.

Typical uses for cold-rolled steel include metal furniture, desks, filing cabinets, tables, chairs, motorcycle exhaust pipes, computer cabinets and hardware, home appliances and components, shelving, lighting fixtures, hinges, tubing, steel drums, lawn mowers, electronic cabinetry, water heaters, metal containers, fan blades, frying pans, wall and ceiling mount kits, and a variety of construction-related products.

For magnesium alloy, Owing to its hexagonal close packed(hcp) crystal structure. magnesium alloy has relatively poor plastic processing property at room temperature，and its temperature range of thermal processing is narrow,

and so magnesium alloy sheets are usually produced by multi-pass hot rolling or warm rolling. Through affecting the mechanism of plastic deformation, the microstructures are directly determined by rolling schedule, then the final macro-mechanical properties of the hot-rolled magnesium alloy sheets were determined by the microstructure [6-8].

In the present research, ECAP (equal channel-angular pressing) and an asymmetric

rolling (ASR) process have been suggested as the methods for changing the texture or microstructure of Mg alloys [9–13]. ECAP process can induce severe shear deformation on materials, which can weaken the basal texture or reduce the grain size, and thereby, enhance the room temperature elongation, While ASR process is suggested to modify texture evolutions and reduce the grain size of AZ31 Mg alloy sheets. In ASR process, the circumferential velocities of the upper and lower rolls are different so shear deformation can be applied throughout the thickness of the sheets [14–17]. The changes in deformation mode from thickness reduction to shear deformation can change the texture from {0002} texture to other components, and redundant shear deformation can reduce the grain size effectively.

Others research also reported that by multi-pass cross hot rolling，uniform，fine and equiaxial grain microstructures can be produced, the anisotropy of hot-rolled magnesium sheet can also be effectively weakened．Strong correlation was observed between the average grain size and tensile property of the hot rolled magnesium alloy sheet. So before the diffusion bonding in the study of this chapter, the magnesium alloy was prior hot rolled. And the effect of hot rolling on microstructure and mechanical property of diffusion bonded Mg/Al alloy was dissertated.

4.2 Experiment on twin roll casting of Mg alloy

The twin roll casting (TRC) is a Liquid forming process where liquid metal is poured to middle zone of two relatively rotating cooling, then metal strip can be directly produced. The twin roll casting technology combines the processes of rapid solidification and processing deformation together [18]. Twin roll casting process has many advantages. Such as:

1. It has an economic advantage of reducing the subsequent rolling operation to produce the final products.

2. Reduce manufacturing cost.

3.Increase production flexibility. And with the characteristic of rapid solidification, some metal alloy that can not be producted by other ordinary processes can be producted.

The TRC process can be mainly divided into two types, vertical and horizontal, based on the arrangement of rolls.There are also several variations of these two types, mostly in an inclined or inverted form [19-21].
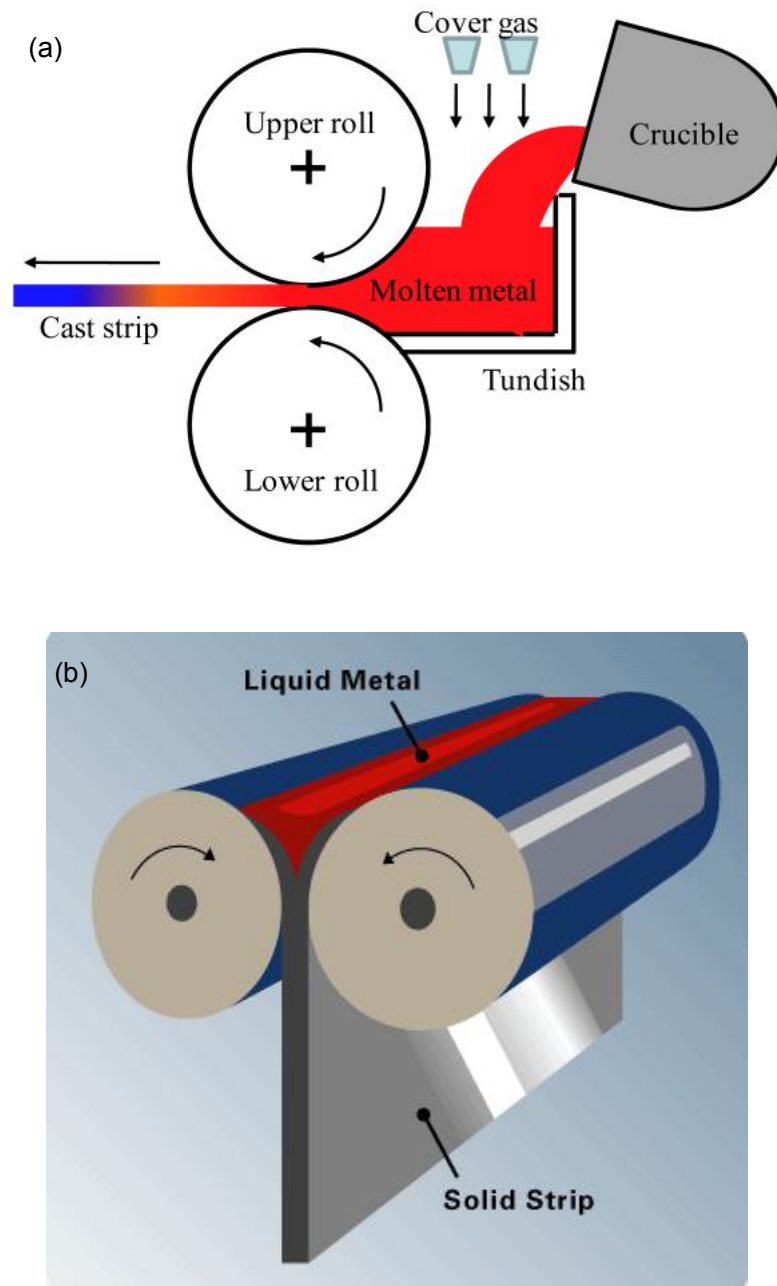
Fig.4.1 Schematic diagram of twin roll casting: (a) horizontal type, (b) vertical type

The vertical TRC is typically used in the steel industry while the horizontal TRC is popular for nonferrous alloys [22], whose selection is mainly based on the needed cooling efficiency of a caster as well as the thermal properties of materials applied. As for Mg alloys, horizontal TRC is preferred since Mg alloys have the thermal

properties similar to those of Al alloys and hence could be handled in a similar manner using a caster utilized for Al alloys. On the other hand, fabrication of Mg alloy strips by vertical TRC has also been reported [23-25]. As it was reported about the study between vertical and horizontal TRC for Mg alloys that horizontal TRC is suitable for producing wide sheets and thus favorable for commercialization due to the relatively easy control of uniform melt distribution while vertical TRC is advantageous with fast casting speed [26]. Despite the difference in the roll arrangement, however, the procedures for operation are substantially similar.

In this study, the vertical TRC process was applied to cast AZ31magnesium alloy. At first, the AZ31 magnesium alloy ingot was heated to 720℃, which   exceeds the melting point, so that the alloy will be fully melted. In order to prevent the magnesium alloy from burning, the mixing gas of CO_2 and SF_6 was used as protection gas. The rotating speed of rolls was set at 18r/min. When the temperature cool down to 680℃, open the furnace and the molten metal will flow into the zone between the two rolls. Then the magnesium alloy sheet will form with the rotation of rolls. The solid trip drops to the oil tank for further cooling after detaching with the rolls.

4.3 Rolling process on Mg alloy

For the purpose of studying the effect of prior rolling on diffusion, the rolling progress on magnesium alloy was carried out with the usage of rolling machine before diffusion bonding progress. The schematic diagram of rolling was shown in Fig.4.2.
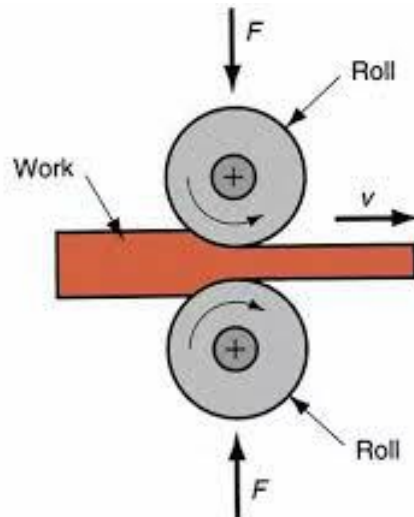
Fig.4.2 The schematic diagram of rolling

The parameters for the rolling progress was shown in Table 4.1.

Table 4.1 The parameters of rolling process

Pass number	Thickness (mm)	Temperature (℃)	Reduction (%)	Rolling speed (m/s)
0	2	250		
1	1.4	250	30	0.15
2	1.0	250	29	0.15

The thickness of sheet was 2mm before the rolling process, after being rolled at 250 ℃ for two times, the thickness turns to be about 1.0 mm.

4.4 Diffusion bonding and annealing process of rolled Mg alloy and Al alloy

At first, the rolled AZ31 magnesium alloy and the magnesium alloy that without rolling were cut together with 6061 aluminum alloy sheets according to the size 50mm*12mm*1mm. Then the oxide layers on the surface of substrate were polished by using abrasive papers #400, and the ground samples were wiped with acetone before joining. After that, the materials were put into the furnace, then closed the door of the furnace.

The next work is to turn on the switch of the pump for vacuum. When the degree of vacuum reached -0.1MPa, turned off the switch, and at the same time, open the embolus of argon gas cylinder and intake valve to insert argon gas into the furnace

until the barometer pointer turned back to 0. Then opened the exhaust valve.

The most important step is the set of temperatures and time for the diffusion joining process. According to the phase diagram, the joining temperature was set as 440℃, and heating time is 10 minutes, holding time is 1 hour. After the temperature setting, turned on the power, the controller started to work, the temperature increased gradually. After cooling down to room temperature in the furnace, specimens were successfully joined.

Besides, in order to improve the microstructures and properties of bonding layers, the samples were used for the annealing treatment experiments. According to the Mg-Al phase graph and annealing experience, the heat treatment temperatures were set as 200℃, 250℃, 300℃, and the holding time was 60min. Then cool down to the room temperature naturally. The annealing treatment experiments were also completed in furnace under argon environment.

4.5 Evaluation of microstructure and mechanical property

For the purpose of studying the effect of rolling process on the microstructures and properties of interfaces, a series of specimens that were treated at different conditions were cut crossing diffusion zone. Then inlaid the component containing diffusion layers into resin for making the specimens to investigate the microstructures. The sections were ground by the grinder with abrasive papers (GRIT 240, 600, 800, 1200). And polished with polishing compound until the microstructure of diffusion zone can be observed clearly. The microstructures and element distribution of the joints were studied respectively by SEM and EPMA. At last, tensile strength was investigated using the tensile machine.

4.5.1 Investigation of microstructure based on SEM

As it is shown in Fig.2.2 in chapter 2, the diffusion zone is named as A, B, and C. Which were investigated as layer A: Al_3Mg_2; layer B: $Mg_{17}Al_{12}$; and layer C: Mg-based solid solution. When with the Mg alloy without being rolled , Mg-based

solid solution occurs in every annealing condition(shown from Fig.4.2 to Fig.4.5). However, when with rolled Mg alloy, Mg-based solid solution occurs only in the annealing condition of 300℃. Comparing with each other, it can be known that the width of the diffusion layer turn to be wider with the increasing annealing temperatures. When compare a with b in every figure, it can be seen that the width of the interface of the specimens with rolled magnesium alloy are thinner than that with magnesium alloy which were not rolled. The reason is that the diffusion speed turns to be faster with the increase of annealing temperatures, that is to say, when the other conditions are the same, only the annealing temperatures change from 200℃ to 300℃, then the width of diffusion zone will be wider with the increase of temperature. Besides, rolling process makes the atomic space of magnesium alloy decrease, then it's difficult for atoms to diffuse between magnesium alloy and aluminium alloy, so that the width of diffusion layers become thinner.
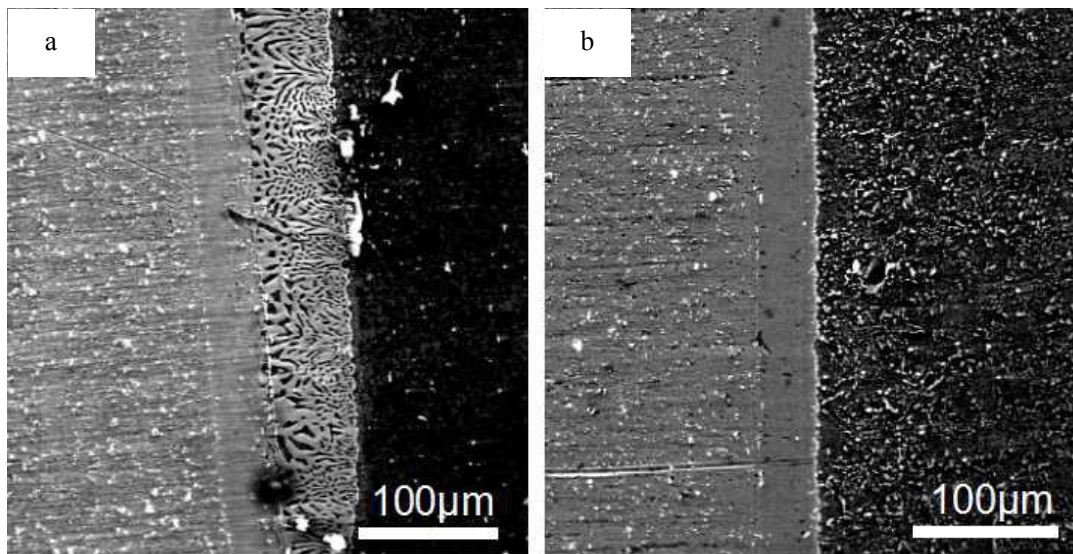
Fig.4.2 The microstructure of bonding layers in the case of annealing absence a: without rolling; b: with rolling
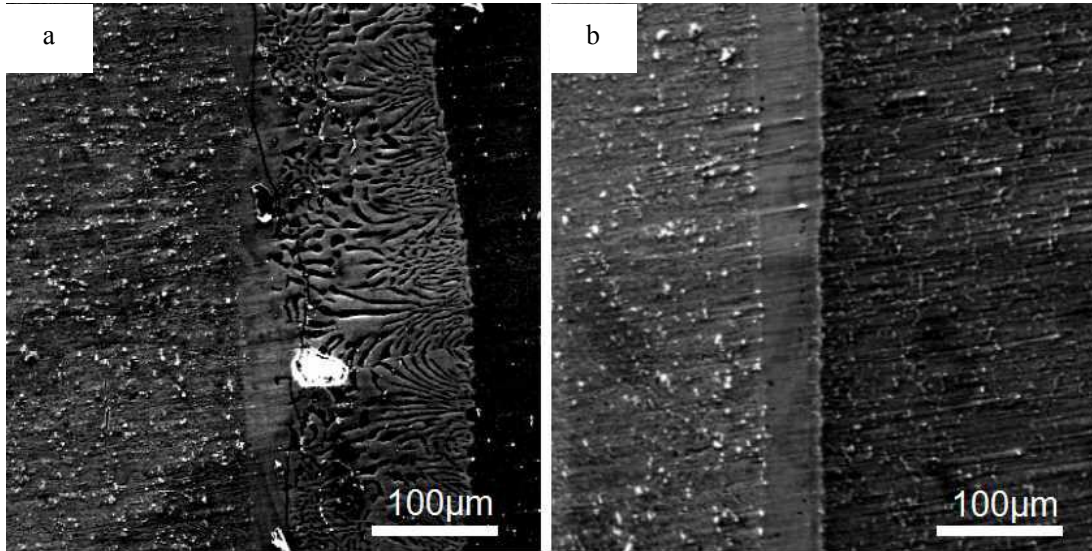
Fig.4.3 The observation results on the microstructure of specimens annealed at200℃
a: without rolling; b: with rolling
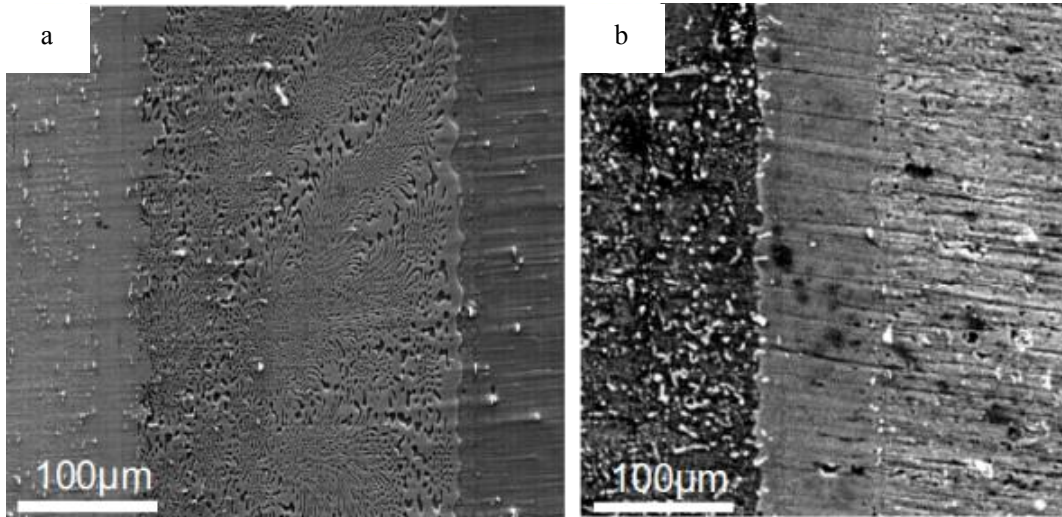
Fig.4.4 The microstructure of bonding layers after annealing at 250℃ a: without rolling;
b: with rolling
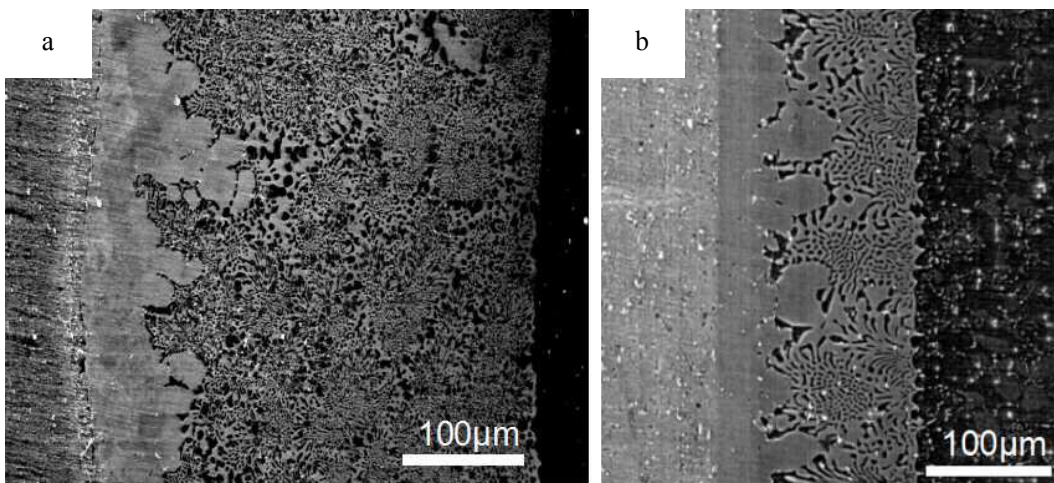
Fig.4.5 The microstructure after annealing at 300℃ a: without rolling; b: with rolling

4.5.2 Analysis of element distribution with the usage of EPMA

The element analysis was carried out with the application of EPMA. Cooling water and protection gas need to be applied before the equipment was started. At first, the specimens with cast magnesium alloy and the specimens with rolled magnesium alloy were stuck with conductive tape respectively, and put   the samples into the different positions of the holder. Secondly, the holder was put into the device called EPMA, then wait for about 30 minutes until the vacuum state is ready. The third step is to open the electron optics system, add the high voltage and adjust the magnitude of the current to 10^{-9}, then select the position of the sample, and adjust the focus, contrast and brightness until the clear optical image and SEM image can be observed. The next step is to set the scanning range as 400μm*400μm. Based on confirming the electron optics conditions, the scan was started. When the scan on one sample was over, save the results of element analysis, then change the observing place for analysis of another specimen. At last, the specimens without annealing and   annealed at 200℃, 250℃, 300℃ were all analyzed. After the data processing, the results of element analysis are shown in the Figs from Fig.4.6 to Fig.4.9.
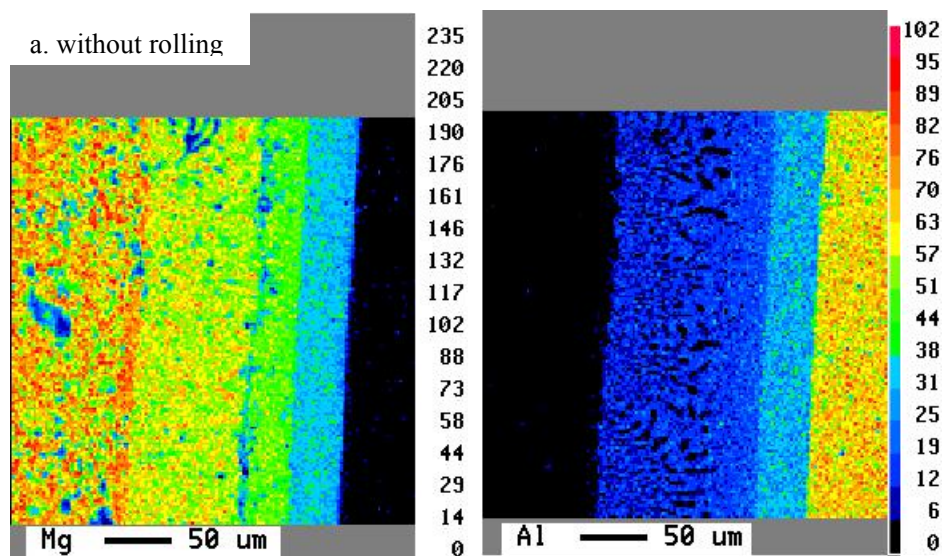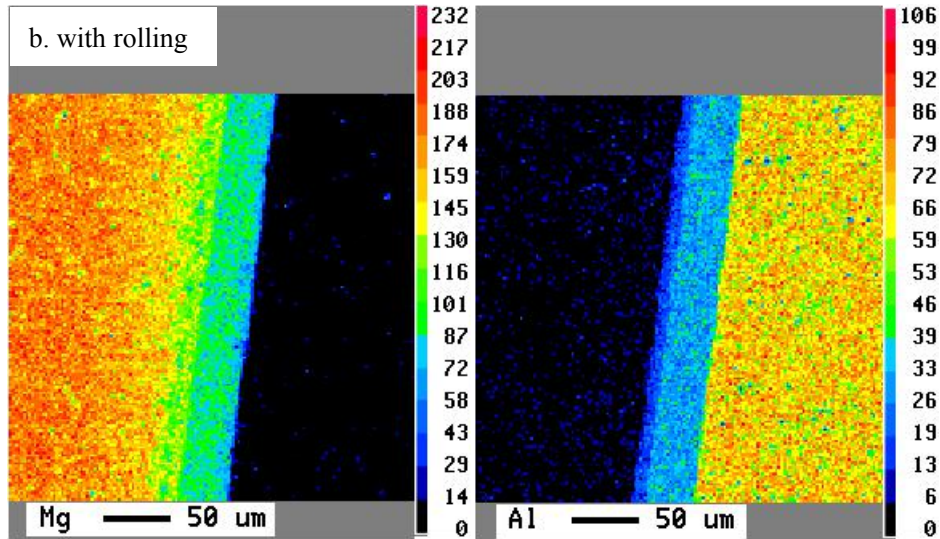
Fig.4.6 The element analysis of the specimens without annealing
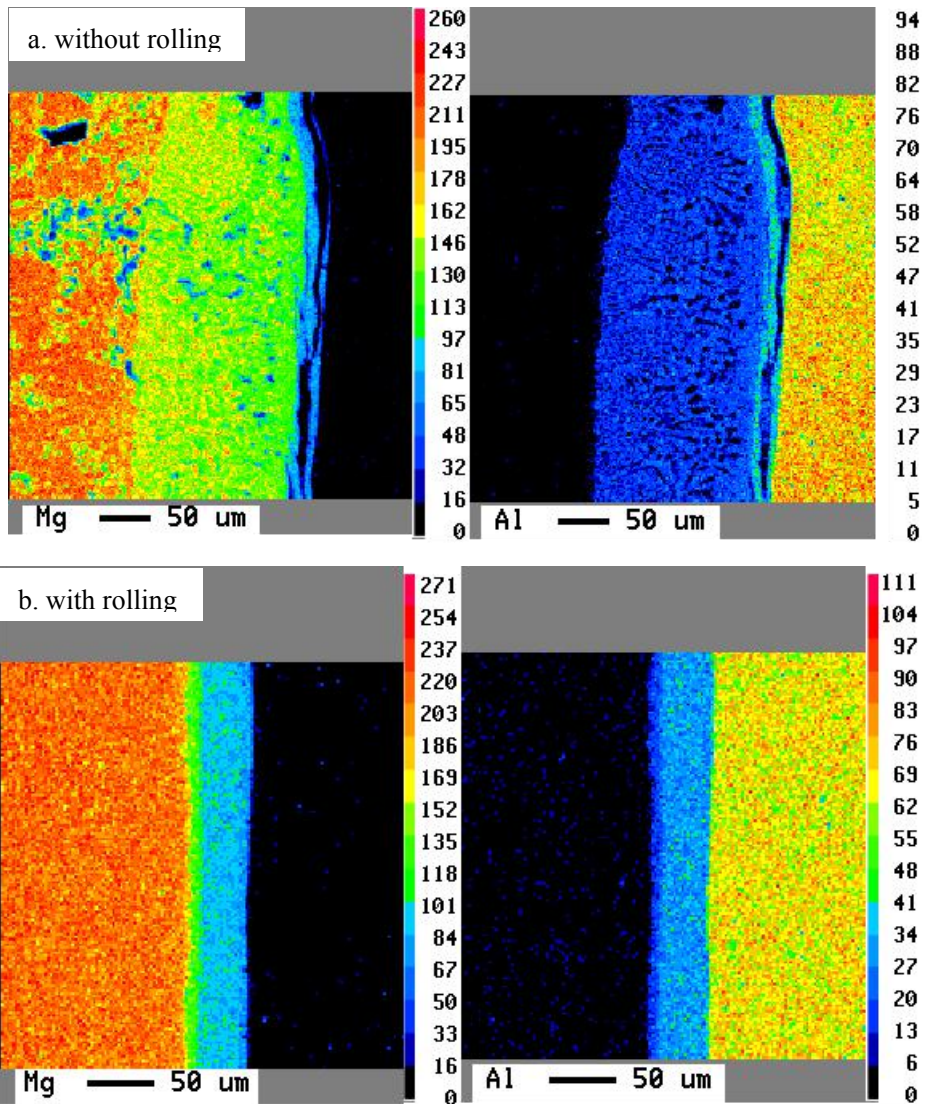
Fig.4.7 The distribution of elements in the case of annealing at 200℃
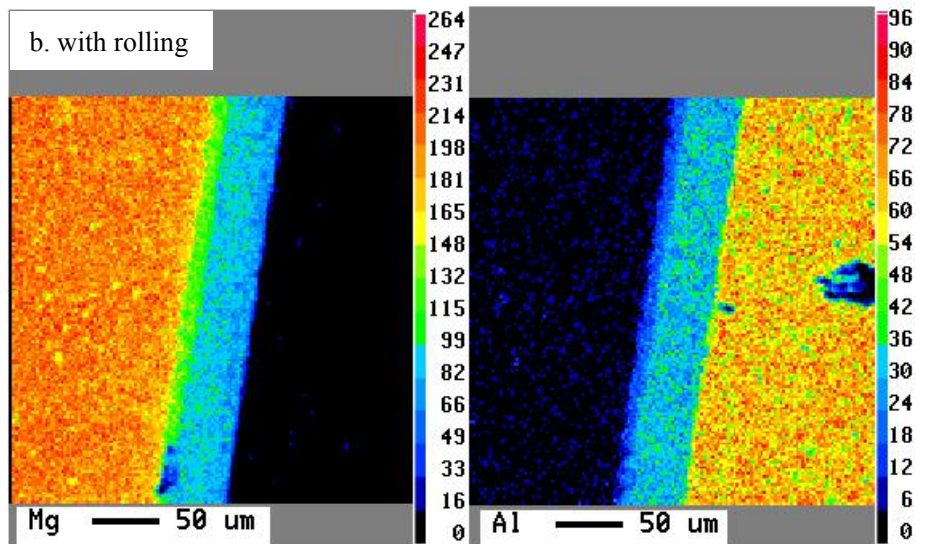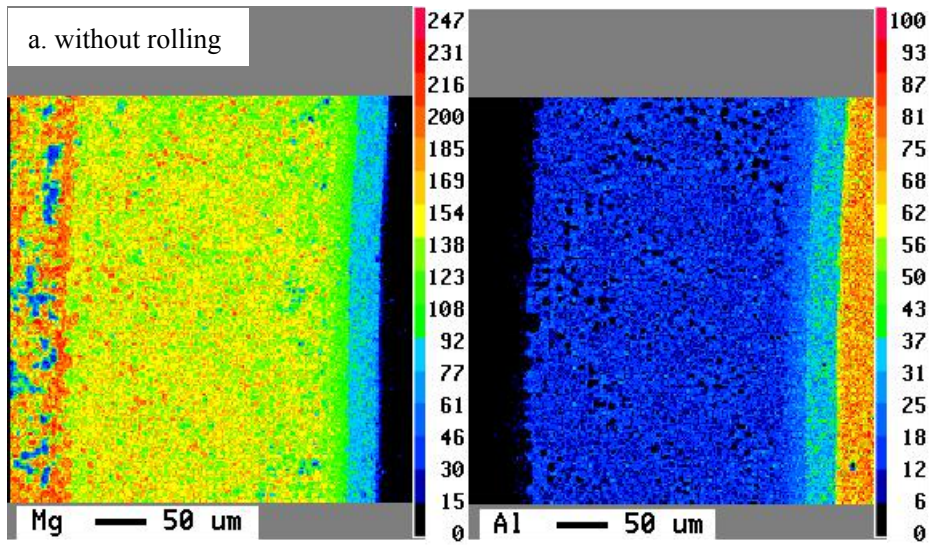
Fig.4.8 The results on element analysis of specimens under the annealing
condition of 250℃
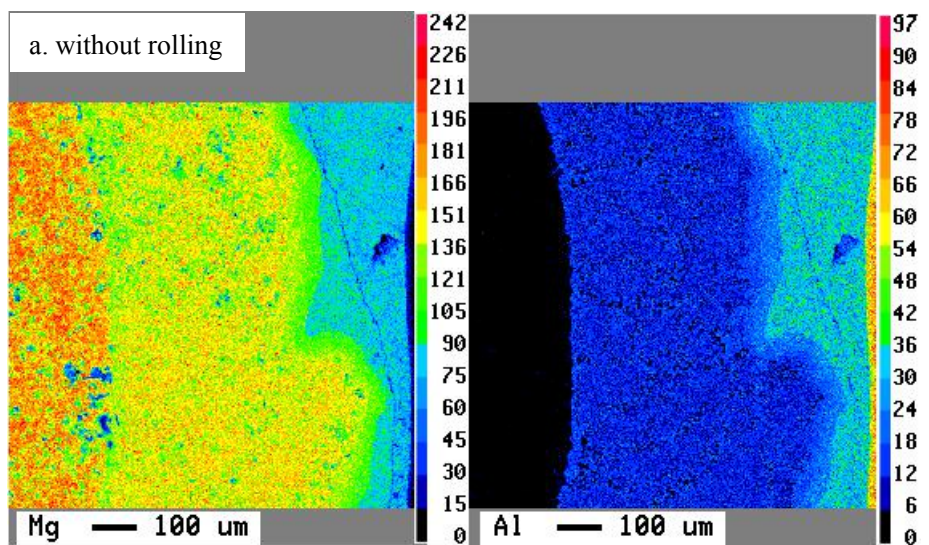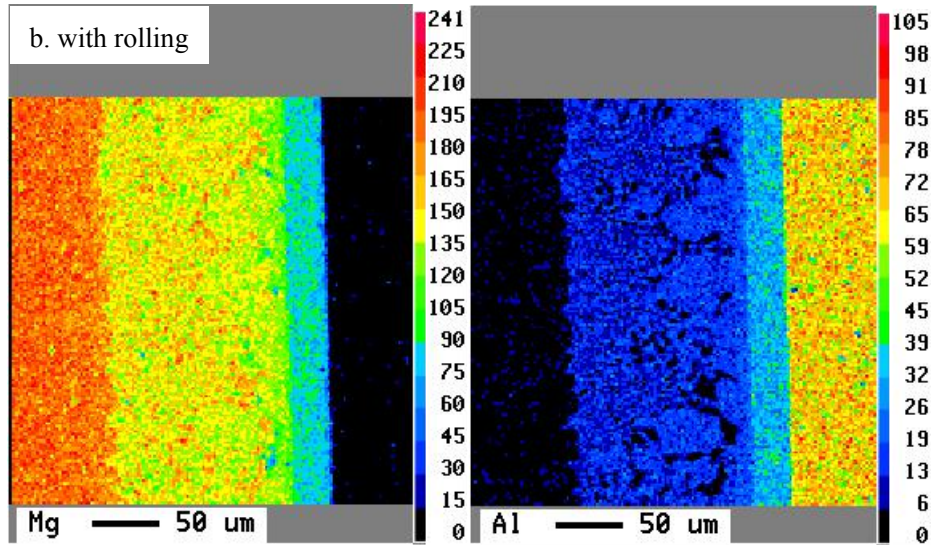
Fig.4.9 The element analysis of the workpieces annealed at 300℃

According to the results, it can be thought that the diffusion layers can be seen clearly. The different colors stand for the quantities of the elements that were detected. The quantities increase with the change of colors from black to white.

First, the same conclusions with microstructure can be got. In another word, the width increase with the increase of annealing temperatures, and the diffusion zones of specimens with rolled magnesium alloy are thinner than the specimens with magnesium alloy without being rolled, Because rolling decreases the atom spacing and make the diffusion not as fast as without rolling. In addition, when rolling process was applied, the element concentration turns to be more than without rolling, because the space between atoms decreases, so that the atomic density increases, and the element content in the same area becomes higher.

4.5.3 Measurement of tensile strength

For the purpose of studying the effect of rolling and annealing on diffusion bonding magnesium alloy and aluminium alloy, the tensile strength were investigated using tension machine. The results are shown from Fig.4.10 to Fig.4.13. The conclusions can be obtained from these results that tensile strength increases with the annealing treatment, but when annealed at 300℃, the strength decreases. In the case of

annealing absence, the results were shown in Fig.4. The conclusion can be obtained that the tensile strenth after rolling was stronger than the one without rolling, but the strain is smaller. Because the rolling process can produce strain hardening effect and work hardening effect. So the strenth of the specimens with rolled magnesium alloy were stronger, while the strain decreased.
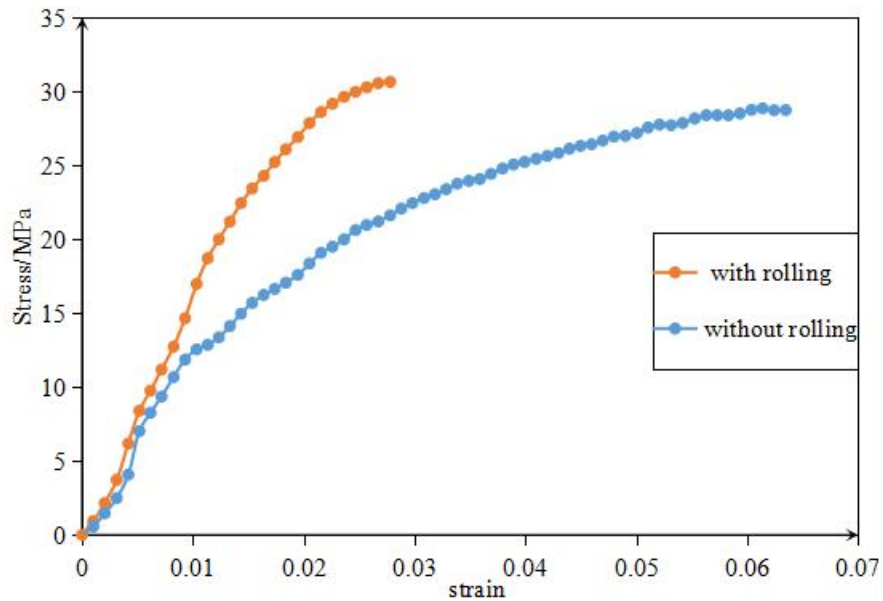
Fig.4.10 Tensile curve of specimen without annealing
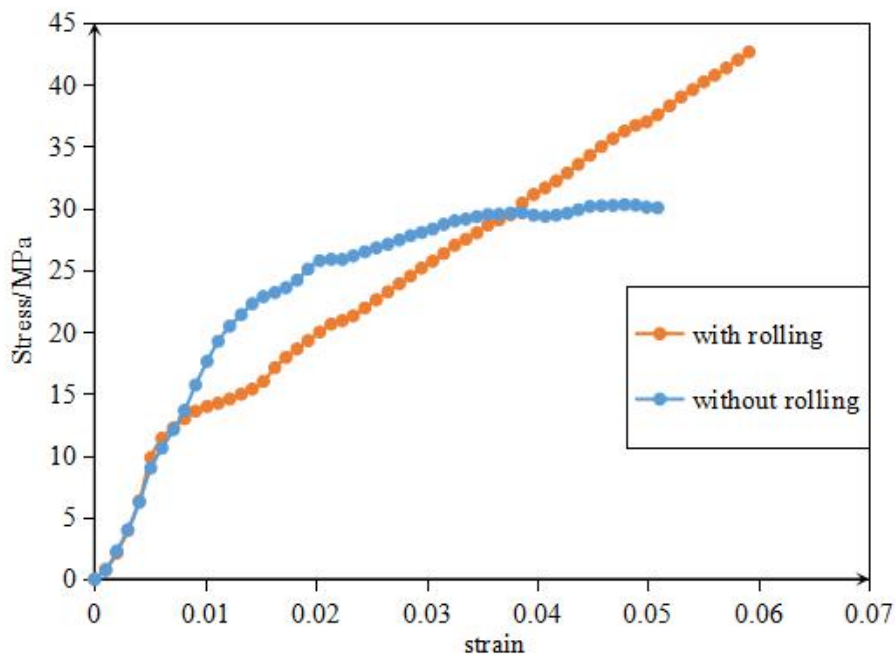
Fig.4.11 Tensile strength of workpiece annealed at 200℃
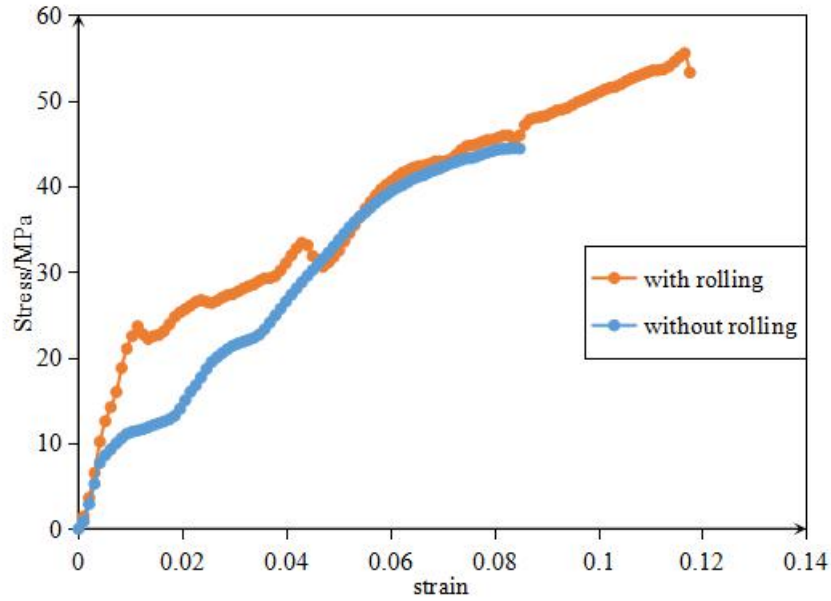
Fig.4.12 Tensile strength in the case of annealing at 250℃
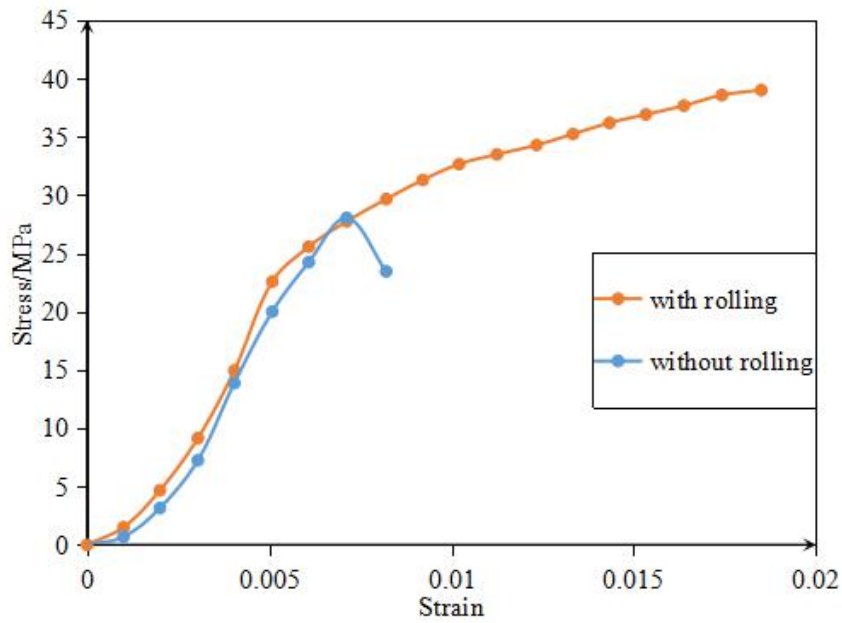
Fig.4.13 Tensile curve under the condition of annealing at 300℃

As shown from Fig.4.11 to Fig.4.13, when without rolling, the maximum of strength is 44MPa, which was obtained after being annealed at 250℃, which was shown in Fig.4.12. As what has been reported in other study, the strength is about 37MPa when without annealing [27]. However, when with rolling, the strength turned to be stonger, in addition, the strain also became bigger. That was because rolling process produced strain hardening effect, and the annealing process decreased the Hardness and

brittleness of specimens. The maximum of strength increased to 53Mpa under the condition of rolling, which was also achieved after being annealed at 250℃. So it can be thought that the most appropriate annealing temperature is 250℃ [28]. What's more, when the strength is compared with each other, it can be seen that the strength is stronger when rolling process is applied. So it's thought that rolling can refine microstructure, and make microstructure more uniform, further more, the mechanical character can be improved.

Concluding remarks

Aiming at refine the microstructure, improving mechanical behaviors, and study the effect of hot rolling, hot rolling process on magnesium alloy and annealing process on diffusion bonded specimens were applied before and after the diffusion bonding experiments. According to the results of the investigations, it can be thought that rolling process on magnesium alloy before welding and annealing after welding can refine the microstructure and have a good effect on tensile strength. And it can be summarized as follows:

1. For the specimens with rolled magnesium alloy, the width of diffusion zone is thinner than the specimens which was made without the rolled magnesium alloy. Rolling process can refine microstructure, so the microstructures and element distribution are more uniform.

2. Annealing and rolling process can refine the microstructure and improve mechanical properties. After being annealed at 250℃, the strength turns to be the strongest. What's more, the strength of the specimen which was with rolled magnesium alloy is stronger than the specimens made with cast magnesium alloy that was not rolled.

3. The width of diffusion layers turns to be wider with the increasing annealing temperatures.

4. 250℃ is the most appropriate annealing temperature.

References

[1] Degarmo, E. Paul, Black, J T., Kohser, Ronald A, Materials and Processes in Manufacturing (9th ed.), Wiley. ISBN 0-471-65653-4. (2003).

[2] Hanliang Zhua, A.K. Ghosh, K. Maruyama, Effect of cold rolling on microstructure and material properties of 5052 alloy sheet produced by continuous casting. Materials Science and Engineering A. 419 (2006) pp.115–121.

[3] A. Di Schino and J. Kenny, Grain refinement strengthening of a micro-crystalline high nitrogen austenitic stainless steel. Mater.Lett.. 57 (2003) pp.1830–1834.

[4] V. V. Stolyarov, Y. T. Zhu, I. V. Alexandrov, T. C. Lowe and R. Z.Valiev, Grain refinement and properties of pure Ti processed by warm ECAP and cold rolling. Mater. Sci. Eng. A. A343 (2003) pp.43–50.

[5] S. C. Sun, J. W. Mu, Z. H. Jiang, C. T. Ji, J. S. Lian and Q. Jiang, Effect of cold rolling on tensile properties and microstructure of high nitrogen alloyed austenitic steel. Materials Science and Technology. 30 (2014) pp.146-151.

[6] Wang H, Zhang E, Nan X, Zhang L，Z Guan, A Comparison of Microstructure and Mechanical Properties of Mg-9A1-1Zn Sheets Rolled from As-cast, cast-rolling and As-extruded Alloys[J]．Materials＆Design．89 (2016) pp. l67-172.

[7] Yuan Y，Ma A，Gou X，et a1, Superior Mechanical Properties of ZK60 Mg Alloy Processed by Equal Channel Angular Pressing and Rolling[J]．Materials Science andEngineering：A. 630 (2015) pp.45—50.

[8] Pu Z，Song G L，Yang S，et a1．Grain Refined and Basal Textured Surface Produced by Burnishing for Improved Corrosion Performance of AZ31B Mg Alloy[J]. Corrosion Science. 57 (2012) pp.192—201.

[9] T. Mukai, M. Yamanoi, H. Watanabe, K. Higashi, Ductility enhancement in AZ31 magnesium alloy by controlling its grain structure. Scr. Mater. 45 (2001) p.89.

[10] W.J. Kim, S.I. Hong, Y.S. Kim, S.H. Min, H.T. Jeong, J.D. Lee, Texture

development and its effect on mechanical properties of an AZ61 magnesium alloy fabricated by equal channel angular processing. Acta Mater. 51 (2003) pp.3293-3307.

[11] S.R. Agnew, J.A. Horton, T.M. Lillo, D.W. Brown, Enhanced ductility in strongly textured magnesium produced by equal channel angular processing. Scr. Mater. 50 (2004) pp.377-381.

[12] Y. Yoshida, L. Cisar, S. Kamado, Y. Kojima, Effect of microstructural factors on tensile properties of an ECAE-processed AZ31 magnesium alloy. Mater. Trans.. JIM 44 (2003) pp.468-475.

[13] L. Jin, D. Lin, D. Mao, X. Zeng, W. Ding, Mechanical properties and microstructure of AZ31 magnesium alloy processed by two-step equal angular channel extrusion. Mater. Lett. 59 (2005) pp.2267-2270.

[14] S.H. Lee, D.N. Lee, Analysis of deformation textures of asymmetrically rolled steel sheets. Int. J. Mech. Sci. 43 (2001) pp.1997-2015.

[15] K.H. Kim, D.N. Lee, Analysis of deformation textures of asymmetrically rolled aluminum sheets. Acta Mater. 49 (2001) pp.2583-2595.

[16] S.H. Kim, J.K. Lee, D.N. Lee, Grain refinement and texture development in asymmetrically rolled aluminum alloy sheets. Ultrafine Grained Materials, TMS, USA. (2002) pp.55-64.

[17] S.H. Kim, J.H. Ryu, K.H. Kim, D.N. Lee, The evolution of shear deformation texture and grain refinement in asymmetrically rolled aluminum sheets. Mater. Sci. Res. Int. 8 (2002) pp.20-25.

[18] Dongying Ju, Hongyang Zhao, Lin Hu, Liangang Zhao, Zhenhu Duan, Progress of twin roll strip casting process. Journal of University of Science and Technology. (2003).

[19] B.Q. Li, Producing thin strips by twin-roll casting-Part 1: Process Aspects and Quality Issues. Journal of Metals, 47(5) (1995) pp. 29–33.

[20] H. Watari et al., Semi-solid manufacturing process of magnesium alloys by twin-roll casting. J. Mater. Proc. Tech.. 155-156 (2004) p.1662-1667.

[21] B.S. You et al., Mater. Sci. Forum, 488-489 (2005) p.337.

[22] R. Kopp, Some current development trends in metal-forming technology. J. Mater. Proc. Tech.. 60 (1996) pp.1-9.

[23] C. Yang et al., The microstructure and processing in twin roll casting of magnesium alloy strip. Mater. Sci. Forum, 488-489 (2005) pp.427-430.

[24] D.Y. Ju, and X.D. Hu, Effect of casting parameters and deformation on microstructure evolution of twin-roll casting magnesium alloy AZ31. Trans. Nonferrous Met. Soc. China. 16 (2006) pp.s874-s877.

[25] T. Haga, H. Watari, and S. Kumai, High speed roll casting of Al alloy and Mg alloy strips, in Continuous Casting: Proceedings of the International Conference on Continuous Casting of Non-Ferrous Metals (ed H. R. Müller), Wiley-VCH Verlag GmbH & Co. KGaA, Weinheim, Germany. doi: 10.1002/9783527607969.ch19. (2005).

[26] P.D. Ding et al., Trans. Nonferrous Met. Soc. China,18 (2008) p.57.

[27] SHANG Jing, WANG Ke-hong, ZHOU Qi, ZHANG De-ku, HUANG Jun, GE Jia-qi, Effect of joining temperature on microstructures and properties of diffusion bonded Mg/Al joints [J]. Transactions of Nonferrous Metals Society of China. 22 (2012) pp.1961-1966.

[28] Yunlong Ding, Jiangang Wang, Ming Zhao, Dongying Ju, Effect of annealing temperature on the joints of diffusion bonded Magnesium Alloy and Aluminum Alloy[J]. Transactions of Nonferrous Metals Society of China. (in press)

Chapter 5 Conclusions and recommendation

5.1 Conclusions

In this thesis, the coupling theory, thermo-elastic plastic deformation, thermal conduction and diffusion in diffusion bonding and annealing process, have been analyzed. And the finite element method was used to the simulation of the diffusion bonding and annealing treatment. The residual stress in the bonding layers is measured and calculated by the improved evaluation technique. The results of residual stress measurement were compared with that of simulations about the residual stress, so that the accuracy was verified. Besides, the effect of the annealing temperature on the microstructure and mechanical properties of the combined Mg/Al alloy has been also studied. The microstructure, element analysis, tensile strength, and micro-hardness of the diffusion zone were investigated. What's more, the influence of hot rolling process on magnesium alloy before diffusion bonding on the microstructure and diffusion bonding properties of the bonding layers is discussed. The evaluation of microstructure, element analysis and mechanical behavior were carried out. The following conclusions can be drawn from the results of experiments and simulations:

1. According to the experimental study on the effect of annealing temperature, the conclusions have been obtained as follows:

(1) It was difficult to obtain enough quality of bonding strength just by diffusion bonding between magnesium and aluminum alloy sheets due to the formation of intermetallic compound layer. In this study, the application of annealing treatment makes it possible.

(2) Annealing temperatures have a great effect on microstructures and mechanical character. The microstructure can be refined by annealing treatment. The element distribution of the annealed specimens is more uniform than the one without annealing.

(3) The width of diffusion layers increases with the rise of annealing temperature,

because diffusion rate turns faster with the increase of temperature.

(4) The hardness of diffusion layers can also be decreased with the usage of annealing process. it's 187HV in interface after the specimen is treated at 250℃. In addition, When the annealing temperature is 250℃, the tensile strength is the strongest, which is about 56MPa.

2. Combining the simulation study and experimental study above, the conclusions can be expressed as follows:

(1) Due to the usage of annealing, the residual stress can be partially released. The stresses near the interface for heat treatment conditions of 200℃, 250℃, and 300℃ are respectively 66MPa, 61MPa and 63MPa. However, the untreated specimens exhibit a stress value of 71MPa.

(2) As the results of experiments, the stresses near the interface for heat treatment conditions of 200℃, 250℃, and 300℃ are respectively 59MPa, 44MPa, 51MPa. The stress of the specimens without annealing is about 65MPa.

(3) It can be depicted that the results obtained from simulation in accord with that of experiments. And 250℃ is the most advisable annealing temperature for the diffusion zone of AZ31B magnesium alloy and 6061 aluminum alloy.

3. According to the results of the study on the effect of prior rolling on microstructure and property of diffusion bonded Mg/Al alloy, it can be depicted that the rolling process on magnesium alloy before welding and annealing after welding can refine the microstructure and have a good effect on tensile strength. And it can be summarized as following:

(1) For the specimens with rolled magnesium alloy, the width of diffusion zone is thinner than the specimens which was made with the magnesium alloy without rolling.

(2) Rolling process can refine microstructure, so the microstructures and elements distribution are more uniform.

(3) Annealing can refine microstructure and improve mechanical property. After being annealed at 250℃, the strength turns to be the strongest. What's more, the strength of the specimen which was with rolled magnesium alloy is stronger than

the one made with cast magnesium alloy that was not rolled.

5.2 Recommendation

In this study, the bonding process was carried out without the welding material between AZ31 Mg alloy and 6061 Al alloy. So the research about the effect of welding materials on the microstructure and mechanical behaviors of the bonding layers will be carried out.

According to the literature that had been read, the element Zn had a good effect on the microstructure of Mg/Al interface. It's said that Zn can reduce the form of intermetallic compounds of Mg and Al. Though intermetallics can be formed, because of the effect of Zn, they will precipitate dispersedly, which can produce precipitation strength.

So with the attempt of other advanced welding technology and equipment, the study on the composition of intermetallic compounds formed by element Mg, Al and Zn, the microstructure, and the mechanical behaviors of welding layers maybe promote the advancement of the field of Mg/Al bonding.

Related publications

1. Yunlong Ding, Jiangang Wang and Dongying Ju, Simulations about the effect of heat treatment temperatures on the properties of diffusion bonded Mg/Al joints. MATEC Web Conferences **130**, 06004, 2017. (Engineering Index)

2. Yunlong Ding, Jiangang Wang, Ming Zhao, Dongying Ju, Effect of annealing temperature on the joints of diffusion bonded Magnesium Alloy and Aluminum Alloy. Transactions of Nonferrous Metals Society of China.(in press) (SCI)

3. Yunlong Ding, Dongying Ju, Finite element analysis of residual stress in the diffusion zone of Mg/Al alloy. Advances in Materials Science and Engineering.(in press) (SCI)

Acknowledgments